Advances in peripheral nerve MR imaging

The application of diffusion MRI in neurological disorders

Wieke Haakma

Advances in peripheral nerve MR imaging - The application of diffusion MRI in neurological disorders

Cover design	Wieke Haakma & Roy Sanders
Cover image	Diffusion MRI of a squid reconstructed with fiber tractography
Lay-out	Roy Sanders
Printed by	Ipskamp Printing, Enschede
ISBN	978-94-028-1130-8

Advances in peripheral nerve MR imaging
The application of diffusion MRI in neurological disorders

Vooruitgang in MR beeldvorming van perifere zenuwen
Het gebruik van diffusie MRI bij neurologische aandoeningen

(met een samenvatting in het Nederlands)

Proefschrift

ter verkrijging van de graad van doctor aan de Universiteit Utrecht
op gezag van de rector magnificus, prof.dr. H.R.B.M. Kummeling,
ingevolge het besluit van het college voor promoties in het openbaar te verdedigen
op dinsdag 9 oktober 2018 des middags te 4.15 uur

door

Wieke Haakma
geboren op 28 januari 1988 te Beetsterzwaag

Promotoren: Prof. dr. J. Hendrikse
Prof. dr. P.R. Luijten

Copromotoren: Dr. M. Froeling
Dr. A. Leemans

Financial support by Sectra and Chipsoft for the publication of this thesis is gratefully acknowledged.

Contents

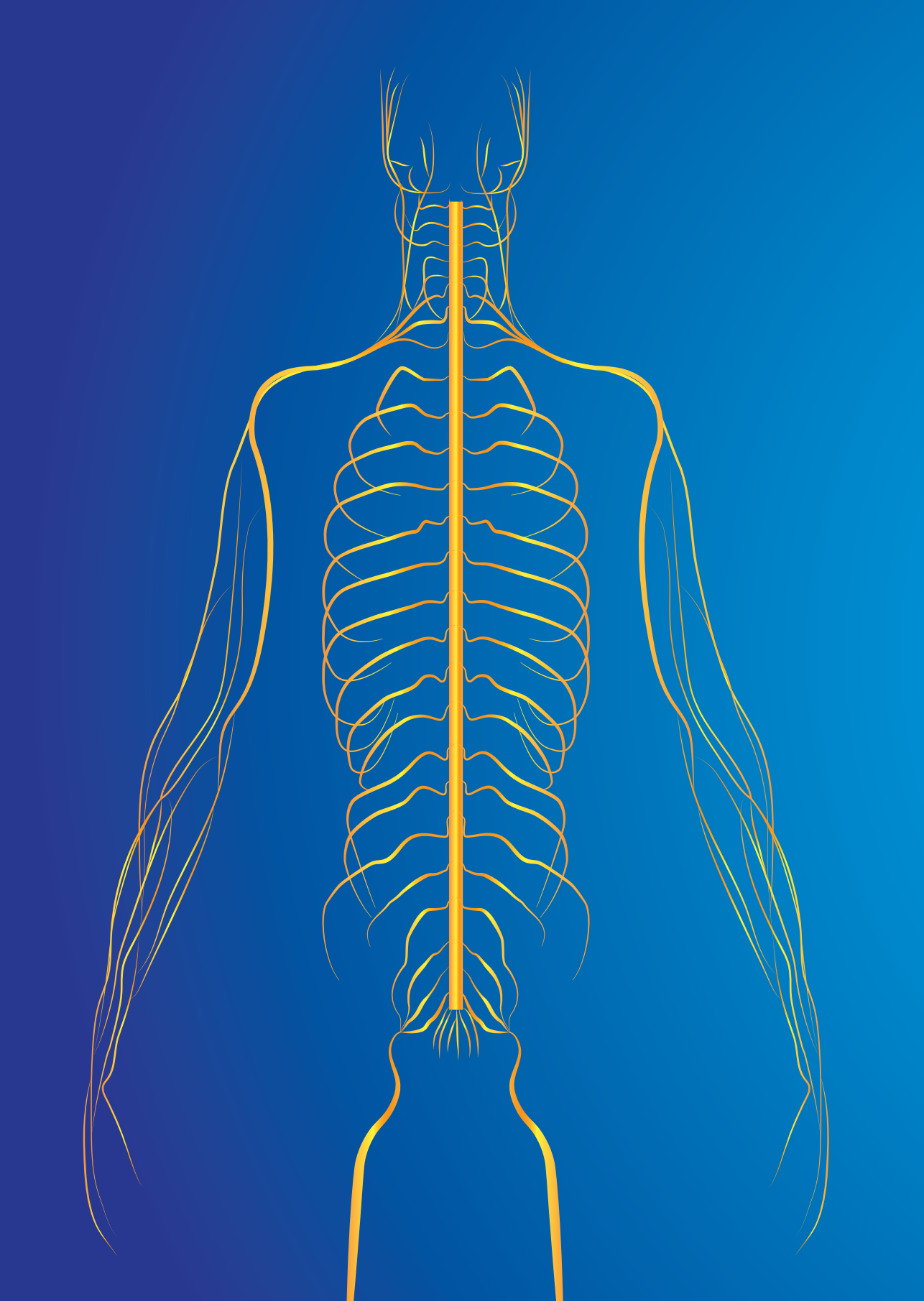

Chapter 1

General introduction

Peripheral nerve anatomy

The peripheral nervous system is a network of nerves which transmits signals from the central nervous system to the body and vice versa. It regulates and controls bodily functions and activity, such as the muscles, hormone secretion, and respiration (1). Peripheral nerve tissue consists of nerves and ganglion tissue. Nerves consist of neurons which enable to rapidly transmit signal or information from one cell to the other. Electrical impulses are sent through the nerve fibers which are called axons. Nerve tissue is composed of connective structures; the endoneurium, perineurium, and epineurium, which form the framework that organizes and protects the nerve fibers (2). Nerve fibers, containing myelinated and unmyelinated axon bundles, carry action potential impulses, whereas ganglion tissue, containing the cell bodies and dendrites, assists in propagation of nerve impulses. Myelin is a lipid structure which is produced by Schwann cells (1,2). Regular intermittent gaps in the myelin sheath are called nodes of Ranvier. Local supporting connective tissue consisting of collagen known as endoneurium supports each myelinated nerve fiber or group of unmyelinated nerve fibers (2). Axons are grouped together in bundles called fascicles. Each fascicle is enveloped by perineurium. The grouped bundles of fascicles are embedded in the epineurium, which forms the outer layer, the nerve sheath (3). A schematic overview of peripheral nerve anatomy is shown in **Figure 1**.

Neurological disorders in peripheral nerves

In the nerves, sensory neurons transmit the signal from the sensory receptors in the peripheral nervous system back to the central nervous system. Motor neurons transmit signal from the central nervous system back to the effectors. Damage to (part of) the nerves may cause distortion in transmission of the signal from the central nervous system to the innervated area and vice versa which may lead to for example muscle weakness or muscle wasting. Pathological changes to the nerve include axonal loss and demyelination. However, most neurological pathologies are mixed, as demyelinating neuropathy can also have a substantial axonal loss, and axonal neuropathy can also show changes in the myelin (4). Neurological disorders can affect the motor neurons and/or the sensory neurons. An example of a purely motor neuropathy is multifocal motor neuropathy (MMN). MMN is a slowly progressive disease which predominantly affects the upper limbs. Patients often present themselves with difficulties in wrist and finger extension or reduced hand grip (5). MMN can mimic the early symptoms of amyotrophic lateral sclerosis (ALS),

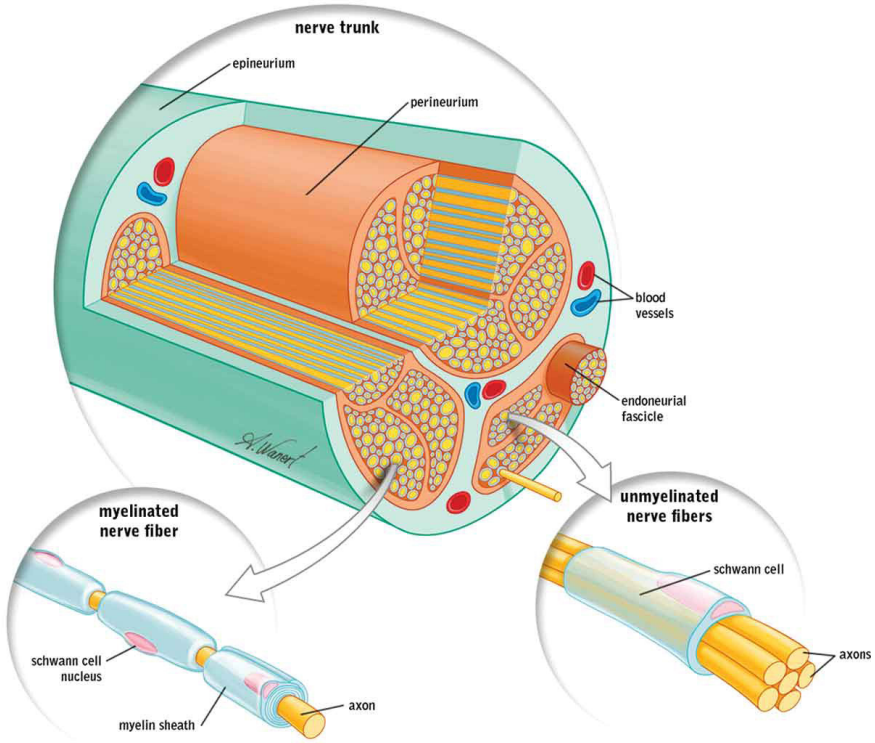

Figure 1: Peripheral nerve anatomy (47)

by which many patients are initially diagnosed with ALS (6). The detection of the characteristic conduction block should distinguish MMN from other pathologies such as ALS, however, these conduction blocks are not always determined (6). High signal intensity on T2-weighted MR images of the brachial plexus and the presence of high CM1-specific IgM antibody titers are also an indication for the diagnosis of MMN (6).

Spinal muscular atrophy (SMA) is another lower motor neuron disease which is characterized by degeneration of spinal cord motor neurons, atrophy of skeletal muscles, and generalized weakness (7). It is caused by homozygous deletion of the survival motor neuron (SMN) 1 gene (8). The SMN protein is involved in the axonal transport in neurons. SMA is classified into four different types, which are characterized by age of symptom onset, and highest motor function achieved (7). SMA type 1 is the most severe and common form and is diagnosed before 6

months of age. These patients usually die within the first 2 years of life. They never acquire the ability to sit unsupported and have severe hypotonia and symmetrical paralysis. SMA type 2 is intermediate severe and starts between 7 and 18 months of age. These children can sit unsupported but are unable to walk independently. Type 3 patients show profound symptom heterogeneity. They usually achieve all major motor milestones, although many need wheelchair support. SMA type 4 typically starts in the second or third decade of life, with mild to moderate muscle weakness symptoms (7,9). SMA is diagnosed using physical examination tests followed by genetic tests (10). The recently approved therapy, i.e. Nusinersen, which was tested in SMA type 1, 2, and 3, showed significant improvement of motor function and a reduction in mortality (11,12). However, the evaluation of this new therapy requires sensitive quantitative outcome measure to determine disease progression and potential treatment effects over time.

Diagnosing neurological disorders in peripheral nerves

There are different methods to detect nerve pathologies. Clinical tests are often used to test reflexes and muscle strength, but those can be quite observer dependent (13). Nerve conduction studies are used to detect the conduction properties of peripheral nerves such as velocity and amplitude. To acquire reliable outcome measures, careful control of body temperature is required and can be hindered by edema, fat or patient intolerance (14,15). Ultrasound can also be used to detect peripheral nerves in neurological disorders non-invasively. However, it can only provide morphological information (14). Furthermore, it is difficult to visualize the more deeply situated nerves such as the lumbosacral nerves, or nerves surrounded by fat or located beneath bones (16,17).

Magnetic resonance imaging and diffusion tensor imaging

A unique in vivo technique to visualize peripheral nerve tissue is magnetic resonance imaging (MRI) (18–20). MRI has proven valuable in the diagnosis and therapeutic workup of peripheral nerve tissue affected by neurological disorders (21,22). Axial T1-weighted images and fat-suppressed T2-weighted images are used to provide insight into the peripheral nerve characteristics, such as signal intensity, course, caliber, fascicular pattern, and size of the nerve. Normal nerves show intermediate signal intensity on T1-weighted images and intermediate to minimally increased signal intensity on T2-weighted images. When nerves are affected, such as in neuropathies the signal intensity increases on T2-weighted images (23). However,

early detection of changes in nerve tissue due to neuropathies are not evident and visible on regular T1 and T2-weighted images. Furthermore, anatomical MRI sequences cannot distinguish between demyelination and axonal injury (24).

Diffusion MRI is an MRI technique which has gained much interest as a diagnostic tool to identify and distinguish between neurological disorders in peripheral nerve tissue and to differentiate between demyelination and axonal injury (24). It is sensitive to the random motion of water molecules (so-called Brownian motion) (25,26). When this movement is unhindered (for example in a glass of water), the water molecules can move freely in each direction, which is called isotropic diffusion. In the human body, the presence of cell membranes can hinder or restrict this diffusion, through which diffusion is predominantly oriented in one direction, also known as anisotropic diffusion (27). By applying multiple diffusion-weighted gradients with different orientations the diffusion tensor can be estimated (25). Diffusion tensor imaging (DTI) provides a way to describe and quantify the magnitude and orientation of the estimated diffusion (25). This allows to determine the microstructural properties of the tissue. Nerves have a strong anisotropy, as diffusion in healthy nerve tissue, is more pronounced along the nerve than perpendicular to its main orientation. The technique to reconstruct the nerves from diffusion data is known as fiber tractography (28).

Diffusion can be described with three so-called eigenvalues; λ_1, λ_2 and λ_3 (i.e. the length of the diffusion in a specific orientation) (27). The diffusion parameters which are typically calculated are: the fractional anisotropy (FA), which approaches 1 when diffusion is predominantly oriented in one direction, the mean diffusion (MD), which is the average of the three eigenvalues ($MD = \frac{\lambda_1+\lambda_2+\lambda_3}{3}$), the axial diffusion (AD), which is defined as the largest eigenvalue, λ_1, and the radial diffusion (RD), which is the average of the second and third eigenvalue ($RD = \frac{\lambda_2+\lambda_3}{2}$).

DTI has been predominantly used in the brain to detect for example ischemia (29). It is now increasingly employed in regions outside the brain such as the lumbosacral nerves (30–32), the brachial plexus (33,34), nerves in the wrist and forearm (35,36), and in the legs (37,38). When the nerve is damaged or affected by pathologies, diffusion characteristics may change. The FA can be associated with a lower AD, a higher RD or a combination of those two parameters (39,40). Changes in MD, for example an increase, may be associated with inflammatory-demyelination processes in the nerve (41). The AD could be associated with axonal density and diameter and may be broadly considered as an axonal marker, whereas RD could be associated with myelin density and thickness, and may therefore be considered

as a myelin marker (42,43). DTI and nerve specific sequences could be beneficial to study physiology and pathology in the nerves. However, these techniques are susceptible to artifacts and misinterpretation (44,45). The application of DTI in various regions outside the brain requires specific design of the protocols. The transition of air to tissue, but also movement of the heart, respiration, or bowel can have negative effects on the image quality of the scans which may influence diffusion estimates (46).

In this thesis the application of MRI and DTI in different parts of the peripheral nervous system in different neurological disorders is investigated. The focus is on the application and validation of DTI in clinical practice to determine the added value of DTI as a clinical tool in the diagnosis, prognosis and potential follow up of different patient groups. Furthermore, pathological mechanisms are explored using this technique.

Outline of this thesis

The studies described in this thesis show the application of DTI to visualize and quantify peripheral nerves and neurological disorders. The main goal was to assess the actual value of DTI in the quantification and visualization of these nerve diseases.

In **chapter 2** the reproducibility of DTI conducted in multiple centers of the lumbar and sacral nerves is investigated. In this study the value of DTI in cross-sectional and longitudinal study design is discussed.

In **chapter 3** the application of DTI in spina bifida patients is shown. This study highlights the potential benefit of DTI to detect and quantify the lumbar and sacral nerves in these patients and shows the differences in diffusion properties and fiber tractography results between patients and healthy controls.

Whereas in chapter 3 a relatively heterogeneous group of patients was included, in **chapter 4,** a more homogeneous group of patients was included, namely patients with an herniated disc at the level of L5 or S1. This study was conducted to determine the added value of DTI to understand the interpretation of diffusion metrics in compressed nerves.

Chapter 5 investigates the use of diffusion MRI in the assessment of the nerves in the forearm in patients with multifocal motor neuropathy, amyotrophic lateral sclerosis, and in healthy controls. In this research an MRI protocol was developed to determine the diffusion parameters and cross-sectional areas of the forearm nerves.

Chapter 6 focusses on spinal muscular atrophy patients, where the spinal cord and nerve roots in the cervical region were analyzed. Diffusion properties and cross-sectional areas of patients were compared to those of healthy controls.

In **chapter 7** the acoustic nerve was investigated with DTI. In this study, single-sided deaf patients were compared to healthy controls.

References

1. Forehand CJ. The action potential, synaptic tranmission, and maintenance of nerve function. Cell Physiol. 2011. 37–61.
2. Flores AJ, Lavernia CJ, Owens PW. Anatomy and physiology of peripheral nerve injury and repair. Vol. 29, American journal of orthopedics. 2000. 167–173.
3. Stewart JD. Peripheral nerve fascicles: anatomy and clinical relevance. Muscle Nerve. 2003;28(5):525–541.
4. Crone C, Krarup C. Neurophysiological approach to disorders of peripheral nerve. 1st ed. Vol. 115, Handbook of Clinical Neurology. Elsevier B.V.; 2013. 81-114.
5. Lawson VH, Arnold WD. Multifocal motor neuropathy: A review of pathogenesis, diagnosis, and treatment. Vol. 10, Neuropsychiatric Disease and Treatment. 2014. 567–576.
6. Vlam L, van der Pol W-L, Cats E a, Straver DC, Piepers S, Franssen H, et al. Multifocal motor neuropathy: diagnosis, pathogenesis and treatment strategies. Nat Rev Neurol. 2012;8:48–58.
7. Lunn MR, Wang CH. Spinal muscular atrophy. Lancet. 2008;371(9630):2120–2133.
8. Wirth B, Herz M, Wetter A, Moskau S, Hahnen E, Rudnik-Schöneborn S, et al. Quantitative analysis of survival motor neuron copies: identification of subtle SMN1 mutations in patients with spinal muscular atrophy, genotype-phenotype correlation, and implications for genetic counseling. Am J Hum Genet. 1999;64(5):1340–1356.
9. d'Ydewalle C, Sumner CJ. Spinal Muscular Atrophy Therapeutics: Where do we Stand? Vol. 12, Neurotherapeutics. 2015. 303–316.
10. Bertini E, Burghes A, Bushby K, Estournet-Mathiaud B, Finkel RS, Hughes RAC, et al. 134th ENMC international workshop: Outcome measures and treatment of spinal muscular atrophy 11-13 February 2005 Naarden, the Netherlands. Neuromuscul Disord. 2005;15(11):802–816.
11. Chiriboga CA. Nusinersen for the treatment of spinal muscular atrophy. Expert Rev Neurother. 2017;17(10):955–962.
12. Finkel RS, Mercuri E, Darras BT, Connolly AM, Kuntz NL, Kirschner J, et al. Nusinersen versus Sham Control in Infantile-Onset Spinal Muscular Atrophy. N Engl J Med. 2017;377(18):1723–1732.
13. MRC. Medical Research Council. Aids to the examination of the peripheral nervous system: Memorandum No 45 (suspending War Memorandum No. 7). The white Rose Press for Her Majesty's Stationery Office. London; 1976.
14. Goedee HS, Brekelmans GJ, van Asseldonk JT, Beekman R, Mess WH, Visser LH. High resolution sonography in the evaluation of the peripheral nervous system in polyneuropathy--a review of the literature. Eur J Neurol. 2013;20(10):1342–1351.
15. Gooch CL, Weimer LH. The Electrodiagnosis of Neuropathy: Basic Principles and Common Pitfalls. Vol. 25, Neurologic Clinics. 2007. 1–28.
16. Beekman R, Visser LH. High-resolution sonography of the peripheral nervous system - A review of the literature. Vol. 11, European Journal of Neurology. 2004. 305–314.
17. Simon NG, Talbott J, Chin CT, Kliot M. Peripheral nerve imaging. 1st ed. Vol. 136, Handbook of Clinical Neurology. Elsevier B.V.; 2016. 811-826.

18. Van Es HW, Van den Berg LH, Franssen H, Witkamp TD, Ramos LM, Notermans NC, et al. Magnetic resonance imaging of the brachial plexus in patients with multifocal motor neuropathy. Neurology. 1997;48:1218–2412.

19. Chhabra A, Belzberg AJ, Rosson GD, Thawait GK, Chalian M, Farahani SJ, et al. Impact of high resolution 3 tesla MR neurography (MRN) on diagnostic thinking and therapeutic patient management. Eur Radiol. 2016;26(5):1235–1244.

20. Kwee RM, Chhabra A, Wang KC, Marker DR, Carrino JA. Accuracy of MRI in diagnosing peripheral nerve disease: a systematic review of the literature. Vol. 203, American Journal of Roentgenology. 2014. 1303–1309.

21. Andreisek G, Burg D, Studer A, Weishaupt D. Upper extremity peripheral neuropathies: Role and impact of MR imaging on patient management. Eur Radiol. 2008;18(9):1953–1961.

22. Kuntz C, Blake L, Britz G, Filler A, Hayes CE, Goodkin R, et al. Magnetic resonance neurography of peripheral nerve lesions in the lower extremity. Neurosurgery. 1996;39(4):750-757.

23. Chhabra A, Andreisek G, Soldatos T, Wang KC, Flammang AJ, Belzberg AJ, et al. MR neurography: Past, present, and future. Vol. 197, American Journal of Roentgenology. 2011. 583–591.

24. Aung W, Mar S, Benzinger T. Diffusion tensor MRI as a biomarker in axonal and myelin damage. Imaging Med. 2013;5(5):427–440.

25. Basser PJ, Mattiello J, LeBihan D. MR diffusion tensor spectroscopy and imaging. Biophys J. 1994;66(1):259–267.

26. Tournier J-D, Mori S, Leemans A. Diffusion tensor imaging and beyond. Magn Reson Med. 2011;65(6):1532–1556.

27. Beaulieu C. The basis of anisotropic water diffusion in the nervous system - a technical review. NMR Biomed. 2002;15(7–8):435–455.

28. Mori S, van Zijl PCM. Fiber tracking: principles and strategies - a technical review. NMR Biomed. 2002;15(7–8):468–480.

29. Sorensen a G, Wu O, Copen W a, Davis TL, Gonzalez RG, Koroshetz WJ, et al. Human acute cerebral ischemia: detection of changes in water diffusion anisotropy by using MR imaging. Radiology. 1999;212(27):785–792.

30. van der Jagt PKN, Dik P, Froeling M, Kwee TC, Nievelstein R a J, ten Haken B, et al. Architectural configuration and microstructural properties of the sacral plexus: a diffusion tensor MRI and fiber tractography study. Neuroimage. 2012;62(3):1792–1799.

31. Haakma W, Dik P, Ten Haken B, Froeling M, Nievelstein R a J, Cuppen I, et al. Diffusion tensor MRI and fiber tractography of the sacral plexus in children with spina bifida. J Urol. 2014;192(3):927–933.

32. Karampinos DC, Melkus G, Shepherd TM, Banerjee S, Saritas EU, Shankaranarayanan A, et al. Diffusion tensor imaging and T2 relaxometry of bilateral lumbar nerve roots: feasibility of in-plane imaging. NMR Biomed. 2013;26(6):630–637.

33. Tagliafico A, Calabrese M, Puntoni M, Pace D, Baio G, Neumaier CE, et al. Brachial plexus MR imaging: accuracy and reproducibility of DTI-derived measurements and fibre tractography at 3.0-T. Eur Radiol. 2011;21(8):1764–1771.

34. Vargas MI, Viallon M, Nguyen D, Delavelle J, Becker M. Diffusion tensor imaging (DTI) and tractography of the brachial plexus: feasibility and initial experience in neoplastic conditions. Neuroradiology. 2010;52(3):237–245.

35. Zhou Y, Narayana P a, Kumaravel M, Athar P, Patel VS, Sheikh K a. High resolution diffusion tensor imaging of human nerves in forearm. J Magn Reson Imaging. 2014;39:1374–1383.

36. Hiltunen J, Kirveskari E, Numminen J, Lindfors N, Goransson H, Hari R. Pre- and post-operative diffusion tensor imaging of the median nerve in carpal tunnel syndrome. Eur Radiol. 2012;22(6):1310–1319.

37. Vaeggemose M, Pham M, Ringgaard S, Tankisi H, Ejskjaer N, Heiland S, et al. Diffusion tensor imaging MR neurography for the detection of polyneuropathy in type 1 diabetes. J Magn Reson Imaging. 2017;45(4):1125–1134.

38. Simon NG, Lagopoulos J, Gallagher T, Kliot M, Kiernan MC. Peripheral nerve diffusion tensor imaging is reliable and reproducible. J Magn Reson Imaging. 2015;43(4):962–969.

39. Takagi T, Nakamura M, Yamada M, Hikishima K, Momoshima S, Fujiyoshi K, et al. Visualization of peripheral nerve degeneration and regeneration: monitoring with diffusion tensor tractography. Neuroimage. 2009;44(3):884–892.

40. Heckel a., Weiler M, Xia A, Ruetters M, Pham M, Bendszus M, et al. Peripheral Nerve Diffusion Tensor Imaging: Assessment of Axon and Myelin Sheath Integrity. PLoS One. 2015;10(6):1–13.

41. Filippi M, Inglese M, Rovaris M, Rocca MA. Diffusion and perfusion MRI in inflammation and demyelination. In: Clinical MR Neuroimaging: Physiological and Functional Techniques, Second Edition. Cambridge University Press; 2011. 488–497.

42. DeBoy CA, Zhang J, Dike S, Shats I, Jones M, Reich DS, et al. High resolution diffusion tensor imaging of axonal damage in focal inflammatory and demyelinating lesions in rat spinal cord. Brain. 2007;130(8):2199–2210.

43. Song S-K, Sun S-W, Ramsbottom MJ, Chang C, Russell J, Cross AH. Dysmyelination Revealed through MRI as Increased Radial (but Unchanged Axial) Diffusion of Water. Neuroimage. 2002;17(3):1429–1436.

44. Jones DK, Cercignani M. Twenty-five pitfalls in the analysis of diffusion MRI data. NMR Biomed. 2010;23(7):803–820.

45. Wheeler-Kingshott CAM, Cercignani M. About "axial" and "radial" diffusivities. Magn Reson Med. 2009;61(5):1255–1260.

46. Irfanoglu MO, Walker L, Sarlls J, Marenco S, Pierpaoli C. Effects of image distortions originating from susceptibility variations and concomitant fields on diffusion MRI tractography results. Neuroimage. 2012;61(1):275–288.

47. Ilfeld BM, Preciado J, Trescot AM. Novel cryoneurolysis device for the treatment of sensory and motor peripheral nerves. Expert Rev Med Devices. 2016;13(8):713–725.

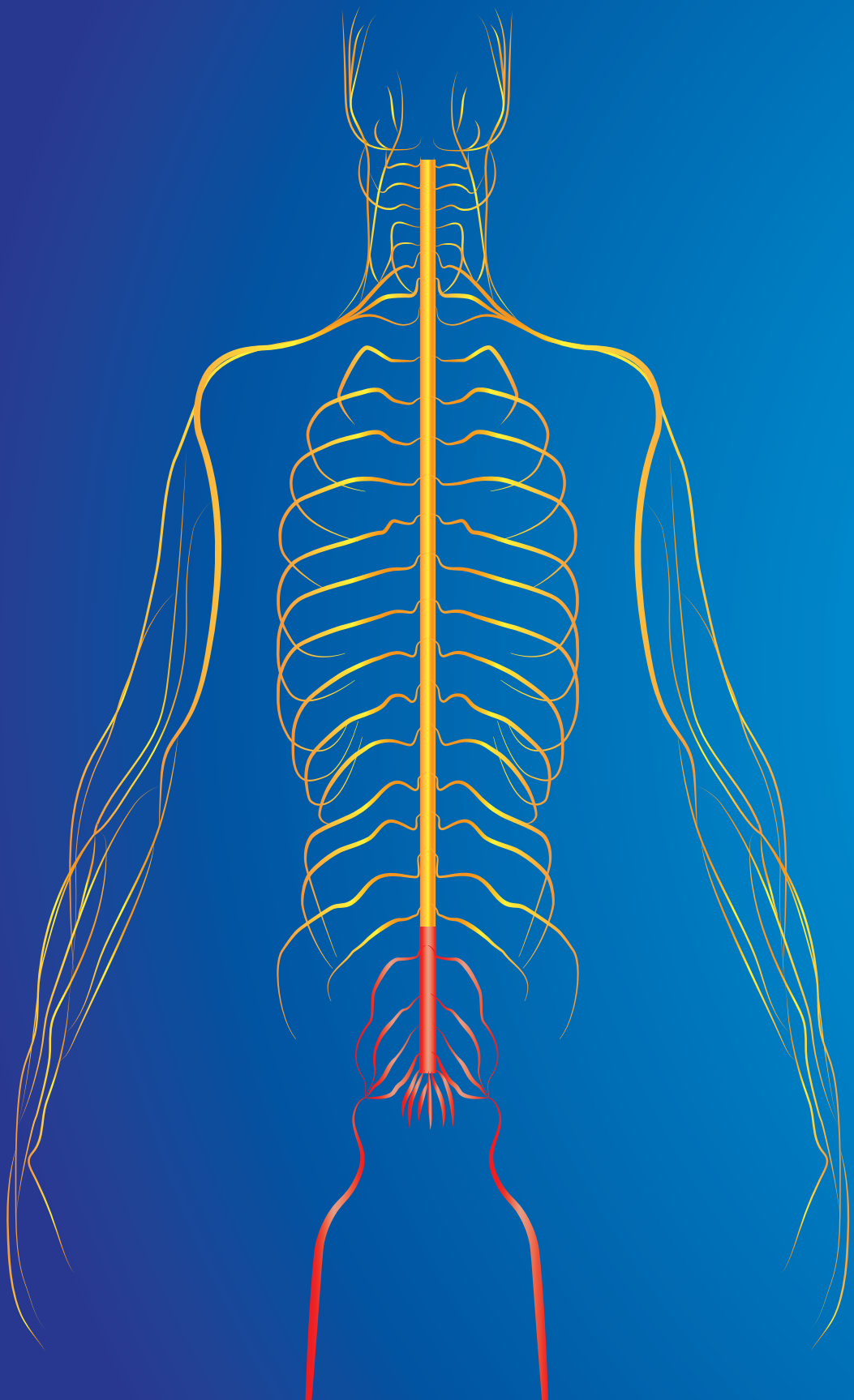

Chapter 2

Multicenter reproducibility study of diffusion MRI and fiber tractography of the lumbosacral nerves

Wieke Haakma
Jeroen Hendrikse
Lars Uhrenholt
Alexander Leemans
Lene Warner Thorup Boel
Michael Pedersen
Martijn Froeling

Journal of Magnetic Resonance and Imaging 2018, DOI: 10.1002/jmri.25964

Abstract

Background

Diffusion tensor imaging (DTI) has been applied in the lumbar and sacral nerves in vivo, but information about the reproducibility of this method is needed before DTI can be used reliably in clinical practice across centers.

Purpose

In this multicenter study the reproducibility of DTI of the lumbosacral nerves in healthy volunteers was investigated.

Study type

Prospective control series

Subjects

Twenty healthy subjects

Field strength/sequence

3T MRI. 3D Turbo Spin Echo, and 3.0 mm isotropic DTI scan.

Assessment

The DTI scan was performed three times (twice in the same session, intra-scan reproducibility, and once after an hour, inter-scan reproducibility). At site 2, one week later, the protocol was repeated (inter-week reproducibility). Fiber tractography (FT) of the lumbar and sacral nerves (L3-S2) was performed to obtain values for fractional anisotropy, mean, axial, and radial diffusivity.

Statistical tests

Reproducibility was determined using intra-class correlation coefficient (ICC), and power calculations were performed.

Results

FT was successful and reproducible in all datasets. ICC's for all diffusion parameters were high for intra-scan (ranging from 0.70-0.85), intermediate for inter-scan (ranging from 0.61-0.73), and inter-week reliability (ranging from 0.58-0.62). There were small but significant differences between the inter-week diffusivity values ($p<0.0005$). Depending on the effect size, nerve location and parameter of interest, power calculations showed that sample sizes between 10 and 232 subjects are needed for cross-sectional studies.

Data conclusion

We found that DTI and FT of the lumbosacral nerves have intermediate to high reproducibility within and between scans. Based on these results, 10-58 subjects are needed to find 10% change in parameters in cross-sectional studies of the lumbar and sacral nerves. The small significant differences of the inter-week comparison suggest that results from longitudinal studies need to be interpreted carefully, since small differences may also be caused by factors other than disease progression or therapeutic effects.

Introduction

Three dimensional magnetic resonance imaging (MRI) and diffusion tensor imaging (DTI) are important imaging modalities to visualize nerve tissue (1,2) and potential nerve damage (3,4). In nervous tissue, diffusion of water molecules is greater along the nerve than perpendicular to it. With DTI, this diffusion profile can be quantified by measuring the diffusion signal along multiple diffusion gradient orientations and estimating a diffusion tensor (5). From the diffusion tensor a 3D reconstruction of nervous tissue architecture can be obtained with fiber tractography (FT). DTI has been used in various peripheral nerve studies (6,7) including the lumbar and sacral nerves (8–10).

MRI and DTI data of the spine is relevant to investigate potential damage due to, for example, disc herniation (11–14) or other degenerative lumbar and sacral disorders (9,15). These studies have shown that diffusion parameters can provide additional information regarding abnormalities in nervous tissue compared to traditional anatomical scans. However, the use of DTI to investigate peripheral nervous tissue, such as the lumbar and sacral nerves, has not been widely adopted and there are no existing standards of how such data should be analyzed. Furthermore, there are different factors which can affect the diffusion measures, such as the moment of performing the scan, the MR scanner, the scanning resolution, and the manual FT segmentation (16–18). Although several studies have demonstrated high scan-rescan reproducibility of manual FT segmentation in the brain (19–21) and in peripheral nerve tissue (22–25), essential information regarding the reproducibility of peripheral nerve DTI measurements is still missing. Such information is needed before DTI can be implemented and used reliably in clinical practice across centers.

The aim of this multicenter study was to investigate and describe different aspects of reproducibility of DTI measurements of the lumbar and sacral nerves using DTI and FT in healthy volunteers.

Materials and methods

The local institutional review boards approved this study and written informed consent was obtained prior to inclusion. The scans were acquired with two 3T Philips Achieva MRI systems (Philips Healthcare, Best, the Netherlands) in two centers; site 1 and site 2. At each site 10 healthy volunteers were included (in total 20 healthy volunteers, six females; mean age of 36 years, range 25-60 years). Healthy volunteers were asymptomatic and did not have any previous history related to spinal diseases.

Scan parameters

At the start of each scan session an anatomical 3D Turbo Spin Echo (3D-TSE) scan was obtained. The scan parameters were: TR=3000 ms, TE=272 ms, TSE factor 180, startup echoes 4, field of view (FOV) 250×250×100 mm^3 selected at the level of L3-S2, slice orientation is coronal, matrix size 250×250×100, reconstruction matrix 512×512×200, resulting in a voxel size of 0.49×0.49×1 mm^3, number of excitations 2, SENSE factor 2, SPAIR fat suppression with inversion delay=240 ms and TR=3000 ms, total acquisition time 5:03 min. Next, at both sites, a series of DTI acquisitions were performed. Due to differences in hardware specifications of the MRI scanners between both sites, the acquisition parameters were also slightly different as is shown in **Table 1**. First, a 3.0 mm isotropic DTI scan was performed (scan 1) which was repeated once in the same session (scan 2) and once after 1 hour (scan 3).

Table 1: DTI sequences at site 1 and site 2 used to visualize the lower lumbar and sacral nerve roots

Sequence parameters	DTI 3.0 mm Site 1	DTI 3.0 mm Site 2	DTI 2.5 mm Site 1	DTI 2.5 mm Site 2
Sequence	SS-EPI	SS-EPI	SS-EPI	SS-EPI
Acquisition plane	Coronal	Coronal	Coronal	Coronal
FOV (mm^2)	336 x 216	336 x 336	320 x 200	320 x 320
TR/TE (ms)	3573 / 45	3451/47	4537 / 45	4400/47
b-value (s/mm^2)	800	800	800	800
Gradient direction	15	15	15	15
EPI factor (ETL)	43	35	47	39
Acquisition matrix	112 x 71	112 x 112	128 x 78	128 x 128
Acquisition voxel size (mm^3)	3.0 x 3.0 x 3.0	3.0 x 3.0 x 3.0	2.5 x 2.56 x 2.5	2.5 x 2.5 x 2.5
Half Fourier scan factor	0.62	0.62	0.62	0.62
Slice thickness/gap (mm)	3.0 / 0	3.0 / 0	2.5 / 0	2.5 / 0
Number of slices	25	25	30	30
Number of excitations	2	2	2	2
Type of fat suppression	SPIR	SPIR	SPIR	SPIR
Total acquisition time (min)	4:20	4:11	5:31	5:21

Additionally, and directly after scan 2, a 2.5 mm isotropic DTI scan was performed (scan 4). At site 2, scan 1, scan 2, and scan 3 were repeated after 1 week (week 2) in the same volunteers.

Data processing and analysis

First, all data were inspected visually to identify artifacts and evaluate the data quality by 2 researchers with 4 years of experience (W.H.), and 10 years of experience (M.F.). The DTI datasets were processed using the *ExploreDTI* diffusion MRI toolbox (www.ExploreDTI.com) (26). Data processing comprised the following steps: 1) A reduced FOV was obtained by selecting a fixed (25) number of slices on both sides of the spine in the coronal plane, which included the spine and its nerve roots from the level of L3 to the sacral nerves, 2) motion and eddy current induced geometrical distortions were corrected, where the diffusion gradients were adjusted using the b-matrix rotation (27), 3) diffusion tensors and subsequently diffusion parameters (fractional anisotropy (FA), mean diffusivity (MD), axial diffusivity (AD), and radial diffusivity (RD)) were calculated with the REKINDLE approach (28), and 4) a standardized fiber tractography approach was used (1) to reconstruct the 3D nerve architecture. Fiber tract pathways were generated by whole volume seeding (seed distance 2.0×2.0×2.0 mm^3). Stopping criteria of the tractography were FA > 0.05, maximum fiber angle change per 1 mm step of 30 degrees, with a minimum fiber length of 10 mm. Two 'AND' ROIs were used to select a segment of 3 cm at each level at each side (L3-S2) starting at the level where the nerves were branching from the spine (**Figure 1** 'segments with ROIs'). The first ROI was placed at the position where the nerve branched from the spine and the second 10 slices lower. The specified FA range together with two 'AND' ROIs allowed to track the nerve roots in a reproducible and reliable manner (8). For each of the 3 cm segments (10 nerves per scan) average values of the diffusion parameters (FA, MD, AD, and RD) were calculated.

Experimental procedures

FT results of the scans were visually compared with the maximal intensity projection (MIP) of the 3D TSE to evaluate their description of the 3D lumbar and sacral nerve anatomy (see **Figure 1**) by two researchers with 4 years of experience (W.H.), and 10 years of experience (M.F.). In total four different experiments were conducted to test for 1) inter-resolution (scan 2 versus scan 4), 2) intra-scan (scan 1 versus scan 2), 3) inter-scan (scan 2 versus scan 3), and 4) inter-week (scans of week 1 versus scans of week 2) reproducibility. As mentioned before, only at site 2 data for experiment 4 was acquired, whereas for the other experiments data from both sites were available and used for analysis. For experiment 1, 2 and 3, where data from

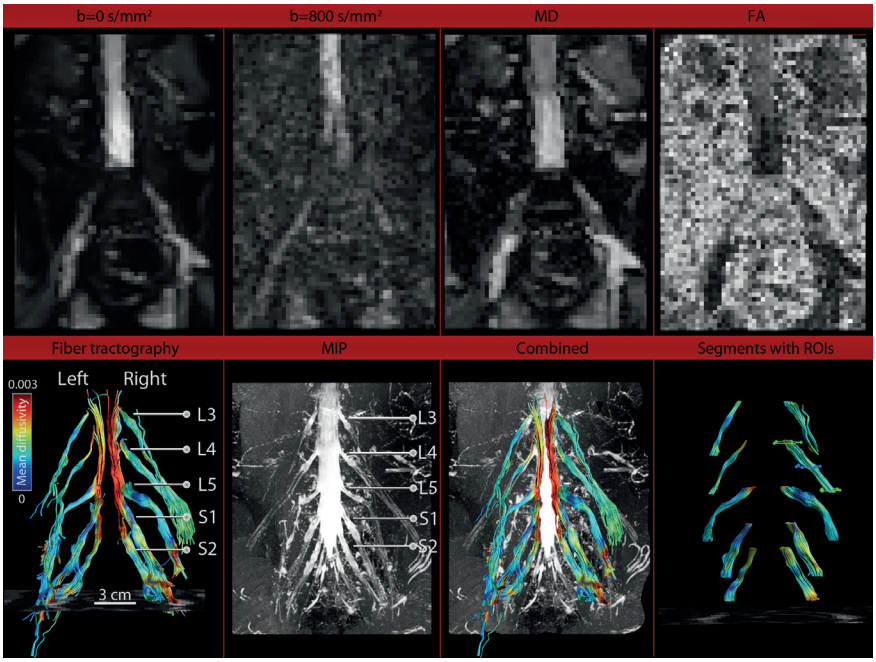

Figure 1: Upper row: b=0 s/mm^2, b=800 s/mm^2, mean diffusivity (MD), and fractional anisotropy (FA) map. Bottom row: Fiber tractography (FT) results of the lumbosacral nerves, a maximal intensity projection (MIP), FT and MIP combined, and display of the segments at each level and 'SEED' (blue) and 'AND' (green) region of interest (ROI) placement.

two sites were available, we present the results for both sites separately and both sites combined. To emphasize, all experiments in this study concern longitudinal assessment and no inter-system comparisons were made.

Statistical analysis

Statistical analyses were performed using the SPSS Statistics version 21.0 (SPSS Inc. Chicago, IL, USA) and comprised of two steps.

First any variation in diffusion parameters were investigated using one-way repeated measures analysis of covariance (ANCOVA) with site and subject ID as co-variates. Three different repeated measures ANCOVA's were performed i.e. 1) inter-resolution analysis, 2) combined intra- and inter-scan analysis, and 3) inter-week analysis, where $p<0.05$ was considered to be significant. Second, the reproducibility of the four different experiments was tested. This was done by means of the inter-class correlation coefficient (ICC) together with the 95% confidence interval (CI),

to check for reliability, and by means of the Bland-Altman analysis, to check for agreement. ICCs were defined as the single measures two-way random model to test for reliability between DTI scans, i.e. how well the measures resemble each other, despite measurement errors. An ICC of < 0.40 was considered a low reproducibility, 0.40 – 0.75 an intermediate to good reproducibility, and > 0.75 a high reproducibility. Bland-Altman analysis was used to test for agreement between DTI measures, i.e. assesses how similar the parameters of repeated measures were. The application conditions of Bland Altman were verified by a visual check for the absence of correlation between the absolute differences and the mean, and whether the differences were normally distributed for which histogram plots were used (29). The 95% limits of agreement (LoA) per diffusion parameter were defined as the mean of paired differences ± 1.96 x its standard deviation (SD). Coefficient of variation (CoV) was calculated ($CoV = 100\% \frac{SD}{Mean}$) to determine both inter-subject and inter-scan variability.

Experiment 1: inter-resolution analysis

In this experiment FT results obtained from the 2.5 mm and the 3.0 mm isotropic scan were compared to each other (scan 2 vs scan 4). Next, diffusion parameters (i.e. FA, MD, AD, and RD) of the scans with different resolution of both sites were compared to each other (*inter-resolution*). For all of the diffusion parameters ICC's were calculated for each site separately and for both sites combined. Finally, Bland-Altman plots were obtained displaying the results of both sites in one graph per diffusion parameter.

Experiment 2: intra-scan analysis

In this experiment, FT results of scan 1 were compared with scan 2. Diffusion parameters (i.e. FA, MD, AD, and RD) of scan 1 and scan 2 with 3 mm isotropic resolution were compared with each other to investigate the *intra-scan* reproducibility, i.e. to what extent scans within the same session vary. Then ICC's were calculated for each site and for both sites combined for all of the diffusion parameters. Finally, Bland-Altman plots were obtained displaying the results of both sites in one graph per diffusion parameter.

Experiment 3: inter-scan analysis

In this experiment FT results of scan 2 were compared with scan 3. Diffusion parameters (i.e. FA, MD, AD, and RD) of scan 2 and scan 3 were compared to each other which were made with a time frame of 1 hour between each other to check

the *inter-scan* reproducibility, i.e. to wat extent scans on two time points vary. ICC's were calculated for each site and for both sites combined for all of the diffusion parameters. Finally, Bland-Altman plots were obtained displaying the results of both sites in one graph per diffusion parameter.

Experiment 4: inter-week analysis

FT results were compared between scans of week 1 and scans of week 2. Diffusion parameters (i.e. FA, MD, AD, and RD) of the scans obtained in week 1 and week 2 (obtained one week later) were compared at site 2. Scan 1 of week 1 was compared with scan 1 of week 2, scan 2 of week 1 with scan 2 of week 2, and scan 3 of week 1 with scan 3 of week 2 to investigate the *inter-week* reproducibility. ICC's were calculated for each site and for both sites combined for all of the diffusion parameters. Finally, Bland-Altman plots were obtained displaying the results of both sites in one graph per diffusion parameter.

Inter-subject versus inter-scan variability and sample size calculation

Box and whisker plots were made to determine the variability between subjects and between scans for each diffusion parameters (i.e. FA, MD, AD, and RD) and each level (L3-S2). Plots were obtained both for site 1 where scan 1, scan 2, and scan 3 were compared, and for site 2 where the results of the scans of week 1 and week 2 were compared. CoV was calculated for each level (i.e. L3-S2) for both subjects (inter-subject variability) and scans (i.e. scan 1, scan 2, and scan 3 for site 1, and the scans of week 1 and week 2 for site 2). These values were then compared. Finally, the sample size was calculated using $sample\ size = \frac{(r+1)}{r} \frac{CoV^2 (Z_{1-\beta} + Z_{\alpha/2})^2}{E^2}$, with a significance level of $\alpha = 0.05$ ($z_{\alpha/2} = 1.96$), a desired power of $\beta = 0.8$ ($z_{1-\beta} = 0.84$), the assumption of an equal number of cases and controls ($r = 1$), and an effect size E of 5% and 10% (30). The CoV used are the inter-subject CoV of site 1 reported in **Table 3**.

Results

Data processing and analyzing

All scans were completed successfully. Based on visual inspection all data had sufficient data quality and did not contain any artifacts that could interfere with the analysis. Raw data of the diffusion scans are shown in **Figure 1** upper row. Lumbar (L3-L5) and sacral nerves (S1-S2) were identified in each subject in the anatomical MIP scans and the locations of the nerves matched the locations of the nerves on the DTI scans. An example is shown in **Figure 1** lower row. In two subjects at

site 1, it was not possible to reconstruct S2, since it was not included in the FOV. Therefore, in total 96 nerve segments at site 1 and 100 nerve segments at site 2 were reconstructed for each of the four scans. The application conditions for Bland Altman were met, as there was no correlation between the mean and the differences, and histogram plots showed normal distributions. However, in eight cases the histogram plots showed long tails (i.e. present in inter-resolution, inter-scan, and inter-week).

Experiment 1: inter-resolution analysis

Figure 2 shows an example of FT of the 2.5 mm isotropic and the 3.0 mm isotropic DTI data. Overall, FT results of the 2.5 mm isotropic protocol were comparable to the 3.0 mm isotropic protocol (Supplemental Material 1 and 2). However, in some cases the nerves of scans obtained from the 2.5 mm isotropic protocol were more difficult to track compared to those from the 3.0 mm isotropic scan (site 1: P2, P9, and P10, site 2: P6, P7, and P10). Inter-resolution mean diffusion parameters and ICCs are displayed in **Table 2**. There were small differences in MD, AD and RD between the two resolutions ($p<0.0005$) with higher values (up to 0.10×10^{-3} mm^2/s) for the 3.0 mm isotropic scan. ICCs were intermediate to good and on average 0.61. The lowest ICC was for AD at site 1 (0.50, with a 95% CI of 0.34 – 0.64), and the highest

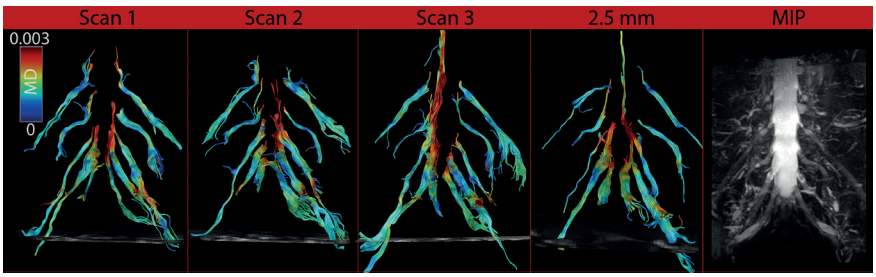

Figure 2: Fiber tractography results of DTI data of scan 1, scan 2, scan 3, scan of 2.5 mm isotropic protocol, and a corresponding intensity projection (MIP) of site 1 displayed as mean diffusivity (MD) color-encoded maps.

for RD at site 2 (0.75, with a 95% CI of 0.65 – 0.83). The top row of **Figure 3** shows the Bland-Altman plots displaying the inter-resolution agreement. LoA were -0.078 – 0.055, (-0.2245 – 0.308) $\times 10^{-3}$ mm^2/s, (-0.286 – 0.382) $\times 10^{-3}$ mm^2/s, and (-0.203 – 0.291) $\times 10^{-3}$ mm^2/s, for FA, MD, AD, and RD, respectively.

Experiment 2: intra-scan analysis

Figures 2 and 4 show similar FT results for DTI scan 1 and scan 2 of two subjects at site 1 (**Figure 2**) and site 2 (**Figure 4**, week 1: A, and B, week 2: E and F). The architectural

Table 2: *Experiment 1, 2, 3, and 4 – inter-resolution, intra-scan, inter-scan, and inter-week reproducibility*. Mean diffusion parameters (FA, MD, AD, and RD) of DTI scans (scan 1=2.5 mm isotropic and, scan 2, 3, and 4=3.0 mm isotropic scanned within the same scan session and after 1 hour) of two sites based on measurements obtained from the level of L3-S2 (per scan; n=96 at site 1 ('1'), n=100 at site 2 ('2'), and n=196 at site 1 and site 2 combined ('c')) and intra-class correlation coefficients (ICC) with 95% confidence interval

				Diffusivity ($\times 10^{-3}$ mm^2/s)		
		Site	FA (mean ± SD)	MD (mean ± SD)	AD (mean ± SD)	RD (mean ± SD)
Week 1						
Scan 1		1	0.30 ± 0.04	1.30 ± 0.14	1.72 ± 0.17	1.08 ± 0.13
		2	0.31 ± 0.04	1.31 ± 0.14	1.76 ± 0.16	1.09 ± 0.13
		c	0.30 ± 0.04	1.30 ± 0.14	1.74 ± 0.16	1.08 ± 0.13
Scan 2		1	0.30 ± 0.05	1.30 ± 0.14	1.73 ± 0.16	1.09 ± 0.13
		2	0.31 ± 0.04	1.31 ± 0.14	1.76 ± 0.16	1.08 ± 0.13
		c	0.31 ± 0.04	1.31 ± 0.14	1.75 ± 0.16	1.09 ± 0.13
Scan 3		1	0.30 ± 0.04	1.27 ± 0.14	1.70 ± 0.17	1.06 ± 0.14
		2	0.31 ± 0.05	1.28 ± 0.12	1.72 ± 0.15	1.06 ± 0.12
		c	0.31 ± 0.05	1.28 ± 0.13	1.71 ± 0.16	1.06 ± 0.13
Scan 4		1	0.31 ± 0.04	1.30 ± 0.19	1.74 ± 0.21	1.08 ± 0.18
		2	0.32 ± 0.04	1.23 ± 0.13	1.66 ± 0.15	1.01 ± 0.13
		c	0.32 ± 0.04	1.26 ± 0.17	1.70 ± 0.19	1.04 ± 0.16
Week 2						
Scan 1		2	0.32 ± 0.04	1.28 ± 0.15	1.72 ± 0.18	1.05 ± 0.14
Scan 2		2	0.32 ± 0.04	1.27 ± 0.15	1.71 ± 0.18	1.04 ± 0.15
Scan 3		2	0.32 ± 0.04	1.26 ± 0.14	1.71 ± 0.18	1.04 ± 0.14
Exp. 1	ICC	1	0.69 (0.56 – 0.78)	0.55 (0.39 – 0.67)	0.50 (0.34 – 0.64)	0.58 (0.43 – 0.70)
		2	0.69 (0.57 – 0.78)	0.74 (0.63 – 0.81)	0.67 (0.55 – 0.77)	0.75 (0.65 – 0.83)
		c	0.69 (0.61 – 0.76)	0.60 (0.50 – 0.68)	0.53 (0.42 – 0.62)	0.63 (0.54 – 0.71)
Exp. 2	ICC	1	0.79 (0.69 – 0.85)	0.81 (0.73 – 0.87)	0.82 (0.74 – 0.88)	0.80 (0.72 – 0.86)
		2	0.70 (0.58 – 0.78)	0.85 (0.78 – 0.90)	0.83 (0.75 – 0.88)	0.84 (0.77 – 0.89)
		c	0.75 (0.68 – 0.80)	0.83 (0.78 – 0.87)	0.82 (0.77 – 0.87)	0.82 (0.77 – 0.86)
Exp. 3	ICC	1	0.64 (0.51 – 0.74)	0.73 (0.61 – 0.81)	0.72 (0.61 – 0.81)	0.72 (0.61 – 0.80)
		2	0.61 (0.47 – 0.72)	0.69 (0.59 – 0.78)	0.62 (0.48 – 0.73)	0.70 (0.59 – 0.79)
		c	0.63 (0.53 – 0.70)	0.71 (0.63 – 0.77)	0.68 (0.59 – 0.75)	0.71 (0.63 – 0.77)
Exp. 4	ICC	2	0.58 (0.50 – 0.65)	0.60 (0.52 – 0.67)	0.57 (0.49-0.64)	0.62 (0.54 – 0.68)

configuration was similar to the MIP (**Figure 4D** and **4H)**. This was also confirmed in all the other subjects (Supplemental Materials 1 and 2). Intra-scan mean diffusion parameters and ICCs are displayed in **Table 2**. There were no significant differences in any of the diffusion values between scan 1 and scan 2. The ICCs for all diffusion parameters for both sites were high, on average 0.81. The lowest ICC was for FA at

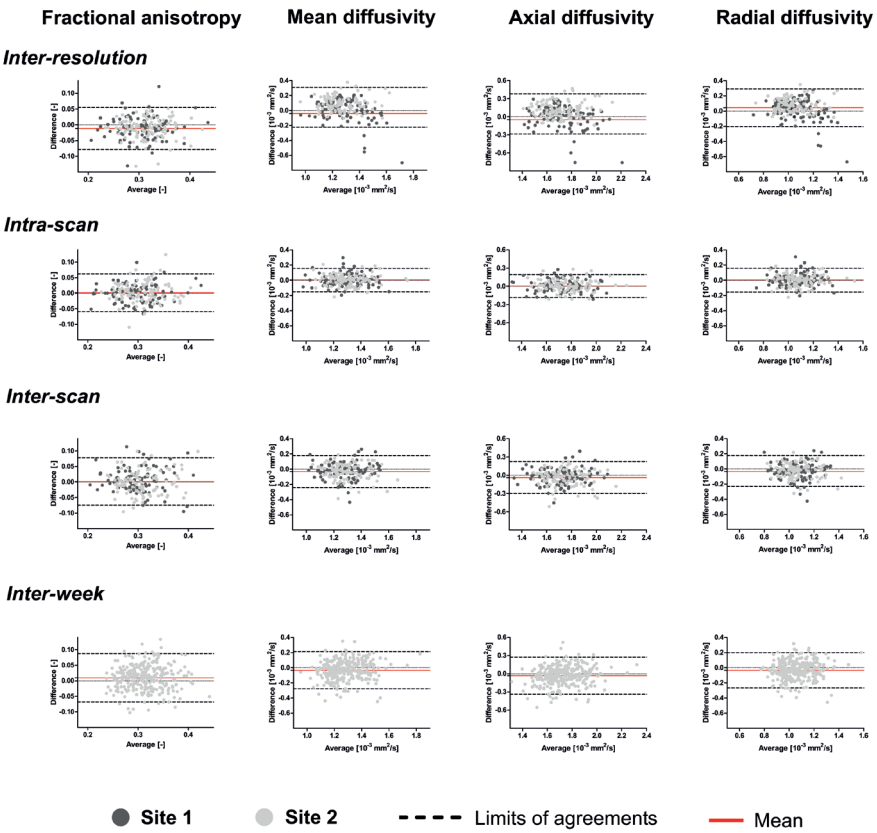

Figure 3: Bland-Altman plots of fiber tractography results of DTI data of the lumbosacral nerves of the inter-resolution, the intra-scan, the inter-scan, and the inter-week agreement of the fractional anisotropy (FA), the mean diffusivity (MD), the axial diffusivity (AD), and the radial diffusivity (RD).

site 2 (0.70, with a 95% CI of 0.58 – 0.78), and the highest was for MD at site 2 (0.85, with a 95% CI of 0.78 – 0.90). The second row of **Figure 3** shows the Bland-Altman plots displaying the intra-scan agreement. LoA were -0.0591 – 0.0623, (-0.152 – 0.157) $\times 10^{-3}$ mm^2/s, (-0.185 – 0.193) $\times 10^{-3}$ mm^2/s, and (-0.155 – 0.158) $\times 10^{-3}$ mm^2/s for FA, MD, AD, and RD, respectively.

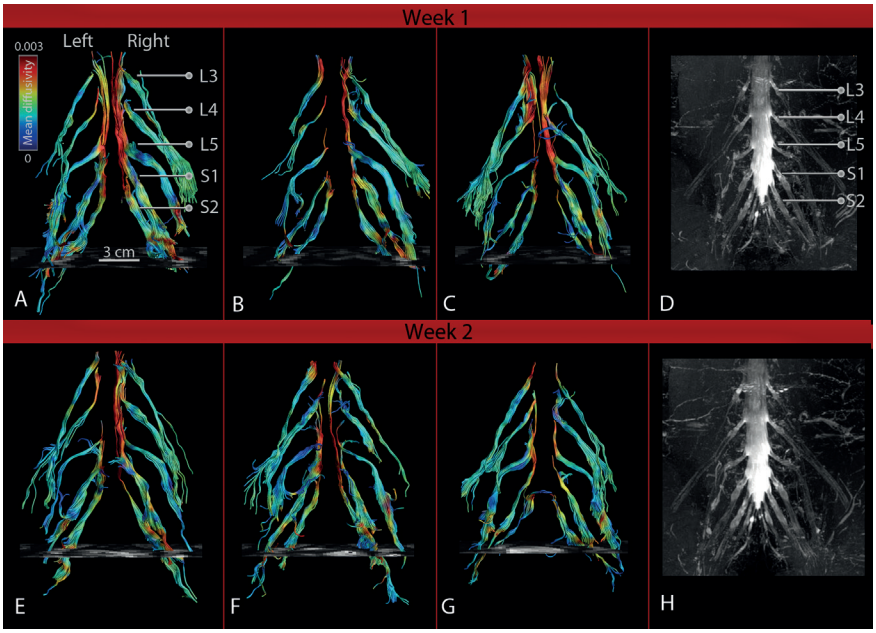

Figure 4: Fiber tractography results of DTI data of scan 1, scan 2, and scan 3 (A, B, C) in week 1, and D) the corresponding maximal intensity projection (MIP), and for week 2 (E, F, G, and H respectively) displayed as mean diffusivity color-encoded maps.

Experiment 3: inter-scan analysis

Figures 2 and **4** show similar FT results for DTI scan 2 and scan 3 of two subjects at site 1 (**Figure 2**) and site 2 (**Figure 4**, week 1: **B**, and **C**, week 2: **F** and **G**). The architectural configuration was similar to the MIP (**Figure 4**, **D** and **H**). This was also confirmed in all the other subjects (**Supplemental Materials 1** and **2**). Inter-scan mean diffusion parameters and ICCs are displayed in **Table 2**. There were no significant differences in any of the diffusion values between scan 2 and scan 3. However, the analysis showed significant differences in MD and AD between sites (p=0.035, and p=0.016 respectively). The ICCs for all diffusion parameters for both sites were intermediate to good, on average 0.68. The lowest ICC was for AD at site 2 (0.62 with a 95% CI of 0.48 – 0.73), and the highest was for MD at site 1 (0.73, with a 95% CI of 0.61 – 0.81). The third row of **Figure 3** shows the Bland-Altman plots displaying the inter-scan agreement on the third line. LoA were -0.0747 – 0.0777, (-0.225 – 0.308) $\times 10^{-3}$ mm^2/s, (-0.286 – 0.382) $\times 10^{-3}$ mm^2/s, and (-0.203 – 0.291) $\times 10^{-3}$ mm^2/s for FA, MD, AD, and RD respectively.

Experiment 4: inter-week analysis

Figure 4 shows similar FT results for a DTI scan of a control subject at site 2 between weeks (week 1: **A**, **B**, and **C**, week 2: **E**, **F**, and **G**). The architectural configuration was similar to the MIP (**D** and **H** respectively). This was also confirmed in the other subjects at site 2 (**Supplemental Material 2**). Inter-week mean diffusion parameters and ICCs are displayed in **Table 2**. There were small but significant differences between scans obtained in week 1 and week 2 for MD, AD, and RD ($p<0.0005$), where scans from week two had slightly lower diffusion values (-0.03 to -0.05 $\times 10^{-3}$ mm^2/s). ICCs were intermediate and on average 0.59. AD had the lowest ICC (0.57, with a 95% CI of 0.49 – 0.64), and the highest was that of RD (0.62, with a 95% CI of 0.54 – 0.68). The bottom row of **Figure 3** shows the Bland-Altman plots displaying the inter-week agreement. LoA were -0.068 – 0.087, (-0.279 – 0.213) $\times 10^{-3}$ mm^2/s, (-0.338 – 0.273) $\times 10^{-3}$ mm^2/s, and (-0.267 – 0.200) $\times 10^{-3}$ mm^2/s, for FA, MD, AD, and RD respectively.

Inter-subject versus inter-scan variability and sample size calculation

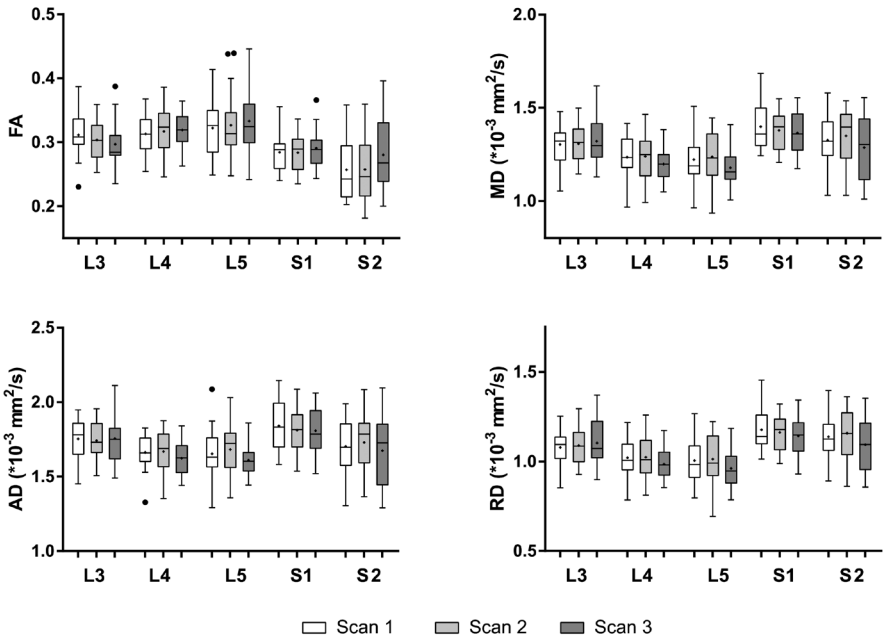

Figure 5: Boxplots with whiskers, outliers, medians, and means (indicated with '+') of the inter-subject variability over measurements (i.e. scan 1, scan 2, and scan 3) of site 1 displayed for all nerve levels (L3-S2) for all diffusion parameters (fractional anisotropy (FA), the mean diffusivity (MD), the axial diffusivity (AD), and the radial diffusivity (RD)).

Figure 5 shows the box and whisker plots of site 1 for all diffusion parameters per scan for each of the nerve levels. The range of the box plots (variability between subjects) is large, whereas the mean of the measurements remains the same over measurements (i.e., scan 1, scan 2, and scan 3).
Figure 6 shows similar results for the inter-week variability between subjects and scans, variability between subjects is large and similar to those of site 1, whereas the mean remains similar between weeks. **Table 3** shows that inter-subject CoV measurements are approximately 2 times higher than the inter-scan CoV measurements. Inter-subject CoV measurements for L3-S2 are on average respectively 9.6%, 9.2%, 12.0%, 9.1%, and 13.9% for site 1, and 11.8%, 9.7%, 10.1%, 11.3%, and 10.8% for the inter-week comparison at site 2. Inter-scan CoV measurements for L3-S2 are on average respectively 5.1%, 5.9%, 5.5%, 4.4%, and 6.6% for site 1, and 5.7%, 5.4%, 6.4%, 6.0%, and 6.3% for the inter-week comparison. **Table 4** shows the calculated sample sizes for an effect size of 5% and 10%. Overall, for FA most samples are needed (i.e. 35

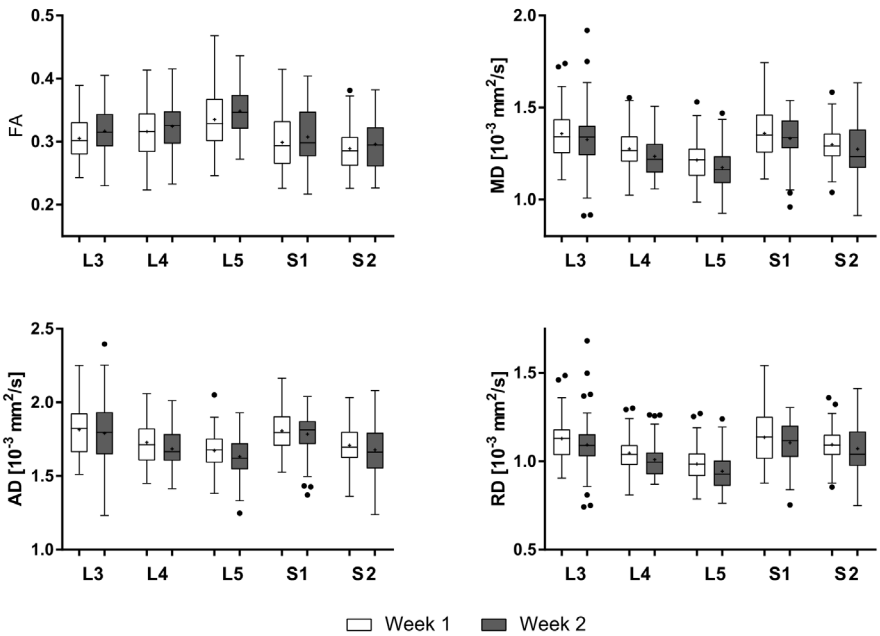

Figure 6: Boxplots with whiskers, outliers, medians, and means (indicated with '+') of the inter-subject variability over measurements of scans of week 1 versus week 2 at site 2 displayed for all nerve levels (L3-S2) for all diffusion parameters (fractional anisotropy (FA), the mean diffusivity (MD), the axial diffusivity (AD), and the radial diffusivity (RD)).

Table 3: Coefficient of variation (CoV) for each nerve level (L3-S2) and for all nerve levels together (overall) for both the inter-subject and inter-scan variability.

	CoV (%)											
	L3		L4		L5		S1		S2		Overall	
	Inter-subject	Inter-scan	Inter-subject	Inter-scan	Inter-subject	Inter-scan	Inter-subject	Inter-scan	Inter-subject	Inter-scan	Inter-subject	Inter-scan
Site 1												
FA	11.1	6.9	10.1	7.2	15.3	7.2	10.4	5.6	19.2	8.5	14.9	7.0
MD	8.9	4.3	8.7	5.3	10.5	4.7	8.5	3.8	11.6	5.8	10.8	4.7
AD	8.1	3.7	7.8	4.6	9.2	4.3	8.4	4.0	12.3	5.3	9.8	4.3
RD	10.3	5.4	10.1	6.3	12.9	5.7	9.2	4.1	12.4	6.6	12.5	5.6
Site 2 inter-week												
FA	11.5	6.7	11.7	5.3	12.0	8.0	14.7	7.4	13.1	6.9	13.7	7.3
MD	11.7	5.3	8.5	5.1	9.2	5.8	10.1	5.4	9.9	6.0	10.9	5.5
AD	11.4	4.9	8.6	5.0	7.8	4.7	7.9	4.4	9.0	6.0	9.7	5.0
RD	12.7	5.8	9.8	6.0	11.2	7.2	12.5	6.6	11.3	6.4	12.8	6.4

Table 4: Sample size calculations for each nerve level (L3-S2) and for all nerve levels together (overall) for an effect size of 5% and 10%

	Sample size											
	L3		L4		L5		S1		S2		Overall	
	5%	10%	5%	10%	5%	10%	5%	10%	5%	10%	5%	10%
FA	78	20	65	17	147	37	68	17	232	58	140	35
MD	50	13	48	12	70	18	46	12	85	22	73	19
AD	42	11	39	10	54	14	45	12	95	24	61	16
RD	67	17	65	17	105	27	54	14	97	25	99	25

samples for an effect size of 10%) whereas AD needs the least (16 samples for an effect size of 10%). The calculated sample sizes vary per nerve, where for L3 the number of needed samples was lowest and for S2 it was highest, i.e. 11-20 and 22-58 for an effect size of 10% respectively.

Discussion

This study describes the reproducibility of DTI of the lumbosacral nerves in healthy volunteers which is essential to appreciate its potential for research and applications in a clinical arena. Intra-scan reliability was high, whereas inter-resolution –, inter-scan –, and inter-week reliability were intermediate to good. However, there were small but significant differences between the diffusivity values of the inter-resolution scans, and inter-week scans. Bland-Altman plots showed high agreement between the intra-scan session results, and LoA were larger for inter-resolution –, inter-scan –, and inter-week agreement, which may be explained by the long tails of the histogram plots of the differences.

Inter-resolution reliability, investigated in experiment 1, was intermediate to high and small, but significant differences in diffusion parameters were found (mean value of site 1 and 2 combined for MD was $1.26 \pm 0.17 \times 10^{-3}$ mm^2/s and $1.31 \pm 0.14 \times 10^{-3}$ mm^2/s, for AD was $1.70 \pm 0.19 \times 10^{-3}$ mm^2/s and $1.75 \pm 0.16 \times 10^{-3}$ mm^2/s, and for RD was $1.04 \pm 0.16 \times 10^{-3}$ mm^2/s and $1.09 \pm 0.13 \times 10^{-3}$ mm^2/s for 2.5 and 3.0 mm isotropic respectively, $p<0.0005$). DTI is very sensitive to the effects of noise, which affect the eigenvalues estimation (31) and reliability of tractography (32). As such, with a voxel size of 2.5 mm isotropic in some cases it proved challenging to reliably track the nerves. We believe that differences in partial volume effects are the cause of the differences we found between the two protocols (33,34), since the higher resolution showed consistently higher diffusion values. Although partial volume of nerve tissue with the surrounding tissue is different for both resolutions (larger voxel size results in more partial volume effects), we experienced that a voxel size of 3.0 mm isotropic is still sufficient to reconstruct and characterize the lumbar and sacral nerves. As the 3.0 mm isotropic resolution protocol has approximately a twofold higher SNR, facilitating more reliable estimation of the tensor eigenvalues and FT, we used this protocol for further analyses.

The intra-scan reproducibility, investigated in experiment 2, of all diffusion measures was high, implying that the DTI sequence is stable, which is in line with previous findings (22). Compared to our results, Simon et al. showed higher reliability (ICCs were on average FA=0.93, AD=0.77, RD=0.83) in the peroneal and

tibial nerve based on three scans obtained at three different time points on one day (22). This could be due to that the peroneal and tibial nerve are approximately two times larger in cross-sectional area than the lumbar and sacral nerves (22,33). Therefore, it is less sensitive to changes in partial volume effects. Furthermore, the knee region is not affected by bowel movement and respiration in contrast to the lumbosacral region, which makes the knee region less sensitive to distortions and motion artifacts which may influence the reproducibility. Our study showed some diversity in ICC values between different positions along lumbar and sacral nerves (with highest range in AD 0.57-0.95 along different points). In general the ICC values of the FA in our study were lowest of all parameters, which is to be expected since the FA contains higher-order terms in the eigenvalues, causing higher degrees of uncertainty (35). Bland Altman plots of the intra-scan and inter-scan agreement showed similar LoA as earlier described in a post-mortem study investigating the lumbar and sacral nerves, taking into account that diffusion values are approximately 3-4 times lower than in vivo results (24).

Inter-scan reproducibility (experiment 3) were intermediate to high, suggesting that the technique is performing sufficient for application in research and clinical studies, which was also confirmed by previous findings (23). Although, inter-week reproducibility (experiment 4) showed intermediate to high ICCs, we did find small but significant differences between the scan measurements obtained in week 1 and week 2 (MD was $1.30\pm0.13 \times10^{-3}$ mm^2/s and $1.27\pm0.15 \times10^{-3}$ mm^2/s, AD was $1.75\pm0.16 \times10^{-3}$ mm^2/s and $1.71\pm0.18 \times10^{-3}$ mm^2/s, and RD was $1.08\pm0.13 \times10^{-3}$ mm^2/s and $1.04\pm0.14 \times10^{-3}$ mm^2/s for week 1 and week 2 respectively). A study investigating the tibial and sciatic nerve in diabetic patients showed no significant differences between scans performed in week 1 and week 2 (25). However, this study investigated a different anatomical region with different cross-sectional areas of the nerves.

The results of our study suggest that for longitudinal studies investigating a small effect size, it is very important to consider how potential findings should be interpreted, since small differences may also be caused by factors other than disease progression or therapeutic effects. Diffusion parameters are very sensitive to change due to many different reasons. Repositioning the subject or the coils can induce small changes to the magnetic field or overall data quality. Partial volume effects are likely to occur, as the nerve size cross-section is generally smaller than the voxel size. Therefore, differences in subject positioning, and changes in surrounding muscle tissue properties (36) may affect the overall diffusion measures

in the nerves (34). The inter-week reproducibility is likely to be more affected compared to the inter-scan reproducibility, which is also represented by the lower ICC values and wider LoA. Further physiological contributions such as the presence of pulsations of arterial vessels, breathing, and bowl movement could affect the diffusion parameters, since DTI is sensitive to motion (22,37).

There have been several studies reporting intra or inter-scan reproducibility of the application of DTI in peripheral nervous tissue (22–24). For future studies investigating the lumbosacral nerves with DTI it is essential to have information regarding the variability in diffusion parameters between subjects versus the variability between scans within one subject. If the variability between subjects is smaller than the variability between scans within one subject, the technique is not sufficient to use in clinical practice. This study shows that the CoV values between subjects are approximately two times higher than those between scans, indicating that DTI of the lumbosacral nerves is reproducible and sensitive to detect potential changes in cross-sectional studies. The calculated CoV and sample sizes are higher for AD than for RD, and highest for FA, which is in accordance to the expected variation due to noise (35,38,39). We have shown that large sample sizes are needed to detect an effect size of 5%. Future studies investigating the lumbosacral nerves should consider this in their study design. However, with improvements in data acquisition and data processing, these sample sizes are likely to decrease.

In this study, the nerves were manually segmented which may induce a rater bias. Nevertheless, since the two AND ROIs do not have to be precise and only tracts spanning the 3cm distance are selected it is unlikely that ROI placement would affect the measures. In future applications, automatic segmentation methods may even further improve the reproducibility of these DTI measures. However, at this point, there is no robust automated method to accurately segment the nerves running from the level of L3-S2. Qualitative assessment further shows that of the FT results of the different scans are comparable, which supports that the experimental design used in this study is sufficient to segment the lumbar and sacral nerves and sample their diffusion parameters in a reliable way.

Several studies have investigated the lumbosacral nerves in a clinical setting using DTI with applications related to lumbar disc herniation (11–14) and neurogenic bladder disorders (9). Our study confirms that the application of DTI and FT in the lumbosacral nerves is reliable for such cross-sectional studies.

We included two sites with 3T MRI systems provided by the same vendors.

However, we could not assess the inter-system reproducibility, since our subjects differed between sites. However, **Table 2** indicates that the diffusion measures are very similar between the two sites. Future studies could determine whether DTI and FT are reproducible even when MRI systems of similar or different vendors are used for the same participants, which is currently unknown for neuro(muscular) applications using diffusion MRI. In addition, it may also be important to determine whether our applied methods are still reproducible when nerves are affected (e.g., due to polyneuropathy or nerve trauma also in post-mortem applications (24)).

In conclusion, this multicenter study showed that the reproducibility of diffusion measures of the lumbar and sacral nerves was intermediate to high, and that FT results were comparable to each other and to the anatomical scans. This confirms that for cross-sectional studies of lumbar and sacral nerves, DTI can be used reliably in a clinical setting. Sample sizes for cross-sectional studies depend on nerve location, parameter of interest, and effect size and can range between 10 to 232 subjects. The small but significant differences of the inter-week comparison highlight that one needs to be careful when interpreting differences in longitudinal studies, since small differences may also be caused by factors other than disease progression or therapeutic effects.

Acknowledgements

We would like to thank all volunteers who participated in this study.

References

1. Basser PJ, Pajevic S, Pierpaoli C, Duda J, Aldroubi A. In vivo fiber tractography using DT-MRI data. Magn Reson Med. 2000;44(4):625–632.
2. Jones DK, Leemans A. Diffusion Tensor Imaging. In: Modo M, Bulte JWM, editors. Magnetic Resonance Neuroimaging. Humana Press; 2011. 127–144.
3. Takagi T, Nakamura M, Yamada M, Hikishima K, Momoshima S, Fujiyoshi K, et al. Visualization of peripheral nerve degeneration and regeneration: monitoring with diffusion tensor tractography. Neuroimage. 2009;44(3):884–892.
4. Stein D, Neufeld A, Pasternak O, Graif M, Patish H, Schwimmer E, et al. Diffusion tensor imaging of the median nerve in healthy and carpal tunnel syndrome subjects. J Magn Reson Imaging. 2009;29(3):657–662.
5. Basser PJ, Mattiello J, LeBihan D. MR diffusion tensor spectroscopy and imaging. Biophys J. 1994;66(1):259–267.
6. Hiltunen J, Suortti T, Arvela S, Seppä M, Joensuu R, Hari R. Diffusion tensor imaging and tractography of distal peripheral nerves at 3 T. Clin Neurophysiol. 2005;116(10):2315–2323.
7. Heckel A, Weiler M, Xia A, Ruetters M, Pham M, Bendszus M, et al. Peripheral Nerve Diffusion Tensor Imaging: Assessment of Axon and Myelin Sheath Integrity. PLoS One. 2015;10(6):1–13.
8. van der Jagt PKN, Dik P, Froeling M, Kwee TC, Nievelstein R a J, ten Haken B, et al. Architectural configuration and microstructural properties of the sacral plexus: a diffusion tensor MRI and fiber tractography study. Neuroimage. 2012;62(3):1792–1799.
9. Haakma W, Dik P, Ten Haken B, Froeling M, Nievelstein R a J, Cuppen I, et al. Diffusion tensor MRI and fiber tractography of the sacral plexus in children with spina bifida. J Urol. 2014;192(3):927–933.
10. Karampinos DC, Melkus G, Shepherd TM, Banerjee S, Saritas EU, Shankaranarayanan A, et al. Diffusion tensor imaging and T2 relaxometry of bilateral lumbar nerve roots: feasibility of in-plane imaging. NMR Biomed. 2013;26(6):630–637.
11. Balbi V, Budzik J-F, Duhamel A, Bera-Louville A, Thuc V, Cotten A. Tractography of lumbar nerve roots: initial results. Eur Radiol. 2011;21(6):1153–1159.
12. Shi Y, Zong M, Xu X, Zou Y, Feng Y, Liu W, et al. Diffusion tensor imaging with quantitative evaluation and fiber tractography of lumbar nerve roots in sciatica. Eur J Radiol. 2015;84(4):690–695.
13. Eguchi Y, Oikawa Y, Suzuki M, Orita S, Yamauchi K, Suzuki M, et al. Diffusion tensor imaging of radiculopathy in patients with lumbar disc herniation: preliminary results. Bone Joint J. 2016;98–B(3):387–394.
14. Chuanting L, Qingzheng W, Wenfeng X, Yiyi H, Bin Z. 3.0T MRI tractography of lumbar nerve roots in disc herniation. Acta Radiol. 2013; 0:1-17
15. Oikawa Y, Eguchi Y, Inoue G, Yamauchi K, Orita S, Kamoda H, et al. Diffusion tensor imaging of lumbar spinal nerve in subjects with degenerative lumbar disorders. Magn Reson Imaging. 2015;33(8):956–961.

16. Hakulinen U, Brander A, Ryymin P, Öhman J, Soimakallio S, Dastidar P, et al. Intra- and Inter-observer Variation of Region-of-Interest Methods in Quantitative Clinical Diffusion Tensor Imaging. In: 5th European Conference of the International Federation for Medical and Biological Engineering. 2011. 551–554.

17. Clerici AM, Bono G, Delodovici ML, Azan G, Cafasso G, Micieli G. A rare association of early-onset inclusion body myositis, rheumatoid arthritis and autoimmune thyroiditis: a case report and literature review. Funct Neurol. 2013;28(2):127–132.

18. Li K, Dortch RD, Welch EB, Bryant ND, Buck AKW, Towse TF, et al. Multi-parametric MRI characterization of healthy human thigh muscles at 3.0 T - relaxation, magnetization transfer, fat/water, and diffusion tensor imaging. NMR Biomed. 2014; 27:1070-1084

19. Heiervang E, Behrens TEJ, Mackay CE, Robson MD, Johansen-Berg H. Between session reproducibility and between subject variability of diffusion MR and tractography measures. Neuroimage. 2006;33(3):867–877.

20. Kristo G, Leemans A, De Gelder B, Raemaekers M, Rutten GJ, Ramsey N. Reliability of the corticospinal tract and arcuate fasciculus reconstructed with DTI-based tractography: Implications for clinical practice. Eur Radiol. 2013;23(1):28–36.

21. Bonilha L, Gleichgerrcht E, Fridriksson J, Breedlove JL, Rorden C, Nesland T, et al. Reproducibility of the structural brain connectome derived from diffusion tensor imaging. PLoS One. 2015;10(9).

22. Simon NG, Lagopoulos J, Gallagher T, Kliot M, Kiernan MC. Peripheral nerve diffusion tensor imaging is reliable and reproducible. J Magn Reson Imaging. 2015;43(4):962–969.

23. Ho MJ, Manoliu A, Kuhn FP, Stieltjes B, Klarhöfer M, Feiweier T, et al. Evaluation of Reproducibility of Diffusion Tensor Imaging in the Brachial Plexus at 3.0 T. Invest Radiol. 2017;52(8):482–487.

24. Haakma W, Pedersen M, Froeling M, Uhrenholt L, Leemans A, Boel LWT. Diffusion tensor imaging of peripheral nerves in non-fixed post-mortem subjects. Forensic Sci Int. 2016;263:139–146.

25. Vaeggemose M, Pham M, Ringgaard S, Tankisi H, Ejskjaer N, Heiland S, et al. Diffusion tensor imaging MR neurography for the detection of polyneuropathy in type 1 diabetes. J Magn Reson Imaging. 2017;45(4):1125–1134.

26. Leemans A, Jeurissen B, Sijbers J, Jones D. ExploreDTI: a graphical toolbox for processing, analyzing, and visualizing diffusion MR data. Proc 17th Sci Meet Int Soc Magn Reson Med. 2009;17(2):3537.

27. Leemans A, Jones DK. The B-matrix must be rotated when correcting for subject motion in DTI data. Magn Reson Med. 2009;61(6):1336–1349.

28. Tax CMW, Otte WM, Viergever M a, Dijkhuizen RM, Leemans A. REKINDLE: Robust extraction of kurtosis INDices with linear estimation. Magn Reson Med. 2014;73(2):794–808.

29. Bland JM, Altman DG. Measuring agreement in method comparison studies. Vol. 8, Statistical Methods in Medical Research. 1999. 135–160.

30. Rosner B. Rosner, B.: Fundamentals of Biostatistics, 7th ed. Boston: Brooks/Cole; 2011.

31. Bastin ME, Armitage PA, Marshall I. A theoretical study of the effect of experimental noise on the measurement of anisotropy in diffusion imaging. Magn Reson Imaging. 1998;16(7):773–785.

32. Froeling M, Nederveen AJ, Nicolay K, Strijkers GJ. DTI of human skeletal muscle: the effects of diffusion encoding parameters, signal-to-noise ratio and T2 on tensor indices and fiber tracts. NMR Biomed. 2013;26(11):1339–1352.

33. Hogan Q. Size of human lower thoracic and lumbosacral nerve roots. Anesthesiology. 1996;85(1):37–42.

34. Vos SB, Jones DK, Viergever MA, Leemans A. Partial volume effect as a hidden covariate in DTI analyses. Neuroimage. 2011;55(4):1566–1576.

35. Farrell JAD, Landman BA, Jones CK, Smith SA, Prince JL, Van Zijl PCM, et al. Effects of signal-to-noise ratio on the accuracy and reproducibility of diffusion tensor imaging-derived fractional anisotropy, mean diffusivity, and principal eigenvector measurements at 1.5T. J Magn Reson Imaging. 2007;26(3):756–767.

36. Froeling M, Oudeman J, Strijkers GJ, Maas M, Drost MR, Nicolay K, et al. Muscle Changes Detected with Diffusion-Tensor Imaging after Long-Distance Running. Radiology. 2015;274(2):548–562.

37. Ries M, Jones RA, Basseau F, Moonen CT, Grenier N. Diffusion tensor MRI of the human kidney. J Magn Reson Imaging. 2001;14(1):42–49.

38. Froeling M, Oudeman J, van den Berg S, Nicolay K, Maas M, Strijkers GJ, et al. Reproducibility of diffusion tensor imaging in human forearm muscles at 3.0 T in a clinical setting. Magn Reson Med. 2010;64(4):1182–1190.

39. Jones DK, Basser PJ. "Squashing peanuts and smashing pumpkins": How noise distorts diffusion-weighted MR data. Magn Reson Med. 2004;52(5):979–993.

Supplemental information

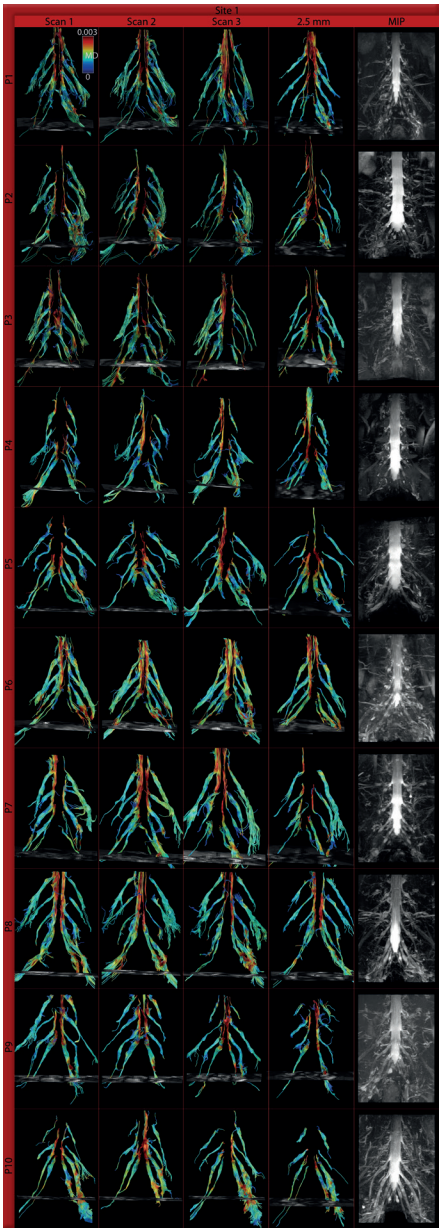

Supplemental Material 1: Fiber tractography of the lumbosacral nerves obtained of three scans with 3.0 mm isotropic voxel size and of one scan with 2.5 mm isotropic voxel size in ten subjects at site 1, displayed as mean diffusivity color-encoded maps together with the corresponding maximal intensity projection (MIP).

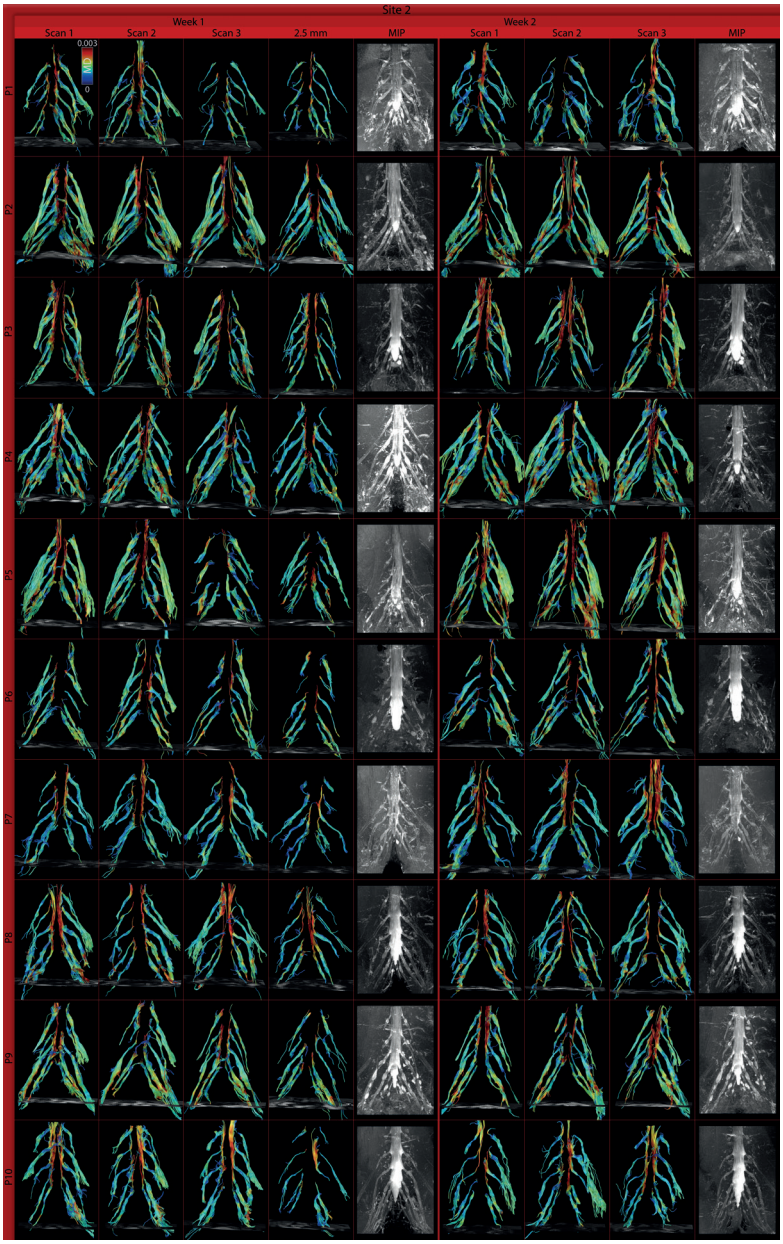

Supplemental Material 2: Fiber tractography of the lumbosacral nerves obtained of three scans with 3.0 mm isotropic voxel size and of one scan with 2.5 mm isotropic voxel size in ten subjects at site 2 and for two different weeks, displayed as mean diffusivity color-encoded maps together with the corresponding maximal intensity projection (MIP).

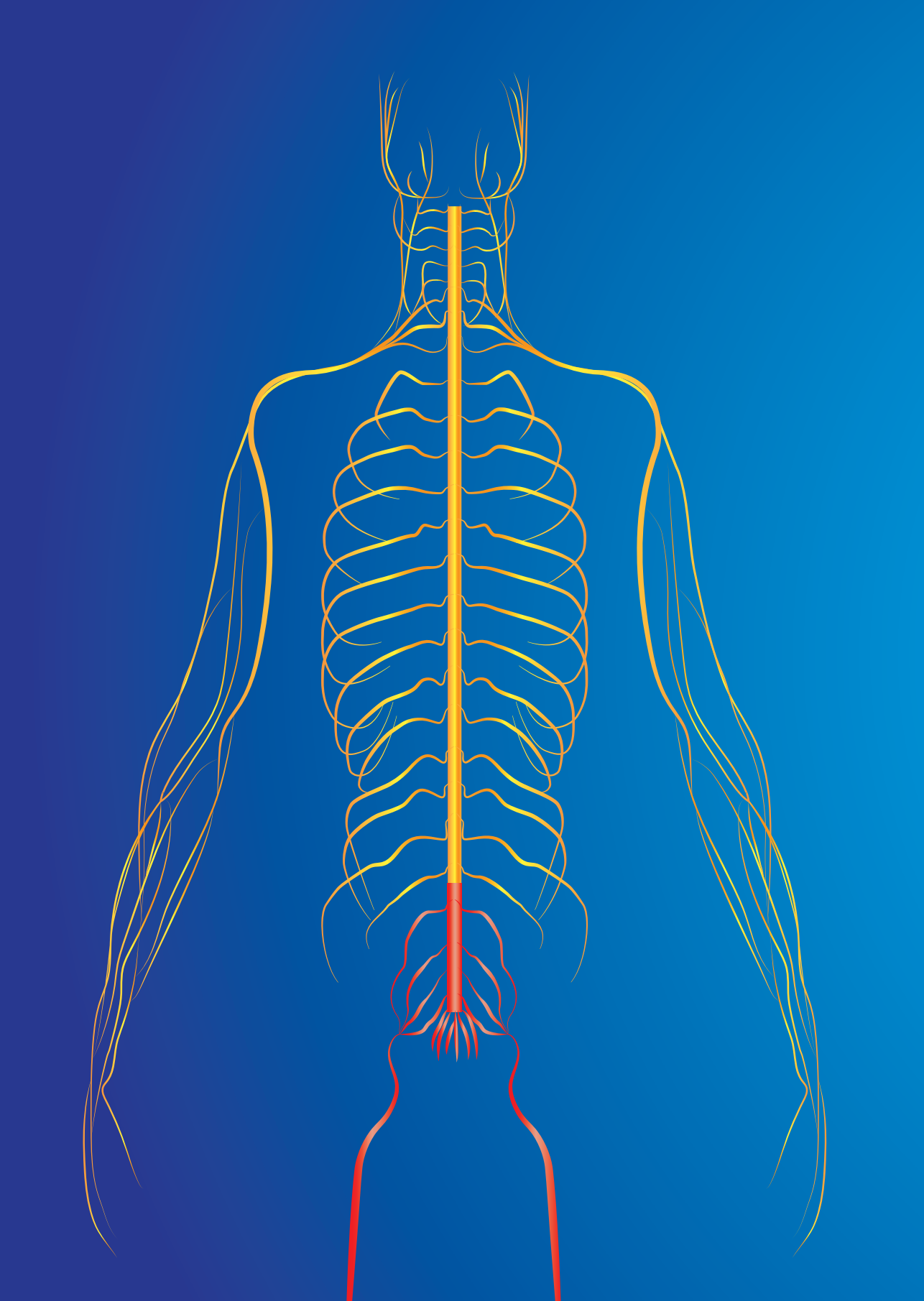

Chapter 3

Diffusion tensor MRI and fiber tractography of the sacral plexus in children with spina bifida

Wieke Haakma
Pieter Dik
Bennie ten Haken
Martijn Froeling
Rutger .A.J. Nievelstein
Inge Cuppen
Tom P.V.M. de Jong
Alexander Leemans

Journal of Urology 2014; 192; 927-933, DOI: 10.1016/j.juro.2014.02.2581

Abstract

Purpose

It is still largely unknown how neural tube defects in spina bifida affect the nerves at the level of the sacral plexus. Visualizing the sacral plexus in 3 dimensions could improve our anatomical understanding regarding neurological problems in patients with spina bifida. We investigate anatomical and microstructural properties of the sacral plexus of spina bifida with diffusion tensor imaging and fiber tractography.

Materials and methods

Ten patients (8 to 16 years old) with spina bifida underwent diffusion tensor imaging on a 3 Tesla magnetic resonance imaging system. Anatomical 3-dimensional reconstructions of the sacral plexus of the 10 patients. Fiber tractography was performed with the diffusion magnetic resonance imaging toolbox *ExploreDTI* to determine the fractional anisotropy, and mean, axial, and radial diffusivity in the sacral plexus of the patients. Results were compared to 10 healthy controls.

Results

Nerves of patients with spina bifida showed asymmetry and disorganisation to a large extent compared to those of healthy controls. Especially at the level of the myelomeningocele it was difficult to find a connection with the cauda equina. Mean, axial, and radial diffusivity values at S1-S3 were significantly lower in the patients.

Conclusions

To our knowledge this 3 Tesla magnetic resonance imaging study showed for the first time sacral plexus asymmetry and disorganization in 10 patients with spina bifida using diffusion tensor imaging and fiber tractography. The observed difference in diffusion values indicate that these methods can be used to identify nerve abnormalities. We expect that this technique could provide a valuable contribution to a better analysis and understanding of the problems of patients with spina bifida in the future.

Introduction

The incidence of spina bifida (SB) worldwide ranges from 0.3-4.5 per 1,000 births (1,2). Patients with SB generally experience neurogenic bladder dysfunction, and lower limb sensory and motor innervation is affected (3). Bladder sphincter contraction and relaxation are coordinated by the central and peripheral nervous systems, and in patients with SB this sphincter function can be affected (4). Without treatment the level to which this function is compromised determines the prognosis of these patients. Early diagnosis is critical to prevent further neurological impairment but it can be quite arduous due to the complex anatomical configuration and high inter-subject variability of peripheral sacral branches (5,6). Currently no reliable in vivo, noninvasive routine clinical technique is available to determine how the sacral plexus is organized on an anatomical or structural level in patients with SB.

A technique that allows for 3D visualization and structural characterization of nerve tissue is diffusion tensor imaging (DTI) (7–9). DTI is a magnetic resonance imaging (MRI) technique that is sensitive to the random movement of diffusing water molecules, the so-called Brownian motion. The diffusion is more pronounced along the nerves than across their main orientation, causing diffusion to show a high degree of anisotropy in such nervous tissue (10). This anisotropy can be quantified by applying a diffusion-weighted MRI acquisition protocol with multiple diffusion gradient orientations and subsequently estimating the diffusion tensor (7). This enables the possibility to reconstruct the 3D architecture of peripheral nerves noninvasively, and is referred to as fiber tractography (FT) (11).

Although DTI has been used in several studies on peripheral nerves (12,13), it has been rarely used in the lumbosacral region (5). The potential value of DTI to quantify peripheral nerve injury or dysfunction seems promising but the extent to which this can be translated to the clinical setting is still questionable given the numerous fiber constituents that may modulate the observed DTI results (10). The 4 diffusion parameters commonly used to investigate tissue microstructural properties are 1) fractional anisotropy (FA), which is high when water molecules move predominantly in 1 direction, 2) mean diffusivity (MD), which is the average of all eigenvalues (overall amount of diffusion), 3) axial diffusivity (AD), which is equal to the largest eigenvalue and 4) radial diffusivity (RD), which is defined as the average of the second and third eigenvalues (**Figure 1**).

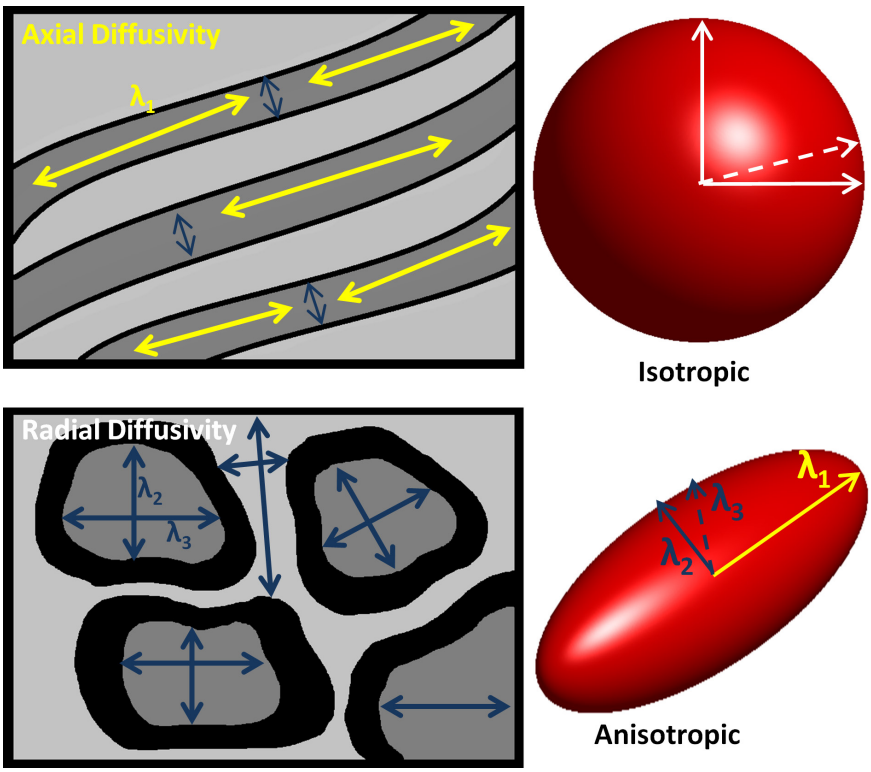

Figure 1: In fluid the random movement of water molecules is isotropic. Diffusion along the nerves (represented as axial diffusivity or λ_1) is higher than perpendicular to the nerves (represented as radial diffusivity or mean of λ_2 and λ_3). λ_1, λ_2, and λ_3 are the eigenvalues (the length of the diffusion) in a particular orientation. This diffusion orientation preference is called anisotropy.

While DTI (7,8) has been widely used to investigate white matter tracts in the brain (11,14–16), its application to peripheral nerves remains limited, mainly due to the greater challenges related to data acquisition (5,12,13). Takagi et al examined the nerve regeneration of the sciatic nerve in rats following contusive injury. The correlation of FA values with both histological and functional changes observed in that work demonstrates the potential clinical value of DTI in peripheral nerve damage and repair with lower FA values indicating damage to peripheral nerves (17). Van der Jagt et al recently reported promising progress in reconstructing and analyzing the peripheral sacral nerves using DTI and FT (5).

We investigated the sacral plexus in 10 children with SB and neurogenic bladder dysfunction using DTI and FT. We compared results to those of healthy controls.

We hypothesized that in these patients with SB the microstructural properties of the sacral plexus would show abnormal values of DTI parameters in nerve regions where the tissue structure was affected. Our results revealed that using DTI and FT 1) peripheral sacral nerves in patients with SB and neurogenic bladder dysfunction could be reconstructed and visualized in great detail, 2) the microstructural tissue organization of the sacral plexus could be characterized in vivo and noninvasively, and 3) peripheral nerve tissue abnormalities could be identified at specific locations in the sacral plexus. We believe that investigating nerve tissue properties with DTI and FT, in addition to conventional MRI, would be helpful to better understand the mechanism of the disturbed innervation of the bladder and lower limb muscles in children with SB.

Materials and methods

Data acquisition

Local institutional review board approval was obtained for this study and written informed consent was provided before MRI. Six girls and 4 boys with a mean age of 11.4 years (range 8 to 16) with SB and neurogenic bladder dysfunction were included in study. Neural tube defects (myelomeningocele) were mostly located in the lumbar sacral region (L5-S2). To decrease variability in the patient group and keep acquisition time to a minimum MRI was performed from the L4 level to the pelvic floor region. As healthy controls, we used participants in the study by van der Jagt et al (5). All imaging was done with a 3 Tesla Philips Achieva MRI System using a 16-channel phased array surface coil. Diffusion-weighted images and anatomical 3D-TSE T2-weighted images were obtained using previously described acquisition protocols (5).

Data processing and analysis

The DTI data sets were processed using the *ExploreDTI* diffusion MRI toolbox (www.ExploreDTI.com) (18). 1) Data were corrected for subject motion and eddy current induced geometrical distortion (19). 2) Diffusion tensors and subsequently diffusion parameters (MD, FA, AD and RD) were calculated using the iteratively weighted linear regression procedure (20). 3) A deterministic streamline tractography approach (21) was used to reconstruct fiber pathways. In each nerve a SEED ROI was placed in the middle of the nerve. A second ROI (AND region) was selected in the nerve root near the cauda equina and another AND ROI was selected more distal along the nerve where it was still traceable. By placing these AND regions according to the 3D-TSE T2-weighted data set fiber we determined trajectories

along the entire nerve. Combining a low FA threshold, i.e. 0.001, with these AND ROIs provides a feasible way to reconstruct tracts with high reproducibility (5). Finally, a pediatric neuroradiologist with more than 15 years of experience with MRI evaluated the accuracy of the fiber tract anatomical locations using the anatomical 3D-TSE T2-weighted images.

Statistical analyses

FA, MD, AD and RD values of nerves L4 to S3 in patients with SB were investigated and compared with values in healthy controls, as determined in the study by van der Jagt et al (5). We investigated variability between the nerves of patients with SB per nerve using the Kruskal-Wallis test. Nerves on the left and right sides were compared using the nonparametric Mann-Whitney U test, which was also used to investigate differences between the nerves of patients with SB and healthy controls. Analysis was done with SPSS (SPSS Inc. Chicago, IL, USA), version 21.0.

Results

With tractography it was possible to obtain 3-dimensional anatomical reconstructions of all 10 patients with SB (see supplemental information). **Figure 2** shows FT results of the lumbosacral plexus of a typical patient with SB. The pseudo color encoding represents the magnitude of the diffusion parameters. **Table 1** lists diffusion measures of patients with SB and healthy controls. Because MD values appeared to be most indicative of nerve abnormalities (see **Table 1**), the fiber tracts were color coded for MD (**Figures 3 to 5**).

Fiber tract evaluation

The sacral plexus of patients with SB were asymmetrical and disorganized compared to that of healthy controls. In 2 patients nerves at the L5 level could not be reconstructed with FT although they were visible on anatomical T2-weighted images (**Figure 3B**). S4 and S5 could not be traced in any patient or control. At that level in most cases they were also not visible on anatomical T2-weighted images.

In patients with SB it was difficult to locate a connection to the cauda equina, especially at the myelomeningocele level (**Figure 4A**). In contrast, this connection was clearly visible in healthy controls (**Figure 4B**).

Diffusion parameters

Statistical testing revealed no significant difference in FA, MD, AD, and RD between the left and right side at the levels L4-S3 ($p>0.05$). Therefore, the 2 sides were pooled for each nerve level. Furthermore, no significant differences were found

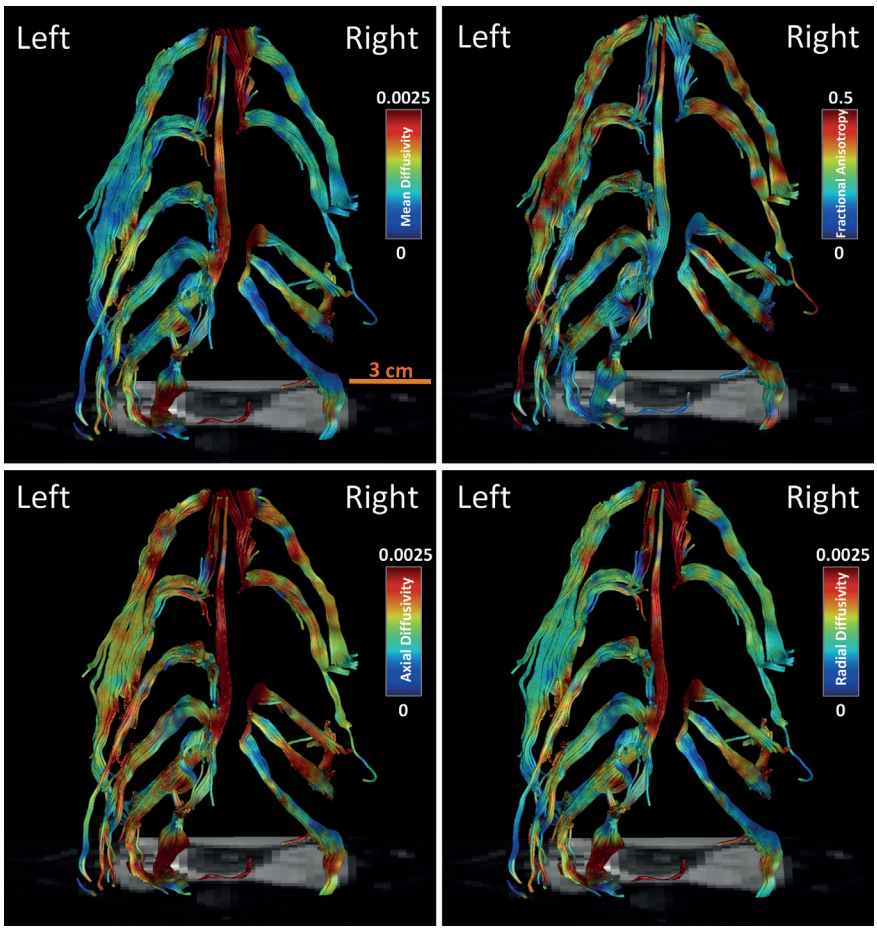

Figure 2: 3D anatomy of the nerves at the level of L3-S3 of a typical spina bifida patient. Color maps of mean diffusivity, fractional anisotropy, axial diffusivity, and radial diffusivity are shown along the fiber pathways. A red color represents a high diffusivity and blue color a low diffusivity.

between individual nerves per level ($p>0.05$). **Table 1** shows that MD at the L4 level in patients with SB was comparable to that in healthy controls.However, from the level of L5 downward, a lower MD value was found, which was significantly different from healthy controls at the levels S1-S3 (S1 and S2: $p<0.001$, S3: $p<0.01$). Similar differences were found for the AD and RD values (S1: $p<0.001$, S2 and S3: $p<0.01$).

Table 1: Diffusion parameters (fractional anisotropy, mean diffusivity, axial diffusivity, and radial diffusivity) and tract length of spina bifida (SB) patients and healthy controls L4-S3

	L4 Mean ± SD	L5 Mean ± SD	S1 Mean ± SD	S2 Mean ± SD	S3 Mean ± SD
FA					
Control	0.28±0.05	0.31±0.03	0.26±0.03	0.23±0.03	0.22±0.03
SB	0.28±0.04	0.29±0.04	0.27±0.05	0.25±0.05	0.26±0.05
MD ($\times 10^{-3}$ mm^2/s)					
Control	1.34±0.22	1.42±0.21	1.83±0.24*	1.73±0.29*	1.62±0.32†
SB	1.32±0.16	1.31±0.24	1.40±0.22*	1.36±0.21*	1.33±0.23†
AD ($\times 10^{-3}$ mm^2/s)					
Control	1.72±0.22	1.86±0.24	2.31±0.27*	2.13±0.36†	1.98±0.39†
SB	1.70±0.18	1.72±0.31	1.78±0.23*	1.70±0.21†	1.66±0.35†
RD ($\times 10^{-3}$ mm^2/s)					
Control	1.15±0.21	1.19±0.20	1.59±0.22*	1.53±0.26†	1.43±0.29†
SB	1.14±0.15	1.11±0.21	1.22±0.23*	1.19±0.22†	1.17±0.22†

*p<0.001; †p<0.01

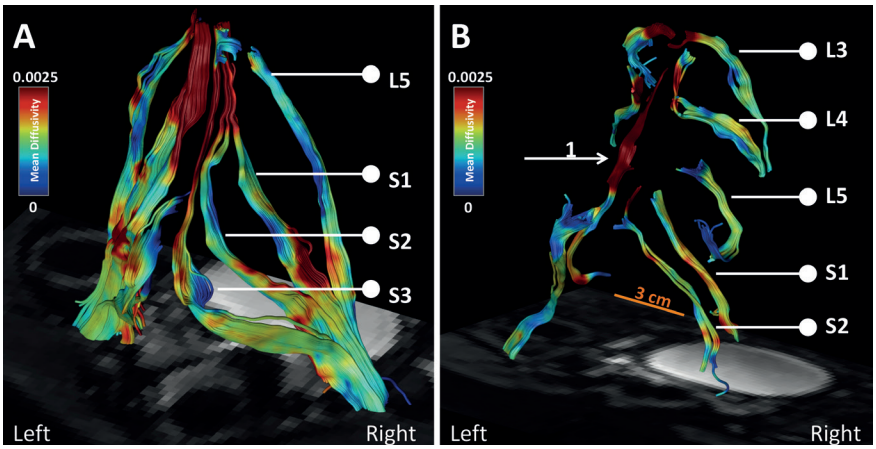

Figure 3: Lower lumbar and sacral nerves, A) healthy control, B) spina bifida patient with myelomeningocele from the level of L5 to caudal. L5 on the left side could not be reconstructed (indicated with "1").

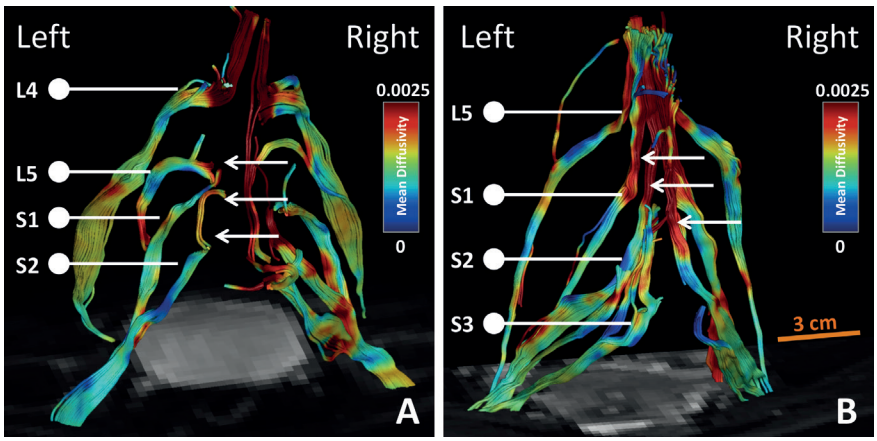

Figure 4: A) Posterior view of a spina bifida patients with myelomeningocele at the level of L5-S1, the sacral nerves do not connect with the cauda equina (indicated with the arrows), B) healthy control in which the nerves show a connection to the cauda equina.

Bladder innervation

In 3 patients we noted a trajectory originating from S2-S4 and continuing to the bladder. **Figure 5A** shows an example in 1 patient. Although this could not be confirmed on anatomical T2-weighted images, it is likely that this was the pudendal nerve since it showed a course similar to that on a schematic anatomy configuration of the sacral plexus (**Figure 5B**).

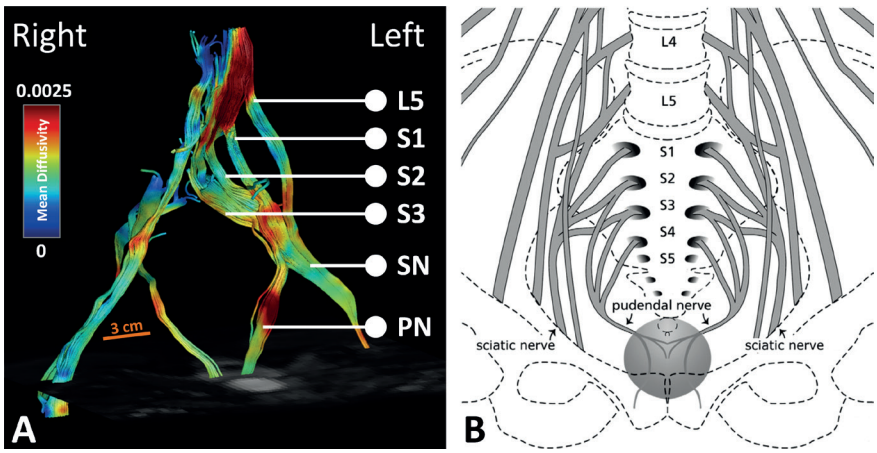

Figure 5: A) Anterior view of a spina bifida patient with myelomeningocele at the level of L1-L4, the pudendal nerve is indicated with "PN", and the sciatic nerve with "SN", B) schematic overview of the lumbosacral nerves. The sacral branches and pudendal nerve (A) correspond with the anatomy (B).

Discussion

To our knowledge we report the first 3 Tesla DTI to reconstruct the 3D architecture of the sacral plexus in 10 patients with SB that detailed L4-S3 individual pathway trajectories and microstructural properties. Differences in anatomy, particularly asymmetry and disorganization, and MD values in the sacral nerves were found in patients with SB compared to healthy controls.

Interpretation

Fiber tractography provides striking images of the sacral plexus non-invasively (5). However, this technology has not been extensively used to investigate peripheral nerves since DTI and FT are not straightforward or trivial to apply. In addition, interpretation is a major difficulty of DTI (22). Therefore, one of the major questions in the use of DTI is whether the images are representative for what we think they present. Abnormalities in fiber reconstructions and diffusion parameters can also be caused by deformations and artifacts in data or limitations of the imaging technique (23,24).

Clinical relevance

In this study MD values from L5 to the caudal level were lower in patients with SB than controls but for L4, which was still intact, MD values were similar in the groups. The decrease in MD could involve reduced intrinsic diffusion in the intra-axonal space due to cytoskeletal breakdown, resulting in increased viscosity (10). It could also be related to myelomeningocele, which in these patients was mostly located at the L5-S1 level. At that level it was also difficult to find a connection to the cauda equina. With some abuse of terminology, if nerves at that level do not work properly, they might be compared to an electric cable that is not adequately plugged into the socket. To investigate whether the lower MD values of these nerves were caused by myelomeningocele, results could be compared to those in patients with SB in whom myelomeningocele is located at a higher level (thoracic or high lumbar).

DTI revealed a trajectory to the bladder that was likely the pudendal nerve. The anatomical image did not show this trajectory. Because the pudendal nerve originates from S2-S4, it would be expected that the pudendal nerve would also have lower MD values. Future studies of the correlation between urodynamic findings and DTI metrics in the sacral plexus of patients with SB may support this

hypothesis. The patient group could be extended by investigating other sacral malformations such as anorectal malformation (25). Lower lesions are often associated with detrusor-sphincter dyssynergia compared to higher lesions. DTI could have an important role in diagnosis and therapy for future neuroanastomotic procedures in these patients.

Limitations

Data were corrected for subject motion and geometric distortions but may still have been misaligned due to the nonlinear behavior of these artifacts (5,9). In addition, due to the relatively large voxel size ($3 \times 3 \times 3$ mm^3) partial volume effects influenced the diffusion parameters and smaller nerve bundles, especially at S3 since those nerves are smaller in diameter than the other nerves (23,26). The control group consisted of healthy adults. Although diffusion properties may change with age, as in brain white matter fiber bundles (27), we expect that differences in AD and RD would be relatively low compared to differences in patients with SB versus healthy adults.

Future work

To determine the extent to which diffusion parameters represent nerve functionality in patients with SB other patient groups with neurological disorders can be investigated. In newborns with SB DTI can be performed before and after closing the spinal cord as a comparison tool to localize potential nerve damage. By improving DTI resolution we believe that in the future it could be possible to visualize small nerves in these infants. Other pathological conditions for which DTI can be used to visualize the peripheral nerves include multiple sclerosis (28) and paraplegia. Finally, DTI could potentially be applied to locate nerves for sacral nerve stimulation, neurostimulator implants and neuroanastomosis procedures (29) in the sacral plexus. Combining electromyogram information with DTI tractography and diffusion parameters may improve our understanding of how to interpret diffusion parameters of peripheral nerves.

At this time DTI cannot replace conventional anatomical imaging modalities, i.e. 2D T1-weighted and T2-weighted sequences or high resolution 3D-TSE protocols. However, it can serve as a complementary tool to better detect and understand neurological problems in patients with SB. Further adjustments of the registration process by fusing anatomical and DTI information may improve analysis of the nerves at each level. Large-scale studies of patients with different types of SB are

needed to further optimize the technique and better determine the exact role of DTI in the diagnosis and follow-up. We expect that abnormal diffusion parameters may indicate affected or dysfunctional nerves.

Conclusion

To our knowledge this 3 Tesla MRI study shows for the first time the asymmetry and disorganization of the sacral plexus in 10 patients with SB using DTI and FT. These abnormalities indicate that the sacral plexus of such patients differs from that of healthy controls. The observed difference in diffusion values shows that these methods can be used to identify nerve abnormalities. Combining 3D-TSE, DTI and FT, and correlating diffusion parameters with the neurological problems of patients with SB are expected to provide a valuable contribution to better analysis and diagnosis of these patients in the future.

Acknowledgements

We would like to thank Niels Blanken (MRI radiographer, department of radiology) for his help in performing the MRI scans.

References

1. de Jong TPVM, Chrzan R, Klijn AJ, Dik P. Treatment of the neurogenic bladder in spina bifida. Pediatr Nephrol. 2008;23(18350321):889–896.
2. Dik P, Klijn AJ, van Gool JD, de Jong-de Vos van Steenwijk CC, de Jong TP. Early start to therapy preserves kidney function in spina bifida patients. Eur Urol. 2006;49(5):908–913.
3. Özek MM, Cinalli G, Maixner WJ. Spina bifida - management and outcome. New York: Springer; 2008.
4. de Groat WC. A neurologic basis for the overactive bladder. Urology. 1997;50(6):36–52.
5. van der Jagt PKN, Dik P, Froeling M, Kwee TC, Nievelstein R a J, ten Haken B, et al. Architectural configuration and microstructural properties of the sacral plexus: a diffusion tensor MRI and fiber tractography study. Neuroimage. 2012;62(3):1792–1799.
6. Matejcik V. Anatomical variations of lumbosacral plexus. Surg Radiol Anat. 2010;32(4):409–414.
7. Basser PJ, Mattiello J, LeBihan D. MR diffusion tensor spectroscopy and imaging. Biophys J. 1994;66(1):259–267.
8. Jones DK, Leemans A. Diffusion Tensor Imaging. In: Modo M, Bulte JWM, editors. Magnetic Resonance Neuroimaging. Humana Press; 2011. 127–144.
9. Tournier J-D, Mori S, Leemans A. Diffusion tensor imaging and beyond. Magn Reson Med. 2011;65(6):1532–1556.
10. Beaulieu C. The basis of anisotropic water diffusion in the nervous system - a technical review. NMR Biomed. 2002;15(7–8):435–455.
11. Mori S, van Zijl PCM. Fiber tracking: principles and strategies - a technical review. NMR Biomed. 2002;15(7–8):468–480.
12. Hiltunen J, Suortti T, Arvela S, Seppa M, Joensuu R, Hari R. Diffusion tensor imaging and tractography of distal peripheral nerves at 3 T. Clin Neurophysiol. 2005;116(10):2315–2323.
13. Vargas MI, Viallon M, Nguyen D, Delavelle J, Becker M. Diffusion tensor imaging (DTI) and tractography of the brachial plexus: feasibility and initial experience in neoplastic conditions. Neuroradiology. 2010;52(3):237–245.
14. Wakana S, Jiang H, Nagae-Poetscher LM, van Zijl PC, Mori S. Fiber tract-based atlas of human white matter anatomy. Radiology. 2004;230(1):77–87.
15. Reijmer YD, Leemans A, Caeyenberghs K, Heringa SM, Koek HL, Biessels GJ. Disruption of cerebral networks and cognitive impairment in Alzheimer disease. Neurology. 2013;80(15):1370–1377.
16. Reijmer YD, Brundel M, de Bresser J, Kappelle LJ, Leemans A, Biessels GJ. Microstructural white matter abnormalities and cognitive functioning in type 2 diabetes: a diffusion tensor imaging study. Diabetes Care. 2013;36(1):137–144.
17. Takagi T, Nakamura M, Yamada M, Hikishima K, Momoshima S, Fujiyoshi K, et al. Visualization of peripheral nerve degeneration and regeneration: monitoring with diffusion tensor tractography. Neuroimage. 2009;44(3):884–892.

18. Leemans A, Jeurissen B, Sijbers J, Jones D. ExploreDTI: a graphical toolbox for processing, analyzing, and visualizing diffusion MR data. Proc 17th Sci Meet Int Soc Magn Reson Med. 2009;17(2):3537.

19. Leemans A, Jones DK. The B-matrix must be rotated when correcting for subject motion in DTI data. Magn Reson Med. 2009;61(6):1336–1349.

20. Veraart J, Sijbers J, Sunaert S, Leemans A, Jeurissen B. Weighted linear least squares estimation of diffusion MRI parameters: Strengths, limitations, and pitfalls. Neuroimage. 2013;81(0):335–346.

21. Basser PJ, Pajevic S, Pierpaoli C, Duda J, Aldroubi A. In vivo fiber tractography using DT-MRI data. Magn Reson Med. 2000;44(4):625–632.

22. Deprez S, Billiet T, Sunaert S, Leemans A. Diffusion tensor MRI of chemotherapy-induced cognitive impairment in non-CNS cancer patients: A review. Vol. 7, Brain Imaging and Behavior. 2013. 409–435.

23. Vos SB, Jones DK, Viergever MA, Leemans A. Partial volume effect as a hidden covariate in DTI analyses. Neuroimage. 2011;55(4):1566–1576.

24. Tournier JD, Calamante F, King MD, Gadian DG, Connelly A. Limitations and requirements of diffusion tensor fiber tracking: An assessment using simulations. Magn Reson Med. 2002;47(4):701–708.

25. Boemers TM, Van Gool JD, De Jong TPVM, Bax KMA. Urodynamic evaluation of children with the caudal regression syndrome (caudal dysplasia sequence). J Urol. 1994;151(4):1038–1040.

26. Hogan Q. Size of human lower thoracic and lumbosacral nerve roots. Anesthesiology. 1996;85(1):37–42.

27. Bennett IJ, Madden DJ, Vaidya CJ, Howard D V, Howard Jr. JH. Age-related differences in multiple measures of white matter integrity: A diffusion tensor imaging study of healthy aging. Hum Brain Mapp. 2010;31(3):378–390.

28. Roosendaal SD, Geurts JJG, Vrenken H, Hulst HE, Cover KS, Castelijns JA, et al. Regional DTI differences in multiple sclerosis patients. Neuroimage. 2009;44(4):1397–1403.

29. Rasmussen MM, Clemmensen D, Rawashdeh YF, Tankisi H, Christensen P, Krogh K. Surgical reinnervation with nerve anastomosis technique for neurogenic bladder and bowel dysfunction. Ugeskr Laeger. 2011;173:2412.

Supplemental information

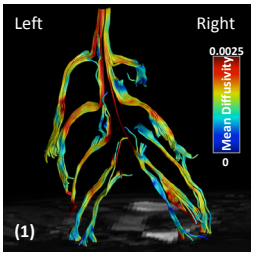

Patient 1	
Myelomening ocele (MMC)	S1
Functional until: Motoric (M) Sensoric (S)	M: L5 S: S2
Patient history	Detruso-rectomy Sling

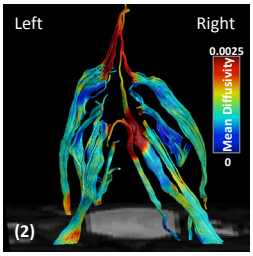

Patient 2	
MMC	S1
Functional until: Motoric (M) Sensoric (S)	M: L4 S: L5
Patient history	Detruso-rectomy Sling CIC Stoma

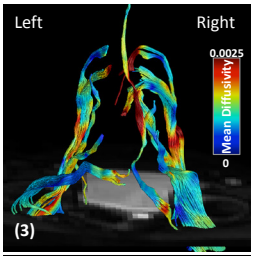

Patient 3	
MMC	L5
Functional until: Motoric (M) Sensoric (S)	M: L4/L5 S: S1
Patient history	Detruso-rectomy

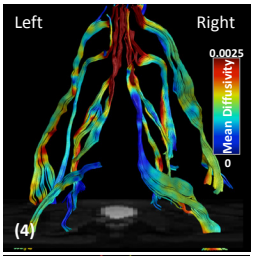

Patient 4	
Meningocele	S1
Functional until: Motoric (M) Sensoric (S)	M: Normal S: Normal
Patient history	Dry with CIC and oxybutynin

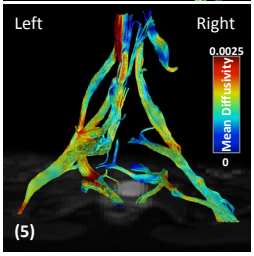

Patient 5	
MMC	L4
Functional until: Motoric (M) Sensoric (S)	M: S1 S: S5
Patient history	Dry with CIC Miction without CIC Split cord

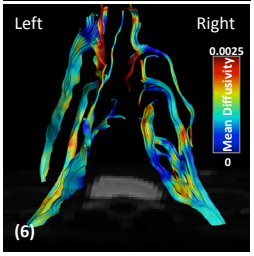

Patient 6	
MMC	S1
Functional until: Motoric (M) Sensoric (S)	M: S2 S: S2
Patient history	Ileocysto-plasty (ICP) with sling CIC Stoma

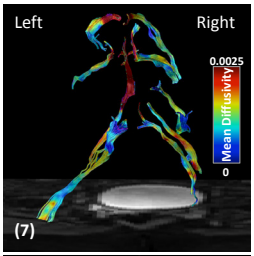

Patient 7	
MMC	L5
Functional until: Motoric (M) Sensoric (S)	M: L5 S: L5
Patient history	Dry with CIC without oxybuty-nin

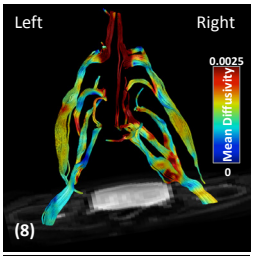

Patient 8	
MMC	S1
Functional until: Motoric (M) Sensoric (S)	M: L4 S: L4
Patient history	Dry with CIC and oxybutynin

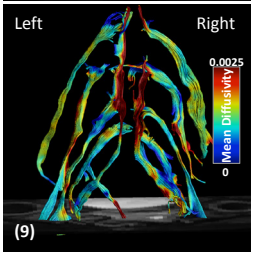

Patient 9	
MMC	L5
Functional until: Motoric (M) Sensoric (S)	M: S2 S: S2
Patient history	Detruso-rectomy Sling CIC and dry

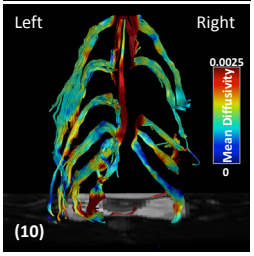

Patient 10	
MMC	S1
Functional until: Motoric (M) Sensoric (S)	M: S1 S: S1
Patient history	ICP Sling CIC Stoma

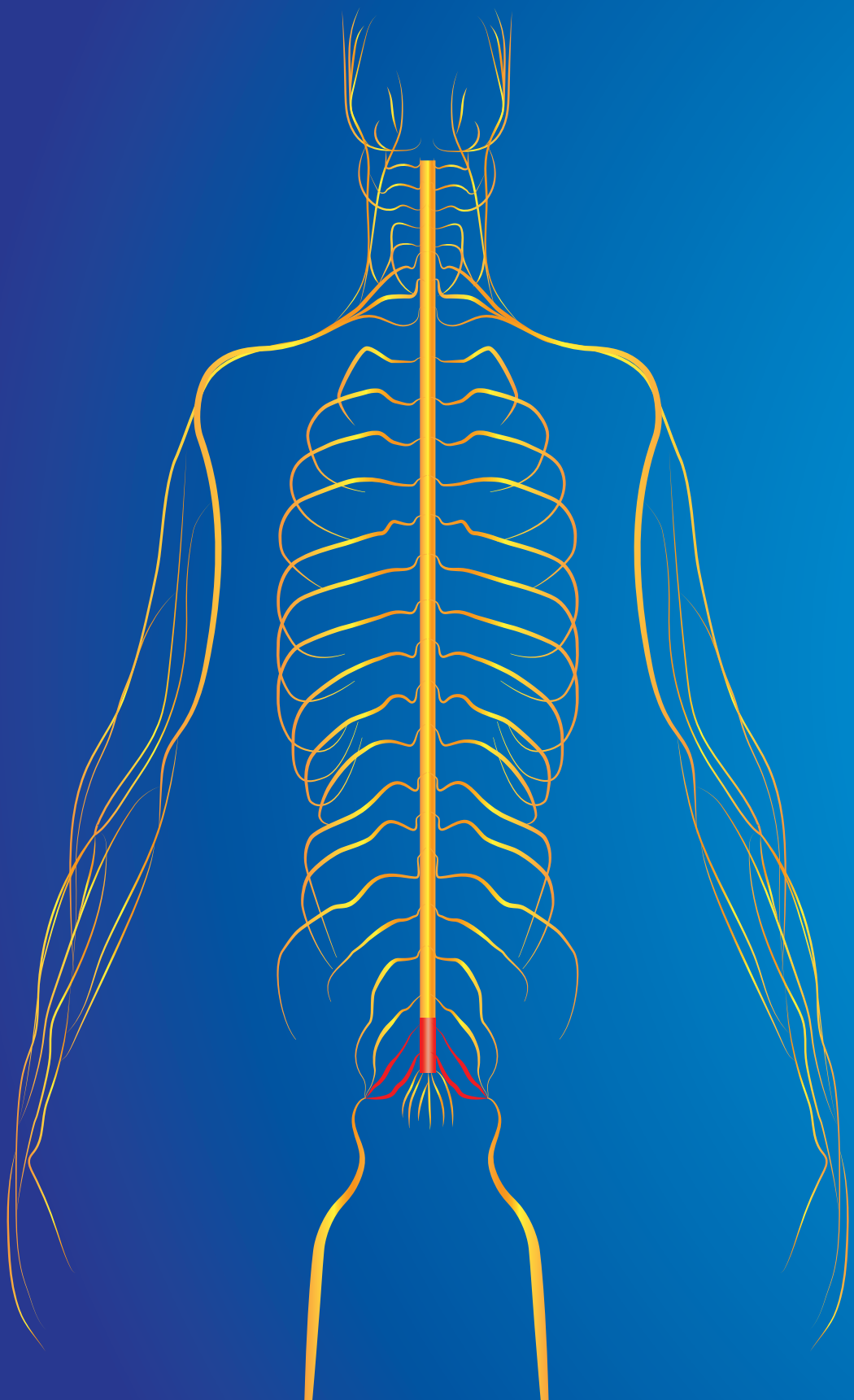

Chapter 4

Diffusion tensor imaging of the compressed nerve roots in lumbar disc herniation

Wieke Haakma
Martijn Froeling
Pieter Dik
Alexander Leemans
Francisca H. H. Linn
Dennis Nieuwkamp
Sanne Dorhout Mees
Geert-Jan Biessels
Jeroen Hendrikse

Submitted

Abstract

Objectives

The aim of this study was to investigate the nerve roots with diffusion tensor imaging (DTI) in patients with herniated disc compressing the nerve at the level of L5 and S1 and compare them with healthy controls.

Methods

Ten patients with lumbar disc herniation and 10 healthy controls were scanned on a 3T MRI scanner. The nerve roots at the level of L5 and S1 were reconstructed using DTI based fiber tractography from which 3 cm tract segments were selected. For these segments diffusion parameters (fractional anisotropy (FA), mean diffusivity (MD), axial diffusivity (AD), and radial diffusivity (RD)) were determined.

Results

There were no differences in the diffusion parameters between the compressed nerve roots in comparison to the contralateral nerve roots. However, significant differences in FA and RD were found between the compressed nerve roots and the nerve roots in healthy controls (0.25±0.03 and 0.29±0.04 for FA, p=0.004, and $1.27\pm0.15 \times 10^{-3}$ mm^2/s and $1.11\pm0.14 \times 10^{-3}$ mm^2/s for RD, p=0.029). No differences were found in the other diffusivity measures. Additionally, we found regional differences in diffusion measures along the nerve segments.

Conclusions

With DTI we found differences in FA and RD between the compressed nerve roots and the nerve roots at the same level in healthy controls, suggesting that there are pathological processes affecting the nerve roots at the level of the compression. Trajectory analysis shows that the location at which diffusion estimates are extracted along the nerve segment is of importance.

Introduction

In patients with compressed nerve roots due to lumbar disc herniation, the nucleus pulposus of the disc breaks through the fibrous ring due to a crack or tear. This can lead to pain radiating in the leg and possible severe functional impairment (1,2). The exact cause of radiating leg pain is not straightforward and the origin of the pain remains rather complex and controversial (3–5). Magnetic resonance imaging (MRI) and diffusion tensor imaging (DTI) are techniques that can be used to investigate and quantify the spinal cord and nerve roots properties and potential nerve damage. T1 and T2-weighted images can display the nerves but do not reveal quantitative functional measures. DTI has the ability to determine diffusion measures which can be associated with for example inflammation processes (6,7). DTI has been used to quantify the diffusion properties of compressed nerve roots due to lumbar disc herniation (4,8–11). However, most of these methods used ROI based analysis which is time consuming and subjective. In comparison tract based methods for analysis of DTI data use fiber tractography to reconstruct the nerves and sample the diffusion parameters. Such methods are less prone to user bias and are commonly used in the analysis of the brain, spinal cord and peripheral nerves (12–14). There is no existing standard and the validation of DTI is not straightforward. Earlier studies investigating the lumbosacral nerves with DTI have shown the feasibility and reproducibility to visualize the lumbosacral nerves (15–18). In this study we examined compressed nerve roots due to the lumbar disc herniation with DTI and analyzed segments of the nerve at the level of the compression together with a segmental analysis along the nerve. The aim is to investigate to what extent it is possible to determine potential changes in the diffusion parameters with DTI in compressed nerve roots due to lumbar disc herniation.

Materials and methods

MRI acquisition and patient characteristics

Local institutional review board approval was obtained for this study and written informed consent was given prior to the MRI examination. 10 patients with nerve root compression at the level of L5 and S1 due to disc herniation underwent DTI on a 3 Tesla MR system (Achieva; Philips Healthcare, Best, The Netherlands) together with 10 healthy asymptomatic age – and gender matched control subjects with no history of low back pain. DTI was performed with diffusion-weighted spin echo single-shot echo planar imaging (EPI) in the coronal plane with the following parameters; TE = 45 ms, TR = 3573 ms, number of excitations = 2, FOV 336 × 216 mm^2, matrix size 112 × 72, 25 slices with thickness = 3.0 mm, resulting in a voxel

size of 3.0 × 3.0 × 3.0 mm^3, half scan 0.62, SPIR fat suppression, b-values 0 and 800 s/mm^2, and 15 gradient directions. The total acquisition time was 4:20 minutes. In addition, T1, and T2, and 3D TSE scans were obtained both in coronal and sagittal plane.

Data processing

First visual inspection of all data was performed to check for artifacts and overall data quality. If the data quality was sufficient DTI analysis and FT were performed with the diffusion MRI-toolbox *ExploreDTI* to determine tract based fractional anisotropy (FA), mean diffusivity (MD), axial diffusivity (AD), and radial diffusivity (RD) in the nerve roots of L5 or S1 of lumbar disc herniated patients and healthy controls (19). Whole volume tractography was performed on all datasets where FT was allowed in all voxels with a FA>0.05 and a MD> 0.8×10^{-3} mm^2/s. Segments of 3 cm were obtained from the level of where the nerve branched with the cauda equina to further distal using 'AND' ROIs (**Figure 1** right image) and included the compression on the nerve root due to disc herniation which was located in the second part of the segment. The T1, T2 and 3D TSE data was used to check the validity of the found tract segments. These segments were then subsampled in 11 different measurements along the nerve root, where diffusion parameters were calculated based on the center line voxels to prevent partial volume effects (12,14,20). The average of these 11 measurement points was used in the statistical analysis.

Statistical analysis

A paired T-test was used to test for any differences in the average diffusion measures of the segments between 1) left and right side of the nerve root in healthy controls, and 2) left and right side of the healthy not compressed nerve roots in patients, and 3) the compressed nerve roots and their contralateral side.

To determine whether the position of sampling along the tract (i.e. beginning/proximal, i.e. measurement point 1, middle, measurement point 6, or end/distal, measurement point 11, of the nerve segment) matters, a one-way repeated measures analysis of covariance (ANCOVA) was used with 'level' and 'groups' as covariate to determine whether there are differences in diffusion measures along the nerve. A p-value of 0.05 was found to be significant for all statistical analyses.

Multivariate ANCOVAs with 'level' as covariate were used to investigate difference in three cases 1) the compressed nerve roots and those of healthy controls, 2) contralateral nerve roots and those of healthy controls, and 3) the healthy nerve roots of patients and those of healthy controls.

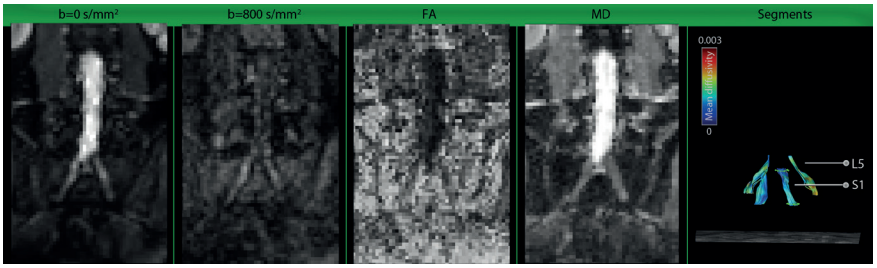

Figure 1: Raw data displayed as b=0 s/mm², b=800 s/mm², fractional anisotropy (FA), and mean diffusivity (MD) maps, from left to right respectively. The most right image indicates fiber tract segments of the nerve roots at the level of L5 and S1 reconstructed with two 'AND' ROIs.

Results

MRI processing and patient characteristics

10 patients (one female) with a mean age 38 years (range 29 –56 years) with disc herniation with compression at the level of L5 right (2 patients), S1 left (7 patients), and S1 right (1 patient) were included. Duration of symptoms before the MRI scan was on average 8.5 months (range 4.5 – 15.5 months). All patients had a typical radicular distribution of the pain associated to the radicular syndrom. In 9 out of 10 patients the symptoms matched with radiological findings. In one case the patient suffered from pain in the right leg but radiological findings showed nerve root compression at S1 left. In addition, 10 healthy controls (one female) with a mean age of 38 years (range 29 – 57 years) were included. Data quality was sufficient in all cases based on visual inspection, and did not contain any artifacts which may interfere with further analysis of the data. An example of the raw DTI data together with the FA and MD maps and the obtained tract segment is displayed in **Figure 1**. Fiber tracts of L5 and S1 were possible to reconstruct in all datasets. **Figure 2** displays fiber tracts of L5 and S1 in a patient and in a healthy control together with the 3D TSE. The compressed nerve root is indicated with an arrow.

Diffusion parameters and fiber tractography

There were no differences in the diffusion parameters of the nerve roots on the left and right side in healthy controls and between the left and right side of the healthy nerve roots in patients. Therefore, the average value of the diffusion parameters of the left and right nerve root side for each level was used for further analysis.

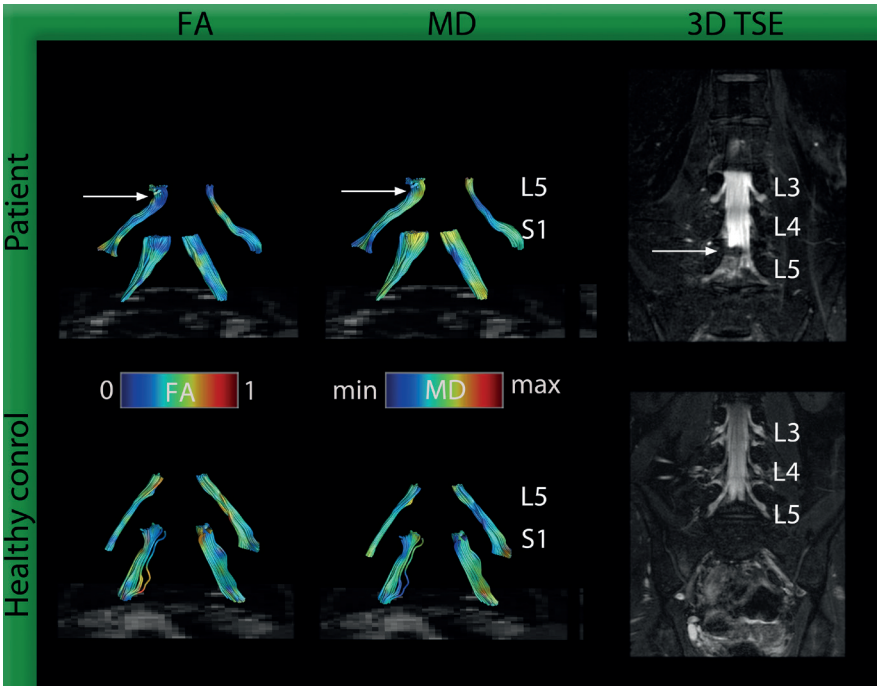

Figure 2: Registered fractional anisotropy (FA) and mean diffusivity (MD) maps with fiber tracts of the segments of L5 and S1 nerves of a patient and a healthy control together with the 3D TSE scan. The arrow indicates the location of the compressed nerve root.

Figure 3 shows plots of the diffusion parameters (FA, MD, AD and RD) over 11 measurements points along the segmented nerve root of the compressed nerve, the contralateral side, and the healthy nerve roots in patients, and the nerve roots in healthy controls at the same level as the patients. More proximal (measurement point 1), FA was lower than in the middle of the nerve (measurement point 6) (0.22 ± 0.06, and 0.28 ± 0.05, $p<0.0005$), and at the end of the nerve root more distal (measurement point 11) (0.31 ± 0.05, $p<0.0005$) for all groups combined. FA at the middle of the nerve was also lower than more distal (measurement point 6 vs 11, $p=0.024$). The MD, and RD were higher more proximal compared to the middle and distal ($1.77 \pm 0.42 \times 10^{-3}$ mm^2/s and $1.28 \pm 0.20 \times 10^{-3}$ mm^2/s for MD, and $1.58 \pm 0.42 \times 10^{-3}$ mm^2/s and $1.08 \pm 0.19 \times 10^{-3}$ mm^2/s for RD for measurement point 1 and 6 respectively, $p<0.0005$). There was no difference in these diffusion measures between the middle of the segment and more distal ($1.20 \pm 0.21 \times 10^{-3}$ mm^2/s for MD, and $1.00 \pm 0.19 \times 10^{-3}$ mm^2/s for RD for measurements 11, $p>0.072$). There were no differences in AD values between these three measurement points along the segment ($2.17 \pm 0.45 \times$

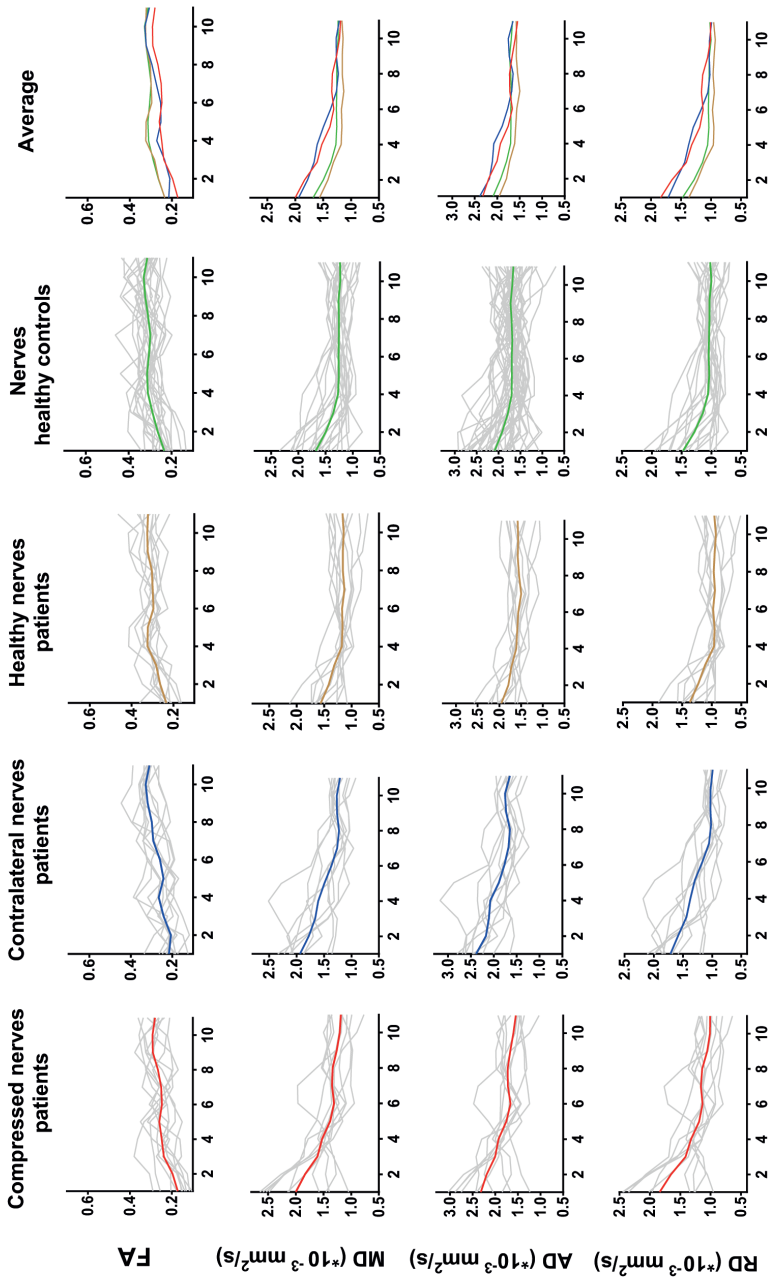

Figure 3: Diffusion parameters (FA, MD, AD, and RD) plotted over the segmented nerve roots starting at measurement 1 (proximal) and ending at measurement 11 (distal) over a segment of 3 cm in patients and healthy controls.

10^{-3} mm^2/s, 1.69 ± 0.24 × 10^{-3} mm^2/s, and 1.62 ± 0.26 × 10^{-3} mm^2/s for measurement point 1, 6 and 11 respectively). The along tract diffusion estimates shown in **Figure 3** shows an apparent difference between the compressed and contralateral nerve roots in patients (blue and red line) compared to the non-compressed healthy nerve roots of patients and healthy controls (green and brown line). However, these differences are mostly in the first part (proximal part) of the tract segments.

Table 1 and **Figure 4** show the average diffusion parameters of the entire nerve roots of the compressed nerves, the contralateral side, and the healthy nerve roots in patients and the nerve roots in healthy controls. There were no differences in any of the diffusion parameters between the compressed versus the contralateral nerve root ($p>0.133$). In comparison, the diffusion parameters of the compressed side in patients compared to nerve roots in healthy controls did reveal significant differences. We found a difference in FA (0.25±0.03 in compressed nerve roots, and 0.30±0.04 in healthy controls, $p=0.004$), and in RD (1.27±0.15 × 10^{-3} mm^2/s in compressed nerve roots, and 1.11±0.14 × 10^{-3} mm^2/s in healthy controls, $p=0.029$) but not in MD ($p=0.14$) or AD ($p=0.96$). There was no difference in any of the diffusion measures between contralateral nerve roots in patients and nerve roots of healthy controls ($p>0.06$), nor between the healthy nerve roots in patients and healthy controls ($p>0.27$).

Table 1: Diffusion parameters of the nerve roots of the compressed nerves and the contralateral side in patients and the mean diffusion values at the same level in healthy controls based of the center line voxels

	Patients			Healthy controls
	Compressed nerve roots	**Contralateral nerve roots**	**Healthy nerves patients**	**Mean of nerve roots**
FA	0.25±0.03*	0.27±0.02	0.30±0.02	0.30±0.04*
MD (× 10^{-3} mm^2/s)	1.45±0.15	1.47±0.18	1.23±0.13	1.32±0.15
AD (× 10^{-3} mm^2/s)	1.83±0.17	1.91±0.22	1.64±0.17	1.76±0.17
RD (× 10^{-3} mm^2/s)	1.27±0.15*	1.26±0.16	1.03±0.11	1.11±0.14*

*Significant different; $p<0.05$

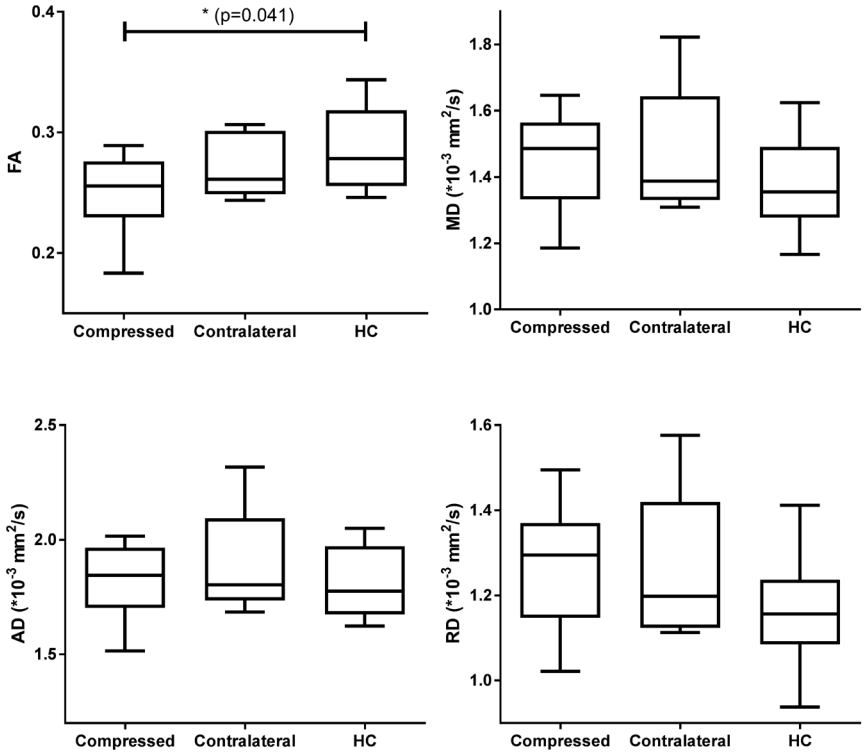

Figure 4. Box plots of the compressed nerve roots in patients, and the contralateral nerve roots in patients, the healthy nerve roots in patients, and the healthy nerve roots in healthy controls. Significant differences were found in the FA and RD between compressed nerve roots and healthy controls (HC) (p=0.004 and p=0.029 respectively). No differences were found in any of the other diffusion parameters.

Discussion

In this study we investigated diffusion parameters in compressed nerve roots (L5 and S1) of patients with lumbar disc herniation and healthy controls. We were not able to detect differences in the average diffusion parameters between the compressed nerve roots and their contralateral side, but we did show significant differences in FA and RD between the compressed nerve roots at the level of the disc hernation and the nerve roots of healthy controls.

Experimental studies report chronic compression and chemical irritation of the lumbar nerve roots which induces different histological changes in the nerve. This involves for example an increase in vascular permeability with disrupted nerve root barrier, development of intraneural oedema and hyperaemia in and around the

nerve. Compression of the nerve roots can induce reduced blood flow and ischaemia which leads to demyelination of nerve fibers, Wallerian degeneration, and endoneural cracking (21–23). This may then lead to a change in water diffusion in the nerve tissue by an increase in space between the axons and axon fascicles, which may explain the lower FA and RD values found in the compressed nerve roots. However, we did not observe any difference in MD values which was previously found in other studies investigating patients suffering from lumbar disc herniations with DTI (4,8,24,25). These earlier studies did not report AD, or RD values of the nerve roots. Chuanting et al reported in compressed nerve roots a higher MD (MD = 2.07×10^{-3} mm^2/s) compared to healthy controls (1.76×10^{-3} mm^2/s), and lower FA in patients (FA = 0.25) compared to healthy controls (FA=0.33). Compared to this study, the MD values in our study were lower (1.45×10^{-3} mm^2/s in patients), but FA values were comparable to the patient group (FA = 0.25 in patients). Wu et al reported diffusion values before and after endoscopic discectomy in patients with lumbar disc herniation (26). Their FA values of the compressed nerve roots are slightly lower (FA=0.16) compared to our study, and the FA of the contralateral side was comparable to healthy controls in our study (FA=0.26). MD values were similar to our results (1.427×10^{-3} mm^2/s in the compressed nerve roots and 1.363×10^{-3} mm^2/s in the contralateral side). Although we did not find a difference in MD, we did find a difference in RD (i.e. the diffusion perpendicular to the main orientation of the nerve), which could be explained by the earlier explained mechanisms such as demyelination of the nerves and is potentially the basis of a higher MD. Furthermore, in contrast to earlier studies reporting diffusion measures of compressed nerves in herniated disc patients, we did not find significant differences between any of the diffusion parameters of the compressed nerve roots and their contralateral side (4,8,11,25,26). A possible explanation for this could be the potential differences in duration of the nerve compression and severity of symptoms, although these factors were not reported in these earlier studies.

Partial volume effects may influence the results, since we used a voxel size of 3 mm isotropic (14,27). Diffusivity estimates obtained from the nerve roots may increase due to their surrounding tissue (14). However, this does not provide an explanation for the observations that there were no significant differences in diffusion parameters between the compressed nerve roots and their contralateral side. Furthermore, we tried to minimize the bias due to partial voluming by including only those voxels that are in the center of the tracts (center line sampling). Further improvement in acquisition protocols and processing strategies will help to more accurately calculate diffusion parameters (28).

We observed that there was a difference of the diffusion measures of the nerve segments along the trajectory of the tracked segment (i.e. proximal, middle and distal part of the nerve segment), indicating that diffusion estimates depend on the location of where the tract is being sampled. High values of MD were found in the first segment, with decreasing values more distal along the nerve root, which is in line with the study of Chiou et al (29). The earlier reported differences between diffusion measures among different studies can be explained by the difference in sampling locations along the nerve (i.e. MD of 2.07×10^{-3} mm^2/s as reported by (4) is likely to be sampled more proximal and MD of 1.45×10^{-3} mm^2/s as reported by (26) is likely to be sampled more distal along the nerve). The difference in diffusion measures (FA and RD) between compressed nerve roots and healthy controls was most prominent in the first part of the nerve segment indicating that potential differences are more likely to be tracked in this part compared to the more distal part of the nerve segment. These are important findings, also in other nerve related injuries, as it can affect segmentation strategies. When performing manual ROI analysis one should take great care to sample all nerves at the same location to prevent any bias due to the positioning of the ROI.

In conclusion, this study showed the use of DTI to investigate nerve roots in patients suffering from nerve root compression due to disc herniation. No differences in diffusion parameters between the compressed nerve roots and their contralateral side were found. We did however find differences in FA and RD between the compressed nerve roots and the nerve roots at the same level in healthy controls. This suggests that there are pathofysiological processes affecting the nerves at the level of the compression. Trajectory analysis shows that the location at which diffusion estimates are extracted along the nerve segment is of importance.

Acknowledgements

We would like to thank all the patients and volunteers who participated in this study.

References

1. Ohnmeiss DD, Vanharanta H, Ekholm J. Degree of disc disruption and lower extremity pain. Spine (Phila Pa 1976). 1997;22(14):1600–1605.
2. Valat J-P, Genevay S, Marty M, Rozenberg S, Koes B. Sciatica. Best Pract Res Clin Rheumatol. 2010;24(2):241–252.
3. Stafford MA, Peng P, Hill DA. Sciatica: a review of history, epidemiology, pathogenesis, and the role of epidural steroid injection in management. Br J Anaesth. 2007;99(4):461–473.
4. Chuanting L, Qingzheng W, Wenfeng X, Yiyi H, Bin Z. 3.0T MRI tractography of lumbar nerve roots in disc herniation. Acta Radiol. 2014; 55(8):969-975.
5. Panagopoulos J, Hush J, Steffens D, Hancock MJ. Do MRI Findings Change over a Period of Up to 1 Year in Patients with Low Back Pain and/or Sciatica? Vol. 42, Spine. 2017. 504–512.
6. Basser PJ, Pajevic S, Pierpaoli C, Duda J, Aldroubi A. In vivo fiber tractography using DT-MRI data. Magn Reson Med. 2000;44(4):625–632.
7. DeBoy CA, Zhang J, Dike S, Shats I, Jones M, Reich DS, et al. High resolution diffusion tensor imaging of axonal damage in focal inflammatory and demyelinating lesions in rat spinal cord. Brain. 2007;130(8):2199–2210.
8. Balbi V, Budzik J-F, Duhamel A, Bera-Louville A, Thuc V, Cotten A. Tractography of lumbar nerve roots: initial results. Eur Radiol. 2011;21(6):1153–1159.
9. Li X, Chen J, Hong G, Sun C, Wu X, Peng MJ, et al. In vivo DTI longitudinal measurements of acute sciatic nerve traction injury and the association with pathological and functional changes. Eur J Radiol. 2013;82(11):e707-714.
10. Eguchi Y, Ohtori S, Orita S, Kamoda H, Arai G, Ishikawa T, et al. Quantitative evaluation and visualization of lumbar foraminal nerve root entrapment by using diffusion tensor imaging: preliminary results. AJNR Am J Neuroradiol. 2011;32(10):1824–1829.
11. Shi Y, Zong M, Xu X, Zou Y, Feng Y, Liu W, et al. Diffusion tensor imaging with quantitative evaluation and fiber tractography of lumbar nerve roots in sciatica. Eur J Radiol. 2015;84(4):690–695.
12. Colby JB, Soderberg L, Lebel C, Dinov ID, Thompson PM, Sowell ER. Along-tract statistics allow for enhanced tractography analysis. Neuroimage. 2012;59(4):3227–3242.
13. Van Hecke W, Leemans A, Sijbers J, Vandervliet E, Van Goethem J, Parizel PM. A tracking-based diffusion tensor imaging segmentation method for the detection of diffusion-related changes of the cervical spinal cord with aging. J Magn Reson Imaging. 2008;27(5):978–991.
14. Vos SB, Jones DK, Viergever MA, Leemans A. Partial volume effect as a hidden covariate in DTI analyses. Neuroimage. 2011;55(4):1566–1576.
15. van der Jagt PKN, Dik P, Froeling M, Kwee TC, Nievelstein R a J, ten Haken B, et al. Architectural configuration and microstructural properties of the sacral plexus: a diffusion tensor MRI and fiber tractography study. Neuroimage. 2012;62(3):1792–1799.
16. Hiltunen J, Suortti T, Arvela S, Seppa M, Joensuu R, Hari R. Diffusion tensor imaging and tractography of distal peripheral nerves at 3 T. Clin Neurophysiol. 2005;116(10):2315–2323.

17. Haakma W, Pedersen M, Froeling M, Uhrenholt L, Leemans A, Boel LWT. Diffusion tensor imaging of peripheral nerves in non-fixed post-mortem subjects. Forensic Sci Int. 2016;263:139–146.

18. Haakma W, Hendrikse J, Uhrenholt L, Leemans A, Warner Thorup Boel L, Pedersen M, et al. Multicenter Reproducibility Study of Diffusion MRI and Fiber Tractography of the Lumbosacral Nerves. J Magn Reson Imaging. 2018;0(0):000–000.

19. Leemans A, Jeurissen B, Sijbers J, Jones D. ExploreDTI: a graphical toolbox for processing, analyzing, and visualizing diffusion MR data. Proc 17th Sci Meet Int Soc Magn Reson Med. 2009;17(2):3537.

20. Perrone D, Aelterman J, Pižurica A, Jeurissen B, Philips W, Leemans A. The effect of Gibbs ringing artifacts on measures derived from diffusion MRI. Neuroimage. 2015;120:441–455.

21. Yoshizawa H, Kobayashi S, Morita T. Chronic nerve root compression. Pathophysiologic mechanism of nerve root dysfunction. Vol. 20, Spine. 1995. 397–407.

22. Beaulieu C, Does MD, Snyder RE, Allen PS. Changes in water diffusion due to Wallerian degeneration in peripheral nerve. Magn Reson Med. 1996;36(4):627–631.

23. Stanisz GJ, Midha R, Munro C a, Henkelman RM. MR properties of rat sciatic nerve following trauma. Magn Reson Med. 2001;45(3):415–420.

24. Eguchi Y, Ohtori S, Yamashita M, Yamauchi K, Suzuki M, Orita S, et al. Diffusion-weighted magnetic resonance imaging of symptomatic nerve root of patients with lumbar disk herniation. Neuroradiology. 2011;53(9):633–641.

25. Zhang J, Zhang F, Xiao F, Xiong Z, Liu D, Hua T, et al. Quantitative Evaluation of the Compressed L5 and S1 Nerve Roots in Unilateral Lumbar Disc Herniation by Using Diffusion Tensor Imaging. Clinical Neuroradiology. 2017. 1–9.

26. Wu W, Liang J, Chen Y, Chen A, Wu B, Yang Z. Microstructural changes in compressed nerve roots treated by percutaneous transforaminal endoscopic discectomy in patients with lumbar disc herniation. Med (United States). 2016;95(40):0–4.

27. Hogan Q. Size of human lower thoracic and lumbosacral nerve roots. Anesthesiology. 1996;85(1):37–42.

28. Cervantes B, Van AT, Weidlich D, Kooijman H, Hock A, Rummeny EJ, et al. Isotropic resolution diffusion tensor imaging of lumbosacral and sciatic nerves using a phase-corrected diffusion-prepared 3D turbo spin echo. Magn Reson Med. 2018; 609-618.

29. Chiou SY, Hellyer PJ, Sharp DJ, Newbould RD, Patel MC, Strutton PH. Relationships between the integrity and function of lumbar nerve roots as assessed by diffusion tensor imaging and neurophysiology. Neuroradiology. 2017;59(9):893–903

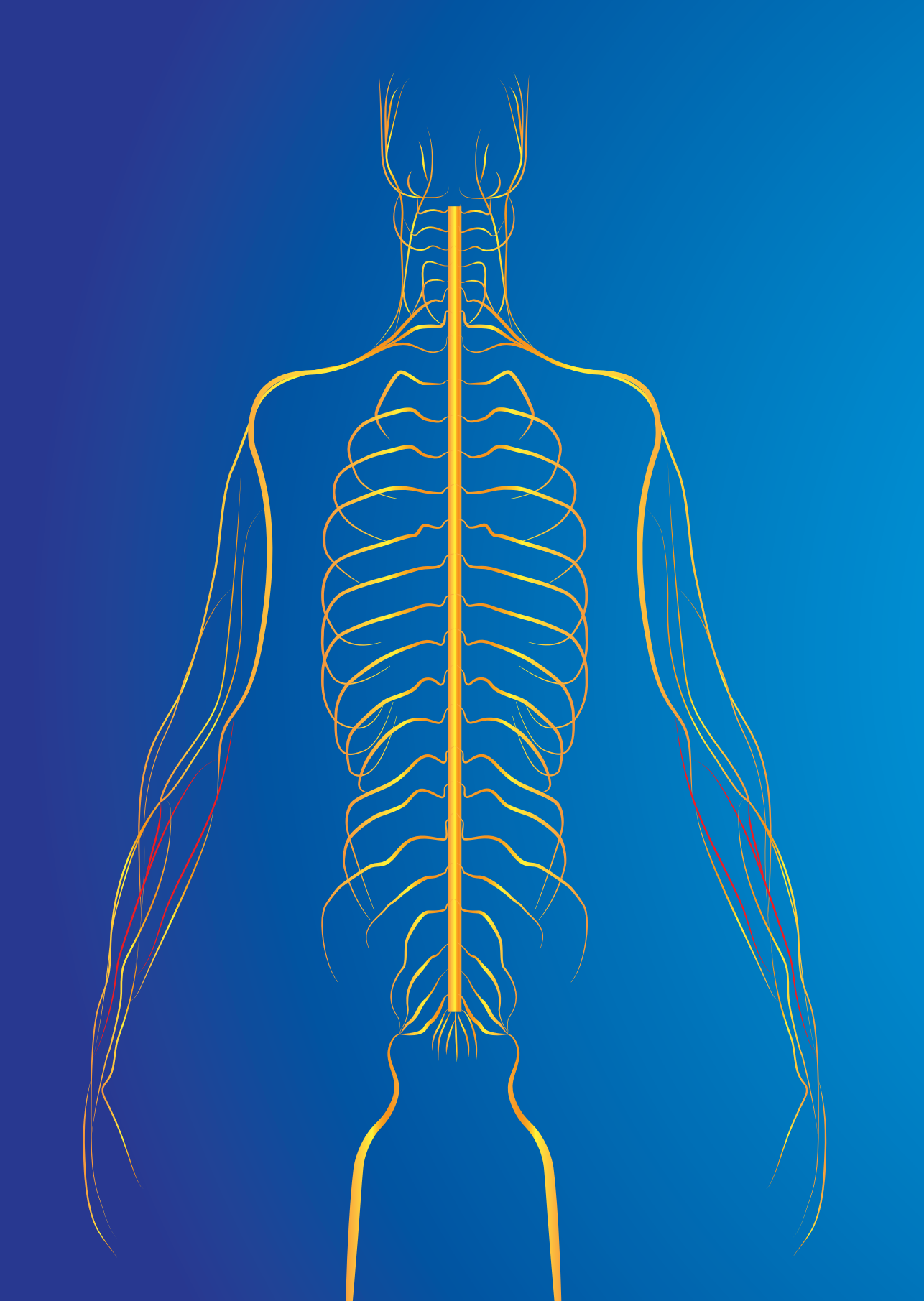

Chapter 5

MRI shows thickening and altered diffusion in the median and ulnar nerves in multifocal motor neuropathy

Wieke Haakma
Bas A. Jongbloed
Martijn Froeling
H. Stephan Goedee
Clemens Bos
Alexander Leemans
Leonard H. van den Berg
Jeroen Hendrikse
W. Ludo van der Pol

European Radiology 2017; 27; 2216-2224, DOI: 10.1007/s00330-016-4575-0

Abstract

Objectives

To study disease mechanisms in multifocal motor neuropathy (MMN) with magnetic resonance imaging (MRI) and diffusion tensor imaging (DTI) of the median and ulnar nerves.

Methods

We enrolled 10 MMN patients, 10 with amyotrophic lateral sclerosis (ALS) and 10 healthy controls (HC). Patients underwent MRI (in prone position) and nerve conduction studies. DTI and fat-suppressed T2-weighted scans of the forearms were performed on a 3.0T MRI scanner. Fiber tractography of the median and ulnar nerve was performed to extract diffusion parameters: fractional anisotropy (FA), mean (MD), axial (AD), and radial (RD) diffusivity. Cross-sectional areas (CSA) were measured on T2-weighted scans.

Results

Forty-five out of 60 arms were included in the analysis. AD was significantly lower in MMN patients ($2.20\pm0.12\times10^{-3}$ mm^2/s) compared to ALS patients ($2.31\pm0.17\times10^{-3}$ mm^2/s; $p<0.05$) and HC ($2.31\pm0.17\times10^{-3}$ mm^2/s; $p<0.05$). Segmental analysis showed significant restriction of AD, RD and MD ($p<0.005$) in the proximal third of the nerves. CSA was significantly larger in MMN patients compared to ALS patients and HC ($p<0.01$).

Conclusions

Thickening of nerves is compatible with changes in myelin sheath structure, whereas lowered AD values suggest axonal dysfunction. These findings suggest that myelin and axons are diffusely involved in MMN pathogenesis.

Introduction

Multifocal motor neuropathy (MMN) is a rare disorder characterized by progressive, asymmetric and predominantly distal limb weakness without any sensory involvement (1). The diagnosis of MMN is mainly based on the combination of clinical characteristics and specific nerve conduction abnormalities, i.e. conduction block. MMN is a mimic of the early phases of amyotrophic lateral sclerosis (ALS) and progressive muscular atrophy from which it needs to be distinguished, since the prognosis of MMN is much better than that of motor neuron disorders. Although patients with MMN respond to treatment with intravenous or subcutaneous immunoglobulins (2–4), progressive weakness of arms and hands due to accumulating axonal damage causes severe disability in a subgroup of patients (1,5).

The pathogenic mechanisms that underlie MMN are incompletely understood. The presence of anti-GM1 IgM antibodies in more than half of the patients may suggest that MMN is caused by anti-GM1 antibody mediated damage at or in the proximity of the nodes of Ranvier. This likely plays a role in the phenomenon of conduction block and in the demyelination or disruption of the compact myelin structure (2,6). Demyelination or disruption of the compact myelin structure represents an alternative pathogenic mechanism that causes MMN (6). There are few pathological studies of affected motor nerves (7,8), and there are no animal models for MMN. There is a need for new methodology to elucidate MMN pathogenesis and to eventually improve treatment strategies.

Magnetic resonance imaging (MRI) can be used to study the brachial plexus and peripheral nerves (9,10). MRI T1 and T2 weighed images can provide anatomical detail and diffusion tensor imaging (DTI) techniques information on the microstructural organization of nervous tissue (11–13) and peripheral nerves (14–17). This unique combination may help to identify relevant disease mechanisms in patients with MMN. In this study, we therefore used MRI and DTI to visualize the median and ulnar nerves in the forearm of patients with MMN, ALS and healthy controls.

Materials and methods

Patient characteristics

We enrolled 10 patients with MMN, 10 patients with ALS and 10 healthy controls at the neuromuscular outpatient clinic of the University Medical Centre Utrecht, a tertiary referral center for neuromuscular disorders. Patients with MMN and ALS

fulfilled diagnostic consensus criteria for definite or probable MMN and the El Escorial criteria for ALS, respectively (4,18). All patients with ALS had clinical signs of lower motor neuron involvement (i.e. weakness, atrophy and/or fasciculations) in the forearm or hand. Patients and healthy controls were matched for age and gender. All patients with MMN were on immunoglobulin maintenance treatment and all patients with ALS used riluzole. All patients and healthy controls underwent a standardized clinical examination including muscle strength testing of the wrist, thumb and finger flexion, opponens pollicis, abductor pollicis brevis, finger spreading and adductor pollicis, together with sensory testing. Clinical examinations, electromyogram and MRI studies were performed on the same day. The local institutional review board approved this study and we obtained written informed consent from each subject prior to inclusion.

Nerve conduction study protocol

Nerve conduction studies were performed using a Nicolet VIKING IV electromyogram machine (CareFusion, Tokyo, Japan) after the limbs were warmed in water at 37°C for 30 minutes. One of us (SG) was unaware of the clinical diagnosis and performed nerve conduction studies using a shortened version of a previously published protocol (4), consisting of motor nerve stimulation of the median nerve (recording m. abductor pollicis brevis) and ulnar nerve (recording m. abductor digiti V) on both sides up to the axilla. We used the definition of conduction block as described in the diagnostic consensus criteria for MMN (18). Axonal loss was defined as a decrease of distal compound muscle action potential (CMAP) below to 2 standard deviations of the lower limit of normal, i.e. a CMAP <3.5mV for the median nerve and a distal CMAP of <2.8mV for the ulnar nerve.

MRI protocol and data acquisition

All subjects underwent MRI of both forearms. Scans were acquired on a 3 Tesla MR system (Achieva, Philips Healthcare, Best, the Netherlands) with a 32-channel phased-array surface coil. Patients were positioned in a prone position with one arm placed above the head as described previously (19). Patients were repositioned when the other arm was scanned. DTI was performed based on diffusion weighted spin echo single-shot echo planar imaging in the axial plane with the following parameters: TE = 66 ms, TR = 6340 ms, SENSE factor 2, FOV 240 × 120 mm^2, matrix size 160 × 80, 60 slices with thickness = 4.0 mm, resulting in a voxel size of 1.5 × 1.5 × 4.0 mm^3, half scan 0.69, SPIR fat suppression, b-values 0, and 800 s/mm^2, NSA = 1, and 15 gradient directions. The total acquisition time was 9:32 minutes. As an anatomical reference, axial fat-suppressed T2-weighted scans were acquired

with the following parameters: TE=90 ms, TR=7139 ms, SENSE factor 1.5, FOV 120 × 120 mm^2, matrix size 240 × 234, slices with thickness of 4.0 mm, and spectral attenuated inversion-recovery fat suppression. One stack was used with 60 slices for both the DTI and the T2-weighted scan. Scans with low quality, evaluated by visual inspection, for example due to movement, were excluded from analysis.

DTI processing

The DTI data was processed using ExploreDTI (www.ExploreDTI.com) (20). Images were corrected for subject motion, eddy current induced distortions, and susceptibility artifacts (21,22). Diffusion tensors were calculated using the REKINDLE method (23) and subsequently diffusion parameters were obtained, which consisted of 1) the fractional anisotropy (FA), 2) the mean diffusivity (MD), 3) the axial diffusivity (AD), and 4) the radial diffusivity (RD) (14). A standardized deterministic streamline approach was used to reconstruct the fiber tract (24).

Fiber tractography and diffusion parameters

To visualize the nerves and extract diffusion parameters, tractography was used. FA range was set to 0.1-0.9, step size of 1 mm, minimum fiber length was set to 100 mm, and the fiber angle was set to 30° per integration step. Fiber tracts, generated by whole volume seeding (1.5×1.5×1.5 mm^3), belonging to the forearm nerves were selected by placing 'AND' region of interests (ROI) in 4 locations in the arm: at the level of the pronator quadratus, 1/3 of the ulna, 2/3 of the ulna, and the junction of the supinator with the radius (16) as shown in **Figure 1**. These locations were chosen as they are relatively easy to locate and therefore provide a reproducible way of selecting the ROIs in each patient in the same way across subjects. 'AND' ROIs only select those tracts that run through all the 'AND' ROIs. This means that from all the fiber tracts generated from whole volume seeding, only those are selected that span all 4 predefined locations in the arm. Resulting tracts were used to calculate the diffusion parameters.

To investigate if DTI parameters were biased by the number of tracts and tract length (25), and to investigate to what extent diffusion metrics are distributed homogeneously along the nerve, additional analyses of shorter nerve segments were performed. For this purpose the forearm was subdivided into three segments defined by the ROI positions as described above and shown in **Figure 1**. Tracts were selected for each of these individual subsections defined by only 2 of the 4 'AND' ROIs and diffusion parameters were calculated for each of the three segments individually.

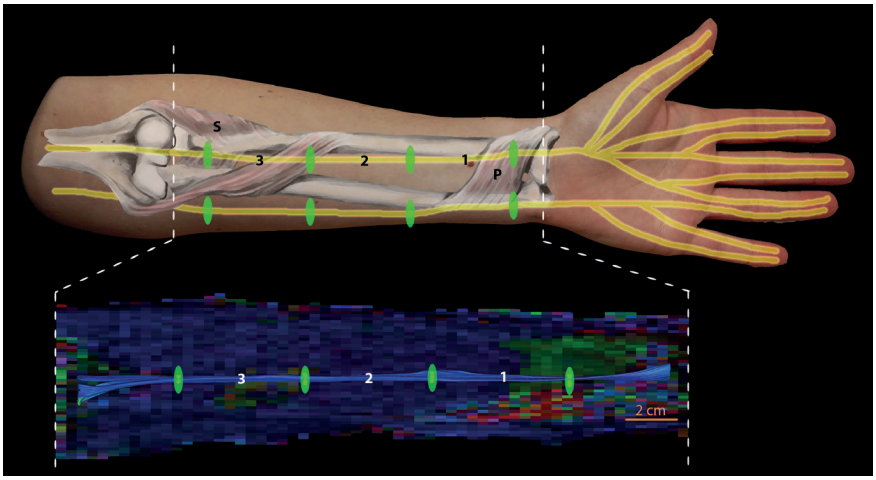

Figure 1: Overview of the region of interest (ROI) positioning along the nerves in the arm (upper image), and the color-encoded DTI (lower image) where green indicates anterior-posterior, red indicates left-right, and blue indicates inferior-superior. The first ROI was placed at the pronator quadratus (P), second and third ROI at 1/3 and 2/3 of the ulna respectively, and the fourth ROI was placed at the location of the junction of the supinator (S) with the radius. The tracts were analyzed along the entire segment, and segment 1, 2, and 3 individually.

Cross-sectional areas

Nerve cross-sectional area (CSA) was assessed on T2-weighted scans, at the predefined 4 locations in the arm: at the level of the pronator quadratus, 1/3 of the ulna, 2/3 of the ulna, and the junction of the supinator with the radius as shown in **Figure 1**. The mean CSA of each nerve was then calculated based on the average CSA of these 4 locations.

Statistical analysis

We used SPSS version 20.0 (SPSS Inc. Chicago, IL, USA) for statistical analysis. A general linear model was used to compare the DTI parameters and the CSA measurements between the three groups. We used Bonferroni correction to correct for multiple testing. The analysis was performed for the whole nerve segment as well as for the individual segments and were based on both median and ulnar nerves. Correction for clustering of the data of scanning two arms in one patient was included into the model, and sex and age were taken into account (13). Pearson correlation was used to check for correlation between the CSA and the diffusion parameters, and between duration of symptoms and diffusion parameters, where $p<0.05$ was considered to be significant.

Results

Patient characteristics and nerve conduction studies

Patient characteristics are summarized in **Table 1**. There was a significant difference in duration of symptoms (p<0.001) between patients with MMN and ALS. Distribution and severity of weakness was similar in both patient groups. Nerve conduction studies showed conduction block in 7 out of 40 (18%) nerves, all in patients with MMN. Distal CMAP amplitudes were consistent with axonal loss.

Table 1: Characteristics of patients with multifocal motor neuropathy (MMN) amyotrophic lateral sclerosis (ALS) and healthy controls

	MMN (n=10)	ALS (n=10)	Healthy controls (n=10)
Mean age in years (range)	54 (29-67)	53 (40-60)	54 (29-67)
Male (%)	8 (80%)	8 (80%)	8 (80%)
Median duration of symptoms in months (range)	52 (11-124)*	11 (6-34)*	-
Median duration of treatment in months (range)	12 (1-39)	4 (1-24)	-
Weakness lower arm (%)	15/20 (75%)	15/20 (75%)	-
Number of conduction blocks (%)	7 (18%)	0 (0%)	0 (0%)
Number of nerves with distal compound muscle action potential < lower limit of normal (%)	6 (15%)	8 (20%)	0 (0%)

*p<0.001

MRI protocol and data acquisition

Data quality in patients was lower than in healthy controls. Based on visual inspection, DTI images of 15 out of 60 arms (7 arms of MMN patients, 6 arms of ALS patients, and 2 arms of healthy controls) had to be excluded due to motion distortion or other MR related problems resulting in a total of 45 scans of arms that were available for analysis. T2-weighted scans of 9 out of 60 arms (3 arms of MMN patients, 4 arms of ALS patients, and 2 arms of healthy controls) had to be excluded, resulting in a total of 51 arms that were used for analysis.

Fiber tractography

The median and ulnar nerves could be reconstructed with fiber tractography in 40 of the 45 datasets. **Figure 2** shows the tracts derived from the median and ulnar nerves in patients with MMN, and ALS as well as in a healthy control. In 5 datasets tracts could not be reconstructed in 7 nerves (6 nerves of 4 MMN patients, and 1 nerve in a healthy control).

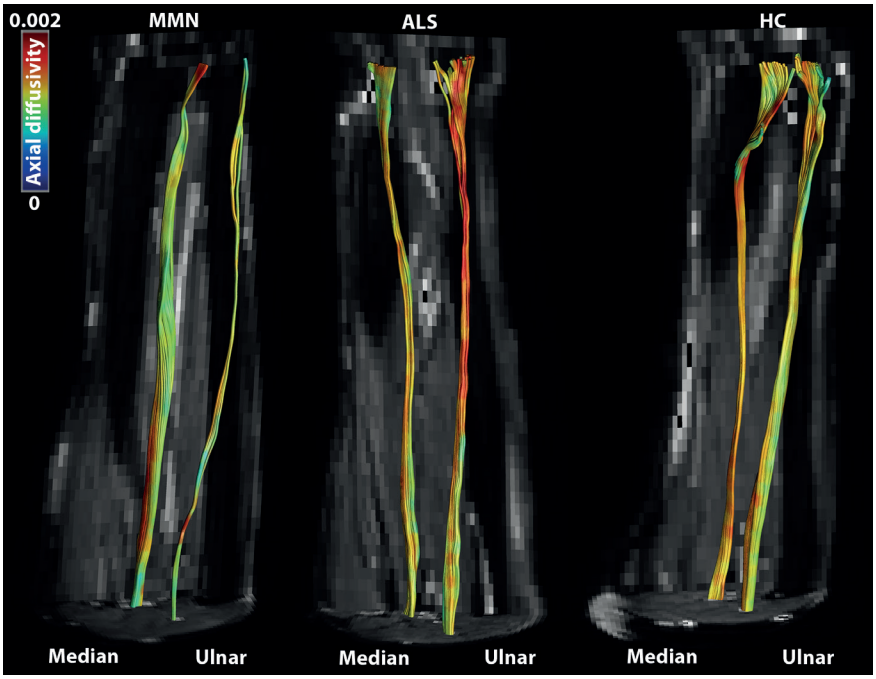

Figure 2: Fiber tractography of the median and ulnar nerve in a multifocal motor neuropathy (MMN) patient, amyotrophic lateral sclerosis (ALS) patient, and healthy control (HC). The color-encoding is according to the axial diffusivity (in units mm^2/s).

In total 4 nerves with conduction blocks and three nerves with axonal damage remained for analyses in the MMN group, and 5 nerves with axonal damage in the ALS group.

Supplementary table 1 shows the number of tracts per nerve and nerve segment. It was not possible to find tracts in 3 nerves of segment 1 and 3, and in 2 nerves of segment 2 in patients with MMN, and in 1 nerve in segment 1 in a healthy control.

Diffusion parameters

There were no significant differences between the two arms. Therefore, left and right arms were combined in the data analysis. The calculated average diffusion parameters of all tracts belonging to the median and ulnar nerves are summarized in **Table 2**. There was a significant difference in AD of nerves of patients with MMN ($2.20\pm0.12 \times10^{-3}$ mm^2/s) compared to patients with ALS ($2.31\pm0.17 \times10^{-3}$ mm^2/s; $p<0.05$) and to healthy controls ($2.31\pm0.17 \times10^{-3}$ mm^2/s; $p<0.05$). There was no significant difference in FA, MD, and RD between the groups.

Table 2: Mean diffusion parameters (fractional anisotropy (FA), mean (MD), axial (AD), and radial (RD) diffusivity) with standard deviation (SD) based on both median and ulnar nerves in patients with multifocal motor neuropathy (MMN), amyotrophic lateral sclerosis (ALS), and healthy controls (HC).

	MMN	ALS	HC
FA			
Entire nerve [I]	0.44 ± 0.04	0.43 ± 0.05	0.44 ± 0.04
Segment 1[II]	0.43 ± 0.05	0.43 ± 0.05	0.43 ± 0.04
Segment 2 [III]	0.44 ± 0.05	0.43 ± 0.05	0.44 ± 0.05
Segment 3 [IV]	0.46 ± 0.06	0.44 ± 0.03	0.45 ± 0.04
MD ($\times 10^{-3}$ mm^2/s)			
Entire nerve	1.44 ± 0.10	1.52 ± 0.15	1.51 ± 0.14
Segment 1	1.50 ± 0.18	1.46 ± 0.17	1.51 ± 0.16
Segment 2	1.43 ± 0.16	1.49 ± 0.18	1.49 ± 0.14
Segment 3	1.38 ± 0.14**	1.50 ± 0.10**	1.45 ± 0.11
AD ($\times 10^{-3}$ mm^2/s)			
Entire nerve	2.20 ± 0.12*	2.31 ± 0.17*	2.31 ± 0.17*
Segment 1	2.26 ± 0.22	2.22 ± 0.20	2.29 ± 0.20
Segment 2	2.19 ± 0.18	2.27 ± 0.22	2.27 ± 0.15
Segment 3	2.16 ± 0.18*	2.30 ± 0.13*	2.25 ± 0.14*
RD ($\times 10^{-3}$ mm^2/s)			
Entire nerve	1.06 ± 0.10	1.13 ± 0.15	1.11± 0.14
Segment 1	1.12 ± 0.18	1.08 ± 0.16	1.11 ± 0.15
Segment 2	1.05 ± 0.16	1.11 ± 0.18	1.09 ± 0.14
Segment 3	0.99 ± 0.14**	1.11 ± 0.09**	1.05 ± 0.11

[I] Whole segment: n=20, n=28, and n=36 for resp. MMN, ALS, and HC
[II] Segment 1: n=23, n=28, and n=35 for resp. MMN, ALS, and HC
[III] Segment 2: n=24, n=28, and n=36 for resp. MMN, ALS, and HC
[IV] Segment 3: n=23, n=28, and n=36 for resp. MMN, ALS, and HC
*Significant difference in MMN versus ALS and controls ($p<0.05$)
**Significant difference in MMN versus ALS ($p<0.005$)

Results of diffusion parameters of nerves with and without reduced distal CMAP are shown in **Table 3**. Nerves with reduced distal CMAP (both MMN and ALS patients) showed lower MD, and RD values ($p<0.05$). The AD in these nerves showed a tendency (not significant $p=0.083$) towards lower values.

Segmental analysis of diffusion parameters also showed a significantly lower AD value in segment 3 for MMN patients compared to ALS patients ($p<0.005$) and healthy controls ($p<0.05$), and additionally significantly lower MD and RD ($p<0.005$) value in patients with MMN compared to those with ALS shown in **Table 2**.

Table 3: Mean diffusion parameters and cross sectional areas (CSA) of the median and ulnar nerves with reduced compound muscle action potential (CMAP) amplitudes, i.e. smaller than the lower limit of normal (LLN) reflecting axonal loss, versus nerves with normal CMAP amplitudes.

	CMAP < LLN N=8	CMAP > LLN N=76
FA	0.47 ± 0.05*	0.44 ± 0.04*
MD ($\times 10^{-3}$ mm^2/s)	1.40 ± 0.12*	1.51 ± 0.14*
AD ($\times 10^{-3}$ mm^2/s)	2.19 ± 0.14	2.30 ± 0.16
RD ($\times 10^{-3}$ mm^2/s)	1.00 ± 0.13*	1.12 ± 0.14*
CSA	7.09 ± 1.29	6.48 ± 1.37

* $p<0.05$

Cross-sectional areas

Figure 3 shows representative examples of CSA of the median nerve of a patient with MMN, ALS, and a healthy control on T2-weighted scans. Mean CSA of the median and ulnar nerves on T2-weighted scans were significantly larger in patients with MMN (median = 9.40±2.87 mm^2, and ulnar = 7.06±1.84 mm^2) compared to those with ALS (median = 7.23±1.47 mm^2, and ulnar = 5.68±0.93 mm^2) and to healthy controls (median = 6.88±1.41 mm^2, and ulnar = 5.36±0.89 mm^2) (Fig 4). There was no correlation between CSA and any of the diffusion parameters (FA, MD, AD, and RD) (max r=0.262), or between duration of symptoms and diffusion parameters

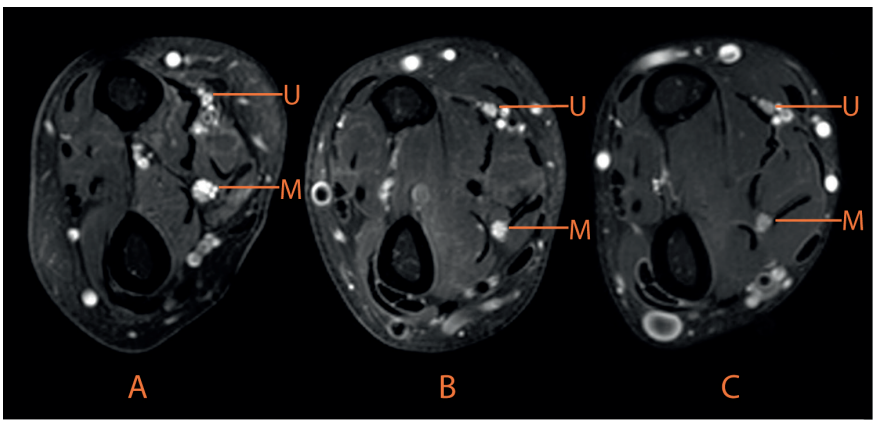

Figure 3: Axial plane of a T2-weighted scans of the forearm with the median (M), and ulnar (U) nerves. A) multifocal motor neuropathy (MMN) patient with enlargement of the median nerve, B) amyotrophic lateral sclerosis (ALS) patient, and C) healthy control.

(max r=0.391). Nerves with reduced CMAP amplitudes did not show a significant difference in CSA compared to nerves with normal CMAP amplitudes (see **Table 3**). There was no correlation between the CSA and any of the diffusion parameters (max r=0.160) in the nerves with reduced CMAP amplitudes.

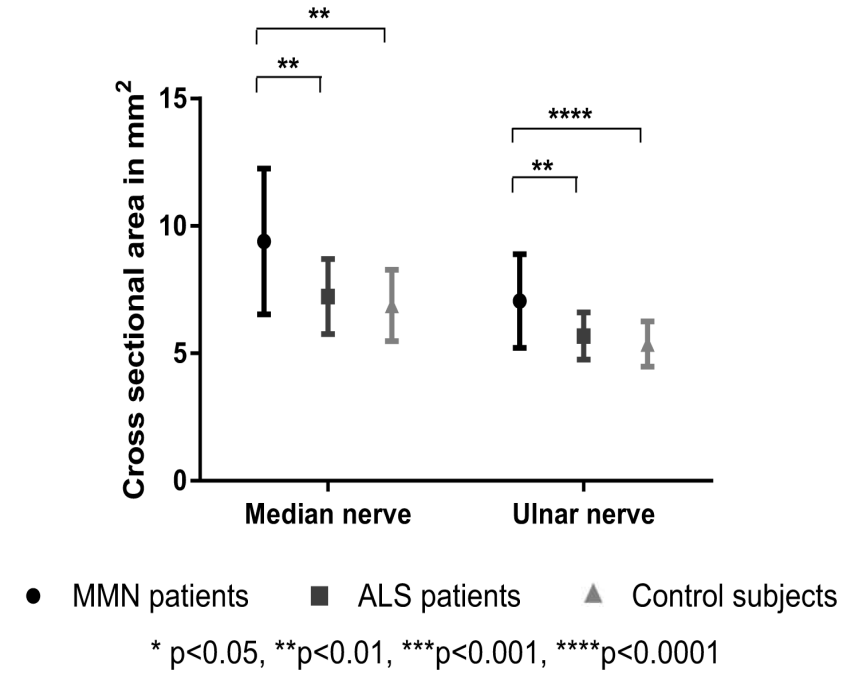

Figure 4: Cross-sectional area of the median and ulnar nerve in the forearm with standard deviation (SD). Multifocal motor neuropathy (MMN) patients differed significantly from amyotrophic lateral sclerosis (ALS) patients and healthy controls.

Discussion

This MRI study shows anatomical and diffusion abnormalities in peripheral nerves from patients with MMN. We found significant nerve enlargement in combination with a significant reduction of axial diffusion. These *in vivo* results suggest that pathogenic mechanisms in MMN might affect both the axon and myelin sheath, as was earlier suggested by pathological abnormalities near the site of conduction block (8).

The median and ulnar nerves of MMN patients were 25-30% larger than those in the healthy controls and ALS patients. The diffuse rather than focal nerve enlargement are in line with high resolution ultrasound studies of peripheral nerves (26,27) and the brachial plexus (9,28). Pathogenic mechanisms underlying MMN therefore seem to affect significant lengths of motor nerves rather than patchy and focal involvement that is suggested by the observed patterns of weakness and conduction block (1,5).

There are clear indications that nerve thickening on MRI reflects involvement of the myelin sheath. It is a consistent feature of both genetic and acquired demyelinating polyneuropathies, i.e. Charcot Marie Tooth type 1 and chronic inflammatory demyelinating polyneuropathy (28,29). This is further supported by the occasional pathological observation of onion bulb formation in nerve biopsy studies in MMN (7,30,31).

Demyelination is probably not the only pathological mechanism that underlies MMN, since it does not explain all disease characteristics, such as the phenomenon of cold paresis (32). Findings in the rabbit model for acute motor axonal neuropathy and human motor neuron model for MMN (33,34) and clinical observations of significant axonal damage in patients with MMN (5,35) suggest additional pathological mechanisms that directly affect the axon (36). The DTI findings in this study, in particular the reduced AD values, support this concept. Reduced AD values reflect pathological changes that impair diffusion in the length of the axon and is associated with Wallerian degeneration in animal studies (11,12,37). In a recently developed *in vitro* model of anti-GM1 IgM antibody-mediated damage to human motor nerves, we observed focal widening of the axon that preceded Wallerian degeneration (34). MRI studies in an ischemia-model of rat sciatic nerve showed that this process of axonal 'beading' was associated with significantly restricted AD and virtually unchanged RD and FA values (38). The reduced AD values may therefore reflect pathological changes in motor axons of patients with MMN. The sub analysis performed on nerves with reduced CMAP amplitudes shows lower FA, MD, and RD values and a tendency of lower AD in the median and ulnar nerves. This tendency of lower AD could be associated with reduction of axon integrity (13). Reduced MD might be due to disruption of the cytoskeleton, increasing the viscosity (39). Detailed analysis of the association of conduction block and MRI and DTI abnormalities would be of added value to further explore the pathophysiological mechanisms behind MMN. However, this was not possible due to the low number of conduction blocks in this patient sample, which would make a statistical analysis severely underpowered. This is a topic for future larger scale studies.

Patients appeared more uncomfortable in the prone scanning position and as a result motion artifacts were more common in patients than in healthy controls. This scanning position was a methodological limitation of this study and resulted in the exclusion of a significant number of scans due to the relatively low quality of this data. During development of the protocol we aimed to obtain a protocol with a sufficiently high resolution to distinguish the nerves and to have sufficient signal to noise ratio (SNR), as the SNR amongst other will influence the precision of the DTI metrics (25,40). Future development of DTI protocols in the forearm should focus on the right tradeoff in SNR, resolution (preferable $<1x1mm^2$ in plane), and scan time, as SNR and resolution will always come at the cost of increased scan time and thus patient discomfort (25). Repositioning patients in supine position and using dedicated arm coils could improve patient comfort and therefore reduce motion artifacts in future studies. This will improve data quality resulting in less data that needs to be rejected due to artifacts.

We used a tract based analyses approach with a minimum length of the fiber tracts of 100 mm to exclude aberrant inclusion of muscle fibers. As a consequence, the number of tracts available for final analysis was small, since only a limited number of fibers can be traced over this range. Moreover, the error accumulation over a long tract range can become substantial and may introduce bias (25). To overcome this problem, we additionally performed segmental analysis, in which smaller segments of the nerves were analyzed resulting in more fiber tracts that were included. The higher number of tracts allows for better sampling of the data. Segmental analysis showed similar AD changes and additional, significant differences in RD values in the proximal segment (segment 3), but not in the distal segments (segment 1 and 2), of the median and ulnar nerves. Decreased RD values further support pathological processes that directly affect the axon, rather than demyelination (11,41).

An obvious limitation of our study is the number of included patients that limits its power. Furthermore, the age range of ALS patients did not fully match those of MMN patients and healthy controls. As ALS and MMN are rare diseases, matching of these two groups is challenging. This was further complicated by the fact that we could only include a selection of ALS patients, who were able to lie still in prone position for a relatively long time. However, mean age, standard deviations and 95% confidence interval of ALS patients was similar to those of patients with MMN and healthy controls.

In line with previous studies we found no differences in diffusion parameters between left and right arms (42). DTI has not been used extensively to investigate forearm nerves and there are few comparable studies of peripheral nerves of the arm in healthy controls (16) or patients with polyneuropathy (43,44). Comparison of previous results with our findings is further complicated by differences in MRI settings (e.g. smaller voxel size and higher b-value), the difference in threshold settings used for tractography (higher FA threshold results in higher FA values (25)), and patient characteristics (43).

Partial volume effects have to be considered when interpreting DTI results in small nerves (45). Partial volume effects are caused by the voxels located on the edges of the nerves and thus partially contain muscle tissue signal, which has a lower AD, and a higher RD than the nerve. As a consequence, partial volume effects would lower the AD and increase the RD values (19). However, partial volume effects cannot explain the current findings of lower AD values as nerves of MMN patients had a larger CSA and consequently lower partial volume effects (45). Partial volume effects could influence the RD values and provide an alternative explanation for the differences found in RD between patients with MMN and controls.

In conclusion, this study shows that MRI and DTI can detect lowered AD and enlarged CSA in patients with MMN compared to ALS and to healthy controls. These results can help to provide insight into pathological mechanisms of MMN. Future studies would be facilitated by improving patient comfort, for example through the use of dedicated arm coils and placing patients in supine position, which could reduce motion artifacts and thus improve data quality. As a result less data needs to be rejected due to artifacts. Comparative DTI studies of patients with MMN and other demyelinating peripheral nerve disorders, such as chronic inflammatory demyelinating polyneuropathy and Charcot-Marie-Tooth type 1A, could help to further clarify the etiology of MMN.

Acknowledgements

We would like to thank Niels Blanken (MRI radiographer, department of radiology) for his help in performing the MRI scans. We would like to thank Dirk Rutgers (radiologist) and Hessel Franssen (neurologist) for sharing their expert opinions on this topic.

References

1. Cats E a., Van Der Pol WL, Piepers S, Franssen H, Jacobs BC, Van Den Berg-Vos RM, et al. Correlates of outcome and response to IVIg in 88 patients with multifocal motor neuropathy. Neurology. 2010;75(9):818–825.
2. Vlam L, van der Pol W-L, Cats E a, Straver DC, Piepers S, Franssen H, et al. Multifocal motor neuropathy: diagnosis, pathogenesis and treatment strategies. Nat Rev Neurol. 2012;8:48–58.
3. Nobile-Orazio E, Cappellari a, Meucci N, Carpo M, Terenghi F, Bersano a, et al. Multifocal motor neuropathy: clinical and immunological features and response to IVIg in relation to the presence and degree of motor conduction block. J Neurol Neurosurg Psychiatry. 2002;72(6):761–766.
4. Van den Berg-Vos RM, Franssen H, Wokke JH, Van Es HW, Van den Berg LH. Multifocal motor neuropathy: diagnostic criteria that predict the response to immunoglobulin treatment. Ann Neurol. 2000;48(6):919–926.
5. Van Asseldonk JTH, Van den Berg LH, Van den Berg-Vos RM, Wieneke GH, Wokke JHJ, Franssen H. Demyelination and axonal loss in multifocal motor neuropathy: Distribution and relation to weakness. Brain. 2003;126(1):186–198.
6. Susuki K, Rasband MN, Tohyama K, Koibuchi K, Okamoto S, Funakoshi K, et al. Anti-GM1 antibodies cause complement-mediated disruption of sodium channel clusters in peripheral motor nerve fibers. J Neurosci. 2007;27(15):3956–3967.
7. Kaji R, Oka N, Tsuji T, Mezaki T, Nishio T, Akiguchi I, et al. Pathological findings at the site of conduction block in multifocal motor neuropathy. Ann Neurol. 1993;33(2):152–158.
8. Taylor B V, Dyck PJB, Engelstad J, Gruener G, Grant I, Dyck PJ. Multifocal motor neuropathy: pathologic alterations at the site of conduction block. J Neuropathol Exp Neurol. 2004;63(2):129–137.
9. Van Es HW, Van den Berg LH, Franssen H, Witkamp TD, Ramos LM, Notermans NC, et al. Magnetic resonance imaging of the brachial plexus in patients with multifocal motor neuropathy. Neurology. 1997;48:1218–1224.
10. Chhabra A, Belzberg AJ, Rosson GD, Thawait GK, Chalian M, Farahani SJ, et al. Impact of high resolution 3 tesla MR neurography (MRN) on diagnostic thinking and therapeutic patient management. Eur Radiol. 2016;26(5):1235–1244.
11. Song S-K, Sun S-W, Ramsbottom MJ, Chang C, Russell J, Cross AH. Dysmyelination Revealed through MRI as Increased Radial (but Unchanged Axial) Diffusion of Water. Neuroimage. 2002;17(3):1429–1436.
12. DeBoy CA, Zhang J, Dike S, Shats I, Jones M, Reich DS, et al. High resolution diffusion tensor imaging of axonal damage in focal inflammatory and demyelinating lesions in rat spinal cord. Brain. 2007;130(8):2199–2210.
13. Heckel a., Weiler M, Xia A, Ruetters M, Pham M, Bendszus M, et al. Peripheral Nerve Diffusion Tensor Imaging: Assessment of Axon and Myelin Sheath Integrity. PLoS One. 2015;10(6):1–13.
14. Haakma W, Dik P, Ten Haken B, Froeling M, Nievelstein R a J, Cuppen I, et al. Diffusion tensor MRI and fiber tractography of the sacral plexus in children with spina bifida. J Urol. 2014;192(3):927–933.

15. Barcelo C, Faruch M, Lapegue F, Bayol M a, Sans N. 3-T MRI with diffusion tensor imaging and tractography of the median nerve. Eur Radiol. 2013;23(11):3124–3130.

16. Zhou Y, Narayana P a, Kumaravel M, Athar P, Patel VS, Sheikh K a. High resolution diffusion tensor imaging of human nerves in forearm. J Magn Reson Imaging. 2014;39:1374–1383.

17. Jengojan S, Kovar F, Breitenseher J, Weber M, Prayer D, Kasprian G. Acute radial nerve entrapment at the spiral groove: detection by DTI-based neurography. Eur Radiol. 2015;25(6):1678–1683.

18. Guideline PNSMMN. European Federation of Neurological Societies/Peripheral Nerve Society guideline on management of multifocal motor neuropathy. Report of a joint task force of the European Federation of Neurological Societies and the Peripheral Nerve Society--first revisi. J Peripher Nerv Syst. 2010;15(4):295–301.

19. Froeling M, Nederveen AJ, Heijtel DF, Lataster A, Bos C, Nicolay K, et al. Diffusion-tensor MRI reveals the complex muscle architecture of the human forearm. J Magn Reson Imaging. 2012;36(1):237–248.

20. Leemans A, Jeurissen B, Sijbers J, Jones D. ExploreDTI: a graphical toolbox for processing, analyzing, and visualizing diffusion MR data. Proc 17th Sci Meet Int Soc Magn Reson Med. 2009;17(2):3537.

21. Leemans A, Jones DK. The B-matrix must be rotated when correcting for subject motion in DTI data. Magn Reson Med. 2009;61(6):1336–1349.

22. Irfanoglu MO, Walker L, Sarlls J, Marenco S, Pierpaoli C. Effects of image distortions originating from susceptibility variations and concomitant fields on diffusion MRI tractography results. Neuroimage. 2012;61(1):275–288.

23. Tax CMW, Otte WM, Viergever M a, Dijkhuizen RM, Leemans A. REKINDLE: Robust extraction of kurtosis INDices with linear estimation. Magn Reson Med. 2014;73(2):794–808.

24. Basser PJ, Pajevic S, Pierpaoli C, Duda J, Aldroubi A. In vivo fiber tractography using DT-MRI data. Magn Reson Med. 2000;44(4):625–632.

25. Froeling M, Nederveen AJ, Nicolay K, Strijkers GJ. DTI of human skeletal muscle: the effects of diffusion encoding parameters, signal-to-noise ratio and T2 on tensor indices and fiber tracts. NMR Biomed. 2013;26(11):1339–1352.

26. Beekman R, van den Berg LH, Franssen H, Visser LH, van Asseldonk JTH, Wokke JHJ. Ultrasonography shows extensive nerve enlargements in multifocal motor neuropathy. Neurology. 2005;65(2):305–307.

27. Grimm A, Décard BF, Athanasopoulou I, Schweikert K, Sinnreich M, Axer H. Nerve ultrasound for differentiation between amyotrophic lateral sclerosis and multifocal motor neuropathy. J Neurol. 2015;262(4):870–880.

28. Shibuya K, Sugiyama A, Ito S, Misawa S, Sekiguchi Y, Mitsuma S, et al. Reconstruction magnetic resonance neurography in chronic inflammatory demyelinating polyneuropathy. Ann Neurol. 2014;77(2):1–5.

29. Hiwatashi A, Togao O, Yamashita K, Kikuchi K, Ogata H, Yamasaki R, et al. Evaluation of chronic inflammatory demyelinating polyneuropathy: 3D nerve-sheath signal increased with inked rest-tissue rapid acquisition of relaxation enhancement imaging (3D SHINKEI). Eur Radiol. 2016;27(2):447-453.

30. Corbo M, Abouzahr MK, Latov N, Iannaccone S, Quattrini A, Nemni R, et al. Motor nerve biopsy studies in motor neuropathy and motor neuron disease. Muscle Nerve. 1997;20(1):15–21.

31. Auer RN, Bell RB, Lee MA. Neuropathy with onion bulb formations and pure motor manifestations. Vol. 16, The Canadian journal of neurological sciences. 1989. 194–197.

32. Straver DCG, van Asseldonk J-TH, Notermans NC, Wokke JHJ, van den Berg LH, Franssen H. Cold paresis in multifocal motor neuropathy. J Neurol. 2011;258(2):212–217.

33. Susuki K, Nishimoto Y, Yamada M, Baba M, Ueda S, Hirata K, et al. Acute motor axonal neuropathy rabbit model: immune attack on nerve root axons. Ann Neurol. 2003;54(3):383–388.

34. Harschnitz O, van den Berg LH, Johansen LE, Jansen MD, Kling S, Vieira De Sá R, et al. Autoantibody pathogenicity in a multifocal motor neuropathy iPSC-derived model. Ann Neurol. 2016;80(1);71-88.

35. Van Asseldonk JTH, Van den Berg LH, Kalmijn S, Van den Berg-Vos RM, Polman CH, Wokke JHJ, et al. Axon loss is an important determinant of weakness in multifocal motor neuropathy. J Neurol Neurosurg Psychiatry. 2006;77(6):743–747.

36. Franssen H, Straver DCG. Pathophysiology of immune-mediated demyelinating neuropathies-Part II: Neurology. Muscle and Nerve. 2014;49(1):4–20.

37. Beaulieu C, Does MD, Snyder RE, Allen PS. Changes in water diffusion due to Wallerian degeneration in peripheral nerve. Magn Reson Med. 1996;36(4):627–631.

38. Budde MD, Frank JA. Neurite beading is sufficient to decrease the apparent diffusion coefficient after ischemic stroke. Proc Natl Acad Sci U S A. 2010;107(32):14472–14477.

39. Beaulieu C. The basis of anisotropic water diffusion in the nervous system - a technical review. NMR Biomed. 2002;15(7–8):435–455.

40. Jones DK. Precision and accuracy in diffusion tensor magnetic resonance imaging. Top Magn Reson Imaging. 2010;21(2):87–99.

41. Song SK, Yoshino J, Le TQ, Lin SJ, Sun SW, Cross AH, et al. Demyelination increases radial diffusivity in corpus callosum of mouse brain. Neuroimage. 2005;26:132–140.

42. Zhou Y, Kumaravel M, Patel VS, Sheikh KA, Narayana PA. Diffusion tensor imaging of forearm nerves in humans. J Magn Reson Imaging. 2012;36(4):920–927.

43. Breckwoldt MO, Stock C, Xia A, Heckel A, Bendszus M, Pham M, et al. Diffusion Tensor Imaging Adds Diagnostic Accuracy in Magnetic Resonance Neurography. Invest Radiol. 2015;50(8):498–504.

44. Kakuda T, Fukuda H, Tanitame K, Takasu M, Date S, Ochi K, et al. Diffusion tensor imaging of peripheral nerve in patients with chronic inflammatory demyelinating polyradiculoneuropathy: A feasibility study. Neuroradiology. 2011;53:955–960.

45. Vos SB, Jones DK, Viergever MA, Leemans A. Partial volume effect as a hidden covariate in DTI analyses. Neuroimage. 2011;55(4):1566–1576.

Supplemental information

Supplementary table 1: Number of tracts (NT) for the entire tract and segments 1, 2, and 3 in patients with multifocal motor neuropathy (MMN), amyotrophic lateral sclerosis (ALS), and healthy controls (HC) (represented as 95% quantile).

NT (number of tracts)	MMN	ALS	HC
Entire nerve	320*****	326*****	**779***
Segment 1	9283	7205	7172
Segment 2	2920	1713	4561
Segment 3	1075	1138	1618

*Significant difference in NT between entire nerve and segment 1, 2 and 3.

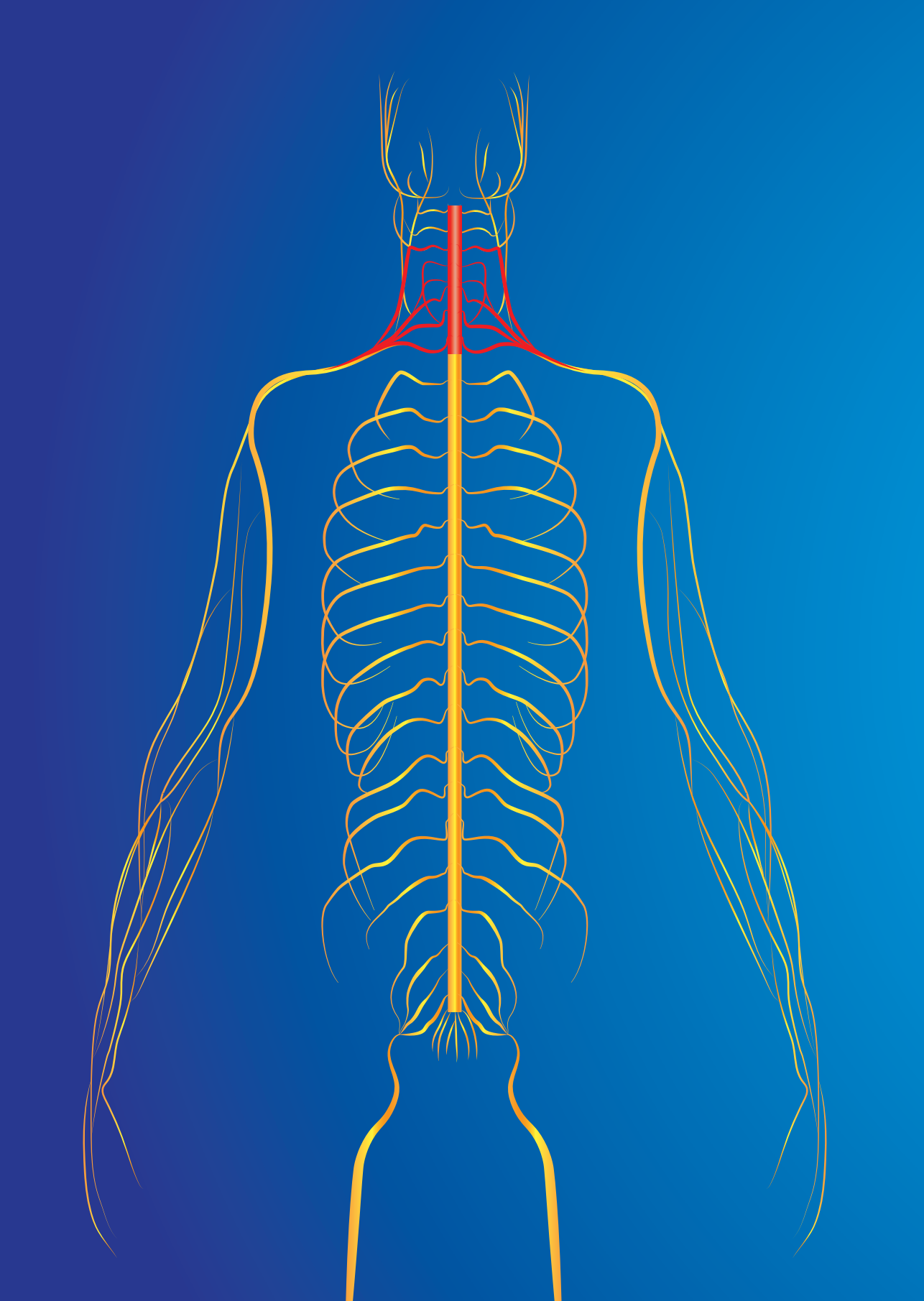

Chapter 6

Magnetic resonance imaging of the spinal cord in spinal muscular atrophy

Wieke Haakma*
Marloes Stam*
Lidy Kuster
Martijn Froeling
Marielle E.P. Philippens
Clemens Bos
Alexander Leemans
Louise A.M. Otto
Leonard H. van den Berg
Jeroen Hendrikse^
W. Ludo van der Pol^

** and ^ these authors contributed equally*

Submitted

Abstract

Objective

In this study we investigated the potential value of magnetic resonance imaging (MRI) and diffusion tensor imaging (DTI) in characterizing changes in the cervical spinal cord and peripheral nerve roots *in vivo* in patients with spinal muscular atrophy (SMA).

Methods

We developed an MRI protocol with 4 sequences to investigate the cervical spinal cord and nerve roots on a 3 Tesla MRI system. We used 2 anatomical MRI sequences to investigate cross-sectional area (CSA) at each spinal segment and the diameter of ventral and dorsal nerve roots, and two diffusion tensor imaging (DTI) techniques to estimate the fractional anisotropy (FA), mean (MD), axial (AD) and radial diffusivity (RD) in 10 SMA patients and 20 healthy controls.

Results

There were no significant differences in CSA ($p>0.1$), although an 8.5% reduction of CSA in patients compared to healthy controls was apparent at segment C7. DTI data showed a higher AD in grey matter of patients compared to healthy controls ($p=0.033$). Significantly lower MD, AD and RD values were found in rostral nerve roots (C3-C5) in patients ($p<0.045$).

Interpretation

We showed feasibility of 4 MRI sequences that allowed differences to be determined between patients and healthy controls, confirming the potential of this technique to assess pathological mechanisms in SMA. These techniques may be used to study disease course of SMA *in vivo*, and evaluate response to survival motor neuron (SMN) augmenting therapy.

Introduction

Hereditary proximal spinal muscular atrophy (SMA) is characterized by dysfunction and degeneration of motor neurons in the anterior horn of the spinal cord and is caused by survival motor neuron (SMN) protein deficiency due to a homozygous loss of function of the SMN1 gene (1). The SMN protein has generic and tissue-specific functions, including pre-mRNA splicing (2) and axonal transport (3,4) of mRNA.

Alterations in the anatomy of the spinal cord and nerve roots of patients with SMA were part of the earliest description of SMA, but have only been documented post-mortem and therefore represent late-stage disease phenomena (5,6). Animal models of SMA have allowed insight into the development of pathology (7,8). However, additional techniques are needed to elucidate the mechanisms *in vivo* that underlie SMA pathogenesis and which can monitor the response to recently introduced SMN protein augmenting therapies at an early stage (9,10) as the execution of clinical trials in SMA is complicated by the lack of sensitive outcome measures (11).

Magnetic resonance imaging (MRI) can provide potential biomarkers for SMA. It has been used to assess muscle volume and fat fraction of the upper and lower extremities (12–14) and spinal cord atrophy (15). Diffusion tensor imaging (DTI), an MRI technique that is sensitive to the random motion of water molecules, can provide additional information on the microstructural organization and status of nervous tissue. DTI has previously been applied in the brain (16), muscle structures (17,18), peripheral nerves (19) and the spinal cord (20) in neuromuscular diseases, but never in SMA. In this study we investigated the potential value of MRI and DTI in characterizing changes in the cervical spinal cord and peripheral nerve roots *in vivo* in SMA patients. We hypothesize that due to pathological changes in SMA there will be a change in the cross-sectional area (CSA) and DTI parameters of the cervical spinal cord and nerve roots.

Methods

Participants

We recruited 10 patients with a genetically confirmed diagnosis of SMA type 2 or 3, aged 12 years and older from the national SMA registry at the University Medical Center Utrecht in the Netherlands, a tertiary referral center for SMA. We used the definition of SMA type established by the 1992 SMA consortium meeting (21) (i.e. type 2: onset between 6 and 18 months, never able to walk; type 3: onset

between 18 months and 30 years, able to walk at some stage in life) with a further delineation of SMA type 3a and 3b based on age at symptom onset before or after 3 years of age (22). All eligible patients in the registry were invited to participate to minimize bias. For each patient, two age- and gender-matched healthy controls were included without history of neuropathy or neuromuscular complaints. Exclusion criteria were: signs of nocturnal hypoventilation (i.e. recurrent morning headaches, night sweats, orthopnea), tracheostomy, any type of (non-)invasive ventilation, pronounced swallowing disorders, a postural change of >15% in forced vital capacity between sitting and supine position, previous trauma or surgery of the (cervical) spinal cord, and any contra-indication for MRI.

Standard Protocol Approvals, Registration and Patient Consent

The Medical Ethics Review Committee (MERC) of the University Medical Center Utrecht approved the study protocol. Informed consent was obtained from all participants and from parents or legal guardians of participants younger than 18 years.

Clinical outcome measures

We used the Medical Research Council (MRC) scale to assess strength of muscles innervated by C5-C8 roots (23). We examined the biceps, triceps, infra- and supraspinatus, pectoralis major, deltoid muscles, wrist flexors and extensors and finger flexors, extensors and abductors. Motor function was evaluated using the Hammersmith Functional Motor Scale Expanded (HFMSE), a 33-item test of motor function developed to evaluate motor performance in patients with SMA types 2 and 3 (24). We recorded the participant's weight and height, since this could potentially influence anatomical measures of the spinal cord. We determined SMN2 copy numbers using Multiplex Ligation-dependent Probe Amplification (MLPA) analysis (SALSA MLPA kit P060 version B2; www.mlpa.com; www.mrcholland.com) (25).

MRI protocol and data acquisition

All subjects were scanned on a 3 Tesla MRI system (Ingenia, Philips Healthcare, Best, the Netherlands) with a neurovascular 15-channel surface coil. Two different areas in the cervical spine were evaluated using 4 different MRI sequences: 1) the cervical spinal cord (spinal segments C4-C8) with a multi-echo steady state free precession (mFFE) sequence and a "high in-plane" resolution DTI scan, and 2) the cervical peripheral nerves (spinal segments C3-C8) with a reversed steady state free precession (T2-FFE) sequence and an "isotropic" resolution DTI scan. Both DTI scans were obtained using b = 100 s/mm^2 (b100) and b = 800 s/mm^2 (b800) to decrease

the influence of cerebral spinal fluid. **Table 1** displays the acquisition parameters of the MRI sequences.

Table 1: MRI acquisition parameters

Sequence name	DTI in-plane	mFFE	DTI isotropic	T2-FFE
Plane	Axial	Axial	Coronal	Axial
TE (ms)	96	TE1=7.8 (ΔTE=9)	62	6
TR (ms)	1657	700	6441	12
NSA	10	2	1	1
Field of view (mm^2)	240 × 240	160×160	280 × 280	200 × 200
Acquisition matrix	256 × 256	560 × 560	112 × 112	432 × 432
Voxel size (mm^3)	0.94×0.94×5.0	0.29×0.29×5.0	2.5×2.5×2.5	0.46 × 0.46 × 0.5
Slices	10	17	30	160
b-value (s/mm^2)	100, 800	-	100, 800	-
Number of gradient directions	10, 10	-	3, 10	-
Acquisition time	5:50	5:47	10:05	5:46

Abbreviations: MRI: magnetic resonance imaging; DTI: diffusion tensor imaging; mFFE: multi-echo fast field echo; T2-FFE: reversed steady state free precession; TE: echo time; TR: repetition time; NSA: number of signal averages

Data processing

Before processing, all data were inspected visually for overall image quality and artifacts (26). Both DTI acquisitions were processed identically using ExploreDTI (www.ExploreDTI.com) (27) consisting of the following steps. First the b100 images were registered, then the b800 images were registered to the mean of the registered b100. Images were corrected for eddy current induced distortions, subject motion, and susceptibility artifacts (28,29). Next, tensors were fitted with the iteratively weighted linear least squares procedure (30). To visualize the nerves and extract the diffusion properties, fiber tractography (FT) was used. Fiber tracts were reconstructed by applying whole volume FT with a fractional anisotropy (FA) threshold of 0.1, minimum fiber length of 15 mm, and maximum fiber angle change per 1 mm step of 30° for both DTI scans. Average diffusion values for each nerve segment were calculated using a tract-based analysis with manually drawn regions of interest (ROIs) to select the appropriate nerve segments.

Spinal cord

Cross-sectional area of the cervical spinal cord

Figure 1B shows an example of how we delineated CSA of the whole spinal cord (spinal segments C4-C8) and grey matter (spinal segments C5-C7) at each segment where the nerve root branched with the spinal cord on the mFFE scan. The white matter CSA was calculated by subtracting the grey matter from the whole spinal cord CSA. We calculated spinal cord atrophy at each segment by expressing the mean difference of CSA between patients and matched controls (controls – patients) as a percentage of the mean of the control.

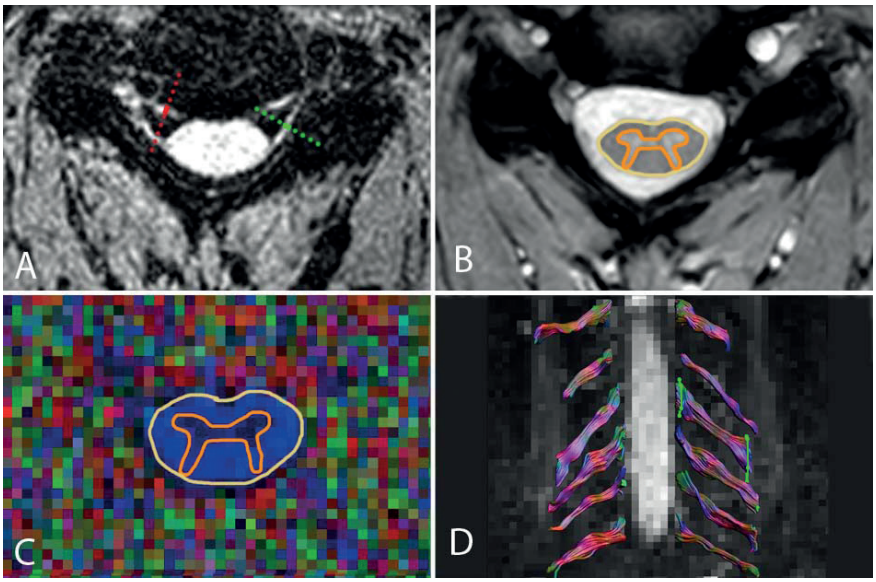

Figure 1: Data acquisition. A) The dotted lines on the reversed steady state free precession (T2-FFE) scan indicate where the diameter of the nerves is measured perpendicular to the nerve. The green line is positioned on the dorsal and the red line on the ventral nerve root. B) Delineation of the grey (orange line) and white matter (yellow line) on the multi-echo fast field echo (mFFE) and C) on the "high in-plane" resolution diffusion tensor imaging (DTI) scan. D) Fiber tractography of the cervical nerve roots from the "isotropic" resolution DTI scan showing two 'AND' ROIs indicating the segment that was used for analysis.

Microstructural properties of the cervical spinal cord

In the "high in-plane" resolution DTI scan we manually segmented the grey matter, white matter, and whole spinal cord at spinal segments C5-C7 (Fig 1C). We used 4 diffusion parameters to investigate the microstructural properties of nervous tissue: the FA which approaches 1 when diffusion is predominantly oriented in one direction, the mean diffusion (MD) which is the average of three eigenvalues (i.e. the length of the diffusion in a specific orientation), the axial diffusivity (AD) which is equal to the largest eigenvalue, and the radial diffusivity (RD) which is the average of the second and third eigenvalues (**Figure 2**). Estimates for the FA, MD, AD and RD were calculated for the grey matter, white matter, and whole spinal cord.

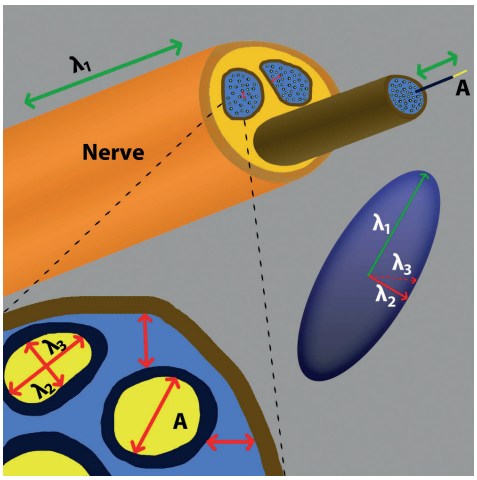

Figure 2: Schematic explanation of diffusion tensor parameters. The main diffusion parameters are calculated from the three eigenvalues λ_1, λ_2 and λ_3: The mean diffusivity (MD) is the average of λ_1 , λ_2, and λ_3.The largest eigenvalue, λ_1 is the axial diffusivity (AD) which represents the diffusivity along the main axis. The diffusion perpendicular to the nerve is the radial diffusivity (RD), which is the average of λ_2 and λ_3. Fractional anisotropy (FA) represents the degree in which diffusion is oriented in one direction. 'A' represents the axon. *("Haakma W. Advances in forensic imaging - CT angiography and diffusion MRI of the nervous system. 2017")*

Cervical nerve roots

Thickness of the ventral and dorsal nerve roots

We measured the diameter of the ventral and dorsal nerve roots on both sides on the T2-FFE, halfway between where the ventral and dorsal nerve roots branch with the spinal cord and where they merge, as displayed in **Figure 1A**.

Microstructural properties of the cervical peripheral nerve roots

We reconstructed the nerves at spinal segments C3-C8 with the data obtained with the "isotropic" resolution DTI scan. Segments of 3 cm of C3-C8 nerve roots were selected where the nerve branched with the spinal cord, as described by

Haakma et al (31). In short, 'SEED', 'AND', and 'NOT' ROIs were used to reconstruct the fiber tracts. For each segment, estimates for the FA MD, AD, and RD were computed (**Figure 1D**).

Data analysis

Statistical analyses of the obtained parameters were performed in IBM SPSS Statistics (version 24; IBM Corp., Armonk, N.Y., USA). We used a mixed analysis of covariance (ANCOVA) with random intercept for the outcome measure as dependent variable and 'segment', 'gender', and 'participant group' as covariates. Fixed effects for the analyses of outcome measures of the "high in-plane" resolution DTI scan and mFFE scan were 'segment', 'gender', 'participant group' and the interaction of 'segment' and 'participant group'. For the outcome measures of the "isotropic" resolution DTI scan the variable 'side' was added to the model as a covariate and fixed effect. Distribution was tested with a Kolmogorov-Smirnov test. We assessed correlations between MRI parameters and clinical scores with Spearman's rank correlation coefficient. We exclusively performed analyses of correlation with clinical scores in patients and only for MRI parameters that were found to be significantly different between patients and controls. For all statistical analyses we considered a p-value of <0.05 to be significant.

Results

Participants

Initially, we included 10 patients with SMA and 20 gender- and age-matched healthy controls. After visual inspection of the imaging data, 2 patients were excluded because of low image quality due to motion artifacts, which made the entire MRI dataset unusable for analysis. We therefore recruited 2 additional patients. Participant characteristics are summarized in **Table 2**.

Spinal cord

Cross-sectional area of the cervical spinal cord

We were able to measure CSA of the whole spinal cord (white and grey matter combined) successfully at segments C4 in 8 patients and 16 controls, at C5 in 5 patients and 18 controls, at C6 in 5 patients and 18 controls, at C7 in 5 patients and 17 controls, and at C8 in 4 patients and 13 controls. Missing values were mainly caused by motion artifacts. We could distinguish grey matter CSA from white matter CSA in 4 patients and 12 controls at C4, in 4 patients and 13 controls at C5, in 4 patients and 14 controls at C6, in 1 patient and 7 controls at C7, and in none at C8.

Table 2: Baseline characteristics

		SMA (n= 10)	SMA type 2 (n= 1)	SMA type 3a (n= 4)	SMA type 3b (n=5)	Healthy controls (n= 20)
Gender, male		6 (60%)	1	3 (75%)	3 (60%)	10 (50%)
Age, y, median (range)		52.9 (17.4-73.6)	71.6	42.9 (17.4-57.8)	51.7 (27.7-73.6)	53.9 (18.1-72.2)
mean MRC upper extremity*, mean (SD)		3.5 (±1.1)	2.2	3.1 (±1.1)	4 (±0.9)	5
mean MRC C5^, mean (SD)		3.1 (±1.4)	1.3	2.8 (±1.6)	3.8 (±1)	5
mean MRC C6°, mean (SD)		3.9 (±1.2)	2.3	3.4 (±1.5)	4.5 (±0.5)	5
mean MRC C7#, mean (SD)		3.6 (±1)	2.7	3.3 (±1.1)	4.1 (±0.8)	5
mean MRC C8~, mean (SD)		4 (±0.7)	3.3	3.6 (±0.5)	4.4 (±0.7)	5
HFMSE score, mean (SD)		25.9 (±22.3)	4	18.8 (±17.3)	38.5 (±24.1)	66
FVC in sitting position, %, median (range)		91 (49-119)	65	84 (49-93)	109 (74-119)	106 (73-116)
FVC in supine position, %, median (range)		94 (67-120)	53	84 (67-97)	105 (77-120)	102 (71-115)
SMN2 copy number	3	4	1	2	1	na
	4	6		2	4	na

*cervical spinal cord innervated muscles: m. supraspinatus, m. infraspinatus, deltoid muscles, m. biceps, m. triceps, m. pectoralis, wrist flexors and extensors, finger extensors, flexors and abductors.
^C5 segment spinal cord innervated muscles: supraspinatus, infraspinatus, deltoid muscle, pectoralis major, biceps
°C6 segment spinal cord innervated muscles: biceps, wrist extensors
#C7 segment spinal cord innervated muscles: triceps, wrist extensors, finger extensors
~C8 segment spinal cord innervated muscles: wrist flexors, finger flexors, finger abductors
Abbreviations: SMA= spinal muscular atrophy; y=years; MRC=Medical Research Council score; SD=standard deviation; HFMSE=Hammersmith Functional Motor Scale Expanded; FVC=forced vital capacity; SMN=survival motor neuron; na=not applicable

The mean CSA of the whole spinal cord was smaller in patients, although this was not statistically significant (p>0.1). The largest difference was found at segment C7 (mean difference: 8.3 mm^2) (**Figure 3A**). There were no significant differences in the grey or white matter CSA between patients and controls (p>0.1) (**Figure 3C-D**). Spinal cord atrophy of the whole spinal cord ranged from 2.7% at segment C8 to 8.5% at segment C7 (**Figure 3B**).

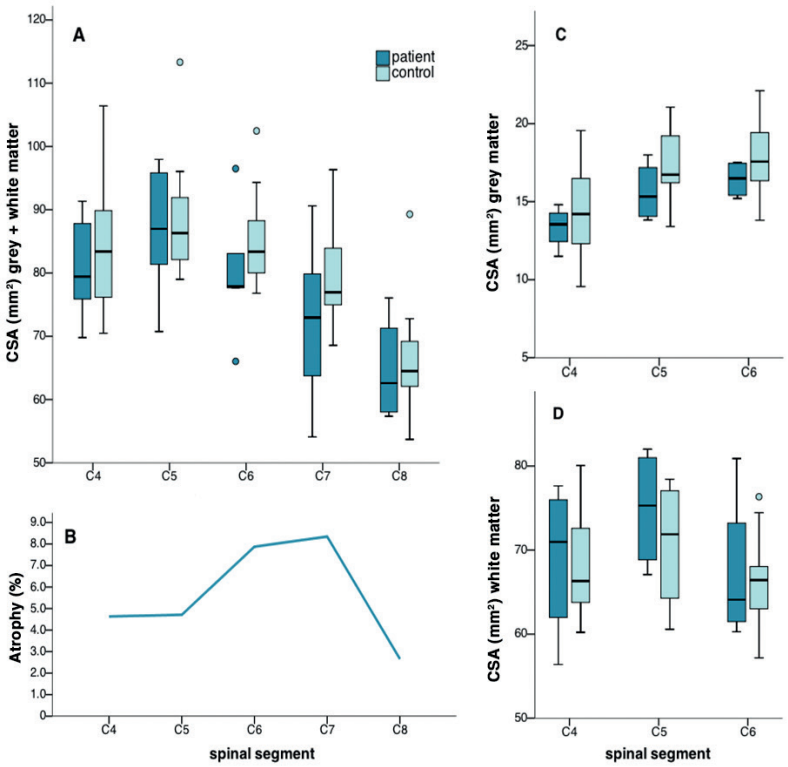

Figure 3: Cross-sectional area of the cervical spinal cord. Group results for SMA patients and healthy controls of CSA per spinal segment for the grey and white matter combined, A). B) Atrophy in SMA patients per spinal segment: The mean difference between patients and controls is depicted as a percentage of the control mean. CSA results of C) grey matter and D) white matter. Abbreviations: CSA=cross-sectional area; C=cervical

Microstructural properties of the cervical spinal cord

DTI scans had sufficient data quality and did not contain artifacts that could interfere with the analysis. Grey matter AD was significantly higher in patients compared to controls (p=0.03). The largest difference was found at segment C7 (mean difference -0.125 $*10^{-3}$ mm^2/s) (**Figure 4**). There were no significant differences between patients and controls in FA, MD and RD (p>0.08). There were no correlations between grey matter AD and HFMSE scores.

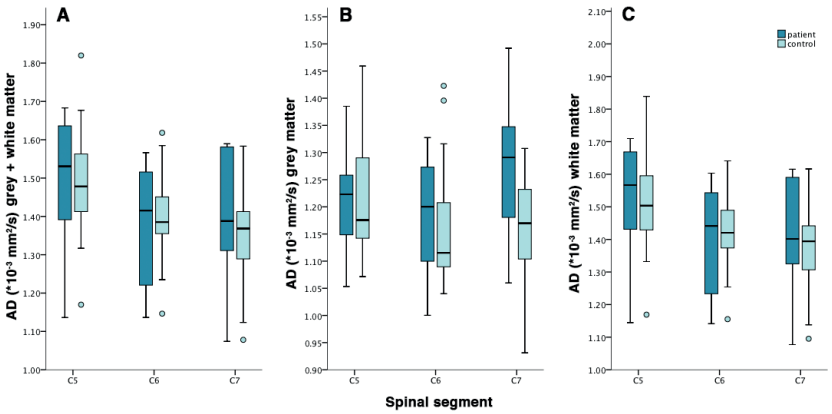

Figure 4: Axial diffusivity values of the cervical spinal cord. AD results per segment for SMA patients and healthy controls, in A) grey and white matter combined, B) grey matter and C) white matter.. Abbreviations: AD=axial diffusivity, C=cervical

Cervical nerve roots

Thickness of the ventral and dorsal nerve roots

Mean thickness of ventral nerve roots (C4-C8) was 0.93±0.13 mm in patients and 1.05±0.27 mm in controls. Mean thickness of dorsal nerve roots overall, was 1.03±0.22 mm in patients and 1.12±0.35 mm in controls. Missing data (patients: 62.5%; controls: 45.5%) precluded meaningful statistical analysis.

Microstructural properties of the cervical peripheral nerve roots

DTI scans had sufficient data quality and did not contain artifacts that interfered with the analysis. Cervical nerve roots could be reconstructed with FT in 357 of

360 nerve roots. FT images of 5 SMA patients and 5 healthy controls are depicted in **Figure 5**. **Figure 6** shows the diffusion parameters per segment for both patients and controls. At spinal segments C4-C8, FA was slightly lower in patients compared to controls (p>0.09) and overall (spinal segments C3-C8) MD, AD and RD were significantly lower in patients (p=0.044, p=0.042 and p=0.039 respectively).

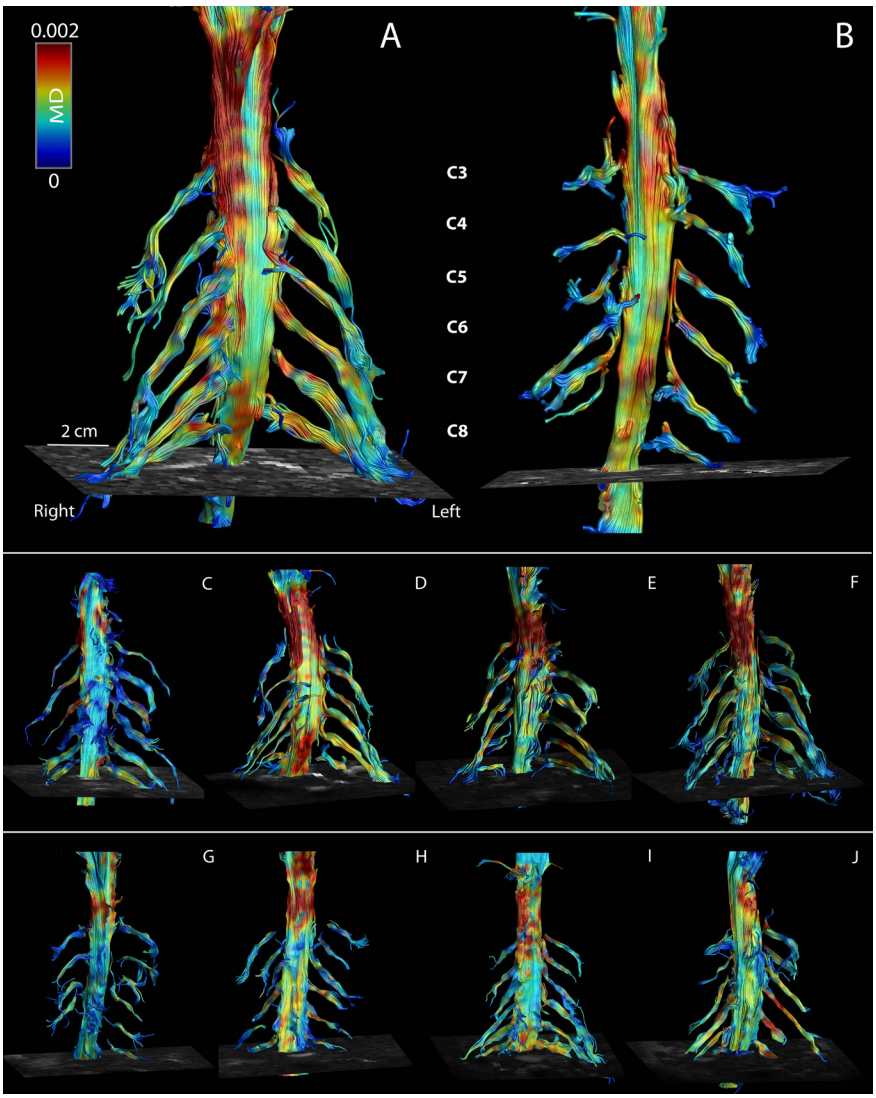

Figure 5: Fiber tractography Fiber tractography images of five randomly chosen SMA patients (B, G, H, I, J) and five healthy controls (A, C, D, E, F).

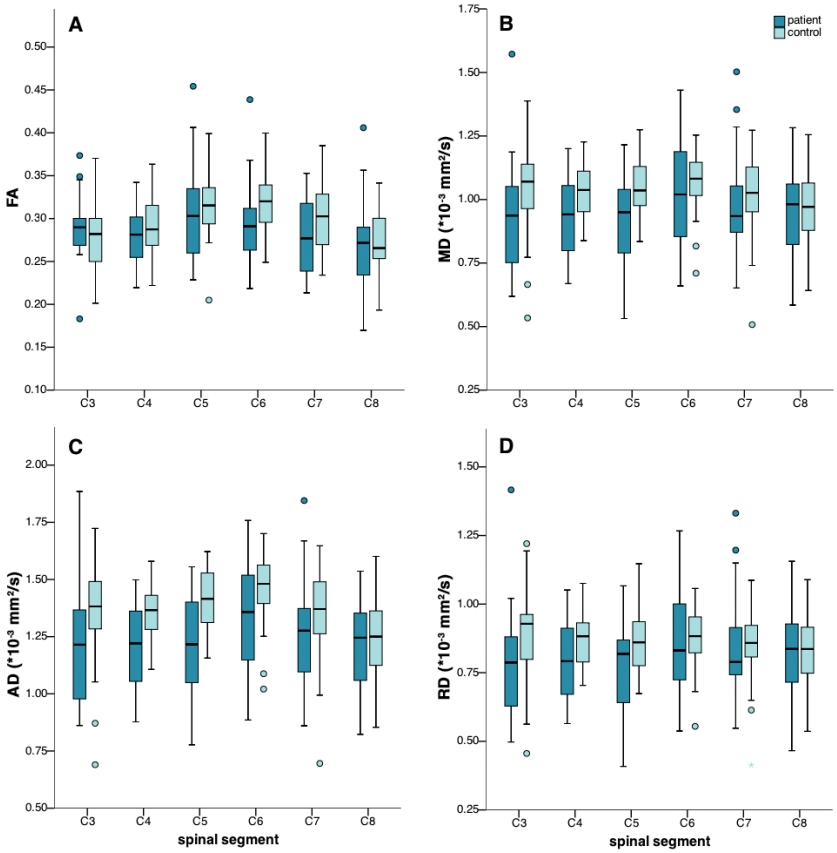

Figure 6: Microstructural properties of the cervical peripheral nerve roots. Group results for SMA patients and healthy controls of the DTI parameters A) fractional anisotropy (FA), B) mean (MD), C) axial (AD) and D) radial diffusivity (RD) for nerve roots at each cervical spinal segment

The largest differences were found at segments C3-C5: with mean differences for MD of 0.117 $*10^{-3}$ mm^2/s (C3), 0.099 $*10^{-3}$ mm^2/s (C4) and 0.133 $*10^{-3}$ mm^2/s (C5); for AD of 0.145 $*10^{-3}$ mm^2/s (C3), 0.154 $*10^{-3}$ mm^2/s (C4) and 0.207 $*10^{-3}$ mm^2/s (C5); and for RD of 0.102 $*10^{-3}$ mm^2/s (C3), 0.072 $*10^{-3}$ mm^2/s (C4) and 0.096 $*10^{-3}$ mm^2/s (C5). There were no correlations of any of the significant parameters with HFMSE score.

Discussion

In this study we investigated the feasibility of various innovative MRI techniques to image the cervical spinal cord and nerve roots in SMA. We developed and applied 2 anatomical MRI sequences, which seem promising for future use. Additionally, we developed and applied 2 DTI sequences to investigate changes in the cervical spinal cord and nerve roots for the first time in SMA patients. We show that DTI parameters can provide important new insights into the pathology of the spinal cord and nerve roots *in vivo* and could potentially be used as a unique biomarker to identify and monitor disease progression.

Spinal cord

The mFFE scan showed a smaller cervical spinal cord CSA in patients compared to controls, with the largest difference at spinal segment C7. The maximal atrophy at segment C7 corresponds to the clinical finding of severe weakness of the triceps in SMA, which are innervated by this segment (23,32,33). The smaller CSA in patients, is in line with the expected motor neuron degeneration, especially since our results indicate that the difference was mainly caused by a difference in grey matter CSA. Furthermore it is in consonance with previous findings which show up to 23% atrophy of the spinal cord in SMA (15). The spinal cord and grey matter were manually delineated to determine CSA, which may induce bias. Automatic segmentation methods may reduce this bias. However, the application of DTI remains challenging, especially at the caudal part of the cervical spinal cord (C7-C8) (34). In some scans, artifacts, for example due to motion, precluded reliable segmentation of grey and white matter. Motion artifacts were more common in patients and may reflect the common symptom of polymyoclonus/ tremor (35). In the caudal segments, there were susceptibility artifacts due to the air in lung tissue. Future studies should focus on developing dedicated methods with less sensitivity to motion artifacts for instance by reducing scan time. Together with findings provided by a study among ALS patients, in whom CSA changed over time and correlated with clinical scores (36), we expect that the mFFE is a promising technique to evaluate the spinal cord in SMA.

We expected to detect a lower FA with the "high in-plane" resolution DTI scan in patients compared to healthy controls, as depletion of motor neurons may lead to an increase in extracellular space and therefore in RD, resulting in a lower FA. Instead, we detected a difference in AD, which was higher in patients compared to controls. With the mFFE scan we found that the CSA of the grey matter is smaller in SMA patients than in healthy controls. As the resolution of the "high in-plane"

resolution DTI scan is only 1 × 1 mm^2 in plane, partial volume effects are likely to influence the results. Moreover, smaller CSA will be more prone to these partial volume effects (37). The diffusion properties of the grey matter are in this case more influenced by the surrounding white matter, which could explain the higher AD values in patients compared to controls. This is further supported by the fact that the difference in AD is largest at segment C7, which is the segment where the CSA reduction suggested atrophy is most pronounced. Future research should therefore aim at developing MRI protocols with a higher in-plane resolution, preferably <0.5 × 0.5 mm^2.

Cervical nerve roots

The T2-FFE scan allowed us to investigate the ventral and dorsal nerve roots. Although the patient sample size was relatively small, we observed differences in size between the ventral and dorsal nerve roots in SMA patients and healthy controls, which indicates the potential value of this technique as a biomarker in SMA *in vivo*. However, missing data were common, for both patients and healthy controls. Multiple artifacts, including local artifacts, e.g. the interference of cerebrospinal fluid at the nerve root, motion artifacts and other MR related artifacts (e.g. susceptibility artifacts), reduced scan quality. In some cases we were not able to detect the nerve despite the scan quality being otherwise good. This may occasionally be caused by reduction of the nerve root size in SMA, e.g. because of axonal abnormalities (3,5–7,38). However, there were also missing data in healthy controls. Future MRI protocol development should focus on reducing these artifacts.

We could reconstruct nearly all nerve roots with FT and calculate DTI parameters with the "isotropic" resolution DTI scan, which was in line with previous findings (39). Although DTI parameters were lower in patients compared to controls at nearly all segments (C3-C8), differences in MD, AD and RD were most pronounced at the more rostral segments (C3-C5). This finding is in line with the characteristic pattern of muscle weakness in SMA, i.e. proximal muscles are usually more affected than distal muscles (40), and with previously described selective vulnerability of motor neurons and findings of cervical nerve root pathology in SMA mice (7). Abnormal DTI values can be explained by a range of SMA-associated anatomical and functional changes. Lower AD values may be associated with reduced diffusion in the length of the axon (41), such as lowered axonal transport in SMA (3,4). Reduced RD may be explained by glial bundles that are frequently described in nerve root pathology in SMA, since they might restrict diffusion perpendicular

to the axon (42,43). Gliosis in the brain has been found associated with increased RD, but this may be explained by a more pronounced glial response (i.e. more cell bodies) in contrast to the presence of more fibrous glial bundles in the nerve roots in SMA (44). In the same study, an increased FA is reported, which supports the restriction of RD by gliosis (44). In addition, compaction of remaining axons in the thinner ventral nerve roots of SMA patients (38) may represent another cause of reduced RD. As a consequence of decreased AD and RD, MD is also reduced.

The diffusion measures of the cervical nerve roots in healthy controls were lower than previously reported (45,46). A factor known to influence FA is the signal-to-noise ratio (SNR), as with lower SNR levels, lower FA values are usually overestimated (47,48). A factor influencing MD is the partial volume effects of surrounding muscular tissue and cerebral spinal fluid. These structures have a higher MD than nervous tissue which may result in the undesirable effect of higher MD estimates in nervous tissue (49). From this, we infer that the lower FA and MD levels found in this study suggest that the data quality was good. The "isotropic" resolution DTI scan allowed the distinction between patients and controls. We believe this represents a promising method to evaluate *in vivo* (changes in) nerve microstructure in SMA.

An obvious limitation of this study is the small sample size, which affects its power. It is clear that additional, longitudinal research in larger groups is necessary to confirm our findings and to evaluate biomarker potential. In the future, it would be interesting also to investigate the lumbar spinal cord with DTI, since lower limbs are usually more affected than upper limbs in SMA. However, the application of DTI in the lower thoracic and higher lumbar spinal cord to investigate grey and white matter is currently still challenging due to several technical issues, such as the presence of susceptibility artifacts caused by the air in lung tissue.

To summarize, we have developed 4 MRI sequences that provide measures of both anatomical and structural changes in SMA. The results suggest that MRI and DTI might provide unique anatomical and functional biomarkers to monitor SMA progression and treatment effects.

Acknowledgements

The authors thank all patients and healthy controls who participated in this study. We would also like to thank Mrs. Bea Nijboer for her contribution in data collection, Mr. Stavros Nikolakopoulos for his statistical advice, and Tuan Nguyen and Ellart Aalbers for their help in acquiring the images.

References

1. Lunn MR, Wang CH. Spinal muscular atrophy. Lancet. 2008;371(9630):2120–2133.
2. Pellizzoni L, Kataoka N, Charroux B, Dreyfuss G. A novel function for SMN, the spinal muscular atrophy disease gene product, in pre-mRNA splicing. Cell. 1998;95(5):615–624.
3. Fallini C, Bassell GJ, Rossoll W. Spinal muscular atrophy: The role of SMN in axonal mRNA regulation. Vol. 1462, Brain Research. 2012. 81–92.
4. Dale JM, Shen H, Barry DM, Garcia VB, Rose FF, Lorson CL, et al. The spinal muscular atrophy mouse model, SMAΔ7, displays altered axonal transport without global neurofilament alterations. Acta Neuropathol. 2011;122(3):331–341.
5. Harding BN, Kariya S, Monani UR, Chung WK, Benton M, Yum SW, et al. Spectrum of neuropathophysiology in spinal muscular atrophy type I. J Neuropathol Exp Neurol. 2015;74(1):15 24.
6. Araki S, Hayashi M, Tamagawa K, Saito M, Kato S, Komori T, et al. Neuropathological analysis in spinal muscular atrophy type II. Acta Neuropathol. 2003;106(5):441–418.
7. Kariya S, Park GH, Maeno-Hikichi Y, Leykekhman O, Lutz C, Arkovitz MS, et al. Reduced SMN protein impairs maturation of the neuromuscular junctions in mouse models of spinal muscular atrophy. Hum Mol Genet. 2008;17(16):2552–2569.
8. D'Errico P, Boido M, Piras A, Valsecchi V, De Amicis E, Locatelli D, et al. Selective vulnerability of spinal and cortical motor neuron subpopulations in delta7 SMA mice. PLoS One. 2013;8(12):e82654.
9. Mendell JR, Al-Zaidy S, Shell R, Arnold WD, Rodino-Klapac LR, Prior TW, et al. Single-Dose Gene-Replacement Therapy for Spinal Muscular Atrophy. N Engl J Med. 2017;377(18):1713–1722.
10. Finkel RS, Mercuri E, Darras BT, Connolly AM, Kuntz NL, Kirschner J, et al. Nusinersen versus Sham Control in Infantile-Onset Spinal Muscular Atrophy. N Engl J Med. 2017;377(18):1723–1732.
11. Bertini E, Burghes A, Bushby K, Estournet-Mathiaud B, Finkel RS, Hughes RAC, et al. 134th ENMC international workshop: Outcome measures and treatment of spinal muscular atrophy 11-13 February 2005 Naarden, the Netherlands. Neuromuscul Disord. 2005;15(11):802–816.
12. Bonati U, Holiga Š, Hellbach N, Risterucci C, Bergauer T, Tang W, et al. Longitudinal characterization of biomarkers for spinal muscular atrophy. Ann Clin Transl Neurol. 2017;4(5):292–304.
13. Sproule DM, Montgomery MJ, Punyanitya M, Shen W, Dashnaw S, Montes J, et al. Thigh muscle volume measured by magnetic resonance imaging is stable over a 6-month interval in spinal muscular atrophy. J Child Neurol. 2011;26(10):1252–1259.
14. Durmus H, Yilmaz R, Gulsen-Parman Y, Oflazer-Serdaroglu P, Cuttini M, Dursun M, et al. Muscle magnetic resonance imaging in spinal muscular atrophy type 3: Selective and progressive involvement. Muscle Nerve. 2017;55(5):651–656.
15. El Mendili MM, Lenglet T, Stojkovic T, Behin A, Guimarães-Costa R, Salachas F, et al. Cervical spinal cord atrophy profile in adult SMN1-linked SMA. PLoS One. 2016;11(4).
16. Müller H-P, Turner MR, Grosskreutz J, Abrahams S, Bede P, Govind V, et al. A large-scale multicentre cerebral diffusion tensor imaging study in amyotrophic lateral sclerosis. J Neurol Neurosurg Psychiatry. 2016;87(6):570–579.

17. Hooijmans MT, Damon BM, Froeling M, Versluis MJ, Burakiewicz J, Verschuuren JJGM, et al. Evaluation of skeletal muscle DTI in patients with duchenne muscular dystrophy. NMR Biomed. 2015;28(11):1589–1597.

18. Oudeman J, Nederveen AJ, Strijkers GJ, Maas M, Luijten PR, Froeling M. Techniques and applications of skeletal muscle diffusion tensor imaging: A review. Vol. 43, Journal of Magnetic Resonance Imaging. 2016. 773–788.

19. Haakma W, Jongbloed BA, Froeling M, Goedee HS, Bos C, Leemans A, et al. MRI shows thickening and altered diffusion in the median and ulnar nerves in multifocal motor neuropathy. Eur Radiol. 2017;27(5):2216–2224.

20. Toosy AT, Kou N, Altmann D, Wheeler-Kingshott CAM, Thompson AJ, Ciccarelli O. Voxel-based cervical spinal cord mapping of diffusion abnormalities in MS-related myelitis. Neurology. 2014;83(15):1321–1325.

21. Munsat TL, Davies KE. International SMA Consortium Meeting (26-28 June 1992, Bonn, Germany). In: Neuromuscular Disorders. 1992. 423–428.

22. Zerres K, Schöneborn SR. Natural History in Proximal Spinal Muscular Atrophy: Clinical Analysis of 445 Patients and Suggestions for a Modification of Existing Classifications. Arch Neurol. 1995;52(5):518–523.

23. MRC. Medical Research Council. Aids to the examination of the peripheral nervous system: Memorandum No 45 (suspending War Memorandum No. 7). The white Rose Press for Her Majesty's Stationery Office. London; 1976.

24. O'Hagen JM, Glanzman AM, McDermott MP, Ryan PA, Flickinger J, Quigley J, et al. An expanded version of the Hammersmith Functional Motor Scale for SMA II and III patients. Neuromuscul Disord. 2007;17(9–10):693–697.

25. Wadman RI, Stam M, Gijzen M, Lemmink HH, Snoeck IN, Wijngaarde CA, et al. Association of motor milestones, SMN2 copy and outcome in spinal muscular atrophy types 0-4. Vol. 88, Journal of Neurology, Neurosurgery and Psychiatry. 2017. 364–367.

26. Tournier J-D, Mori S, Leemans A. Diffusion tensor imaging and beyond. Magn Reson Med. 2011;65(6):1532–1556.

27. Leemans A, Jeurissen B, Sijbers J, Jones D. ExploreDTI: a graphical toolbox for processing, analyzing, and visualizing diffusion MR data. Proc 17th Sci Meet Int Soc Magn Reson Med. 2009;17(2):3537.

28. Leemans A, Jones DK. The B-matrix must be rotated when correcting for subject motion in DTI data. Magn Reson Med. 2009;61(6):1336–1349.

29. Irfanoglu MO, Walker L, Sarlls J, Marenco S, Pierpaoli C. Effects of image distortions originating from susceptibility variations and concomitant fields on diffusion MRI tractography results. Neuroimage. 2012;61(1):275–288.

30. Veraart J, Sijbers J, Sunaert S, Leemans A, Jeurissen B. Weighted linear least squares estimation of diffusion MRI parameters: Strengths, limitations, and pitfalls. Neuroimage. 2013;81(0):335–346.

31. Haakma W, Pedersen M, Froeling M, Uhrenholt L, Leemans A, Boel LWT. Diffusion tensor imaging of peripheral nerves in non-fixed post-mortem subjects. Forensic Sci Int. 2016;263:139–146.

32. Deymeer F, Serdaroglu P, Parman Y, Poda M. Natural history of SMA IIIb: Muscle strength decreases in a predictable sequence and magnitude. Neurology. 2008;71(9):644–649.

33. Piepers S, Berg LH, Brugman F, Scheffer H, Ruiterkamp-Versteeg M, Engelen BG, et al. Natural history of SMA IIIb: muscle strength decreases in a predictable sequence and magnitude. Neurology. 2009;72(23):2057–2058.

34. Tang L, Wen Y, Zhou Z, von Deneen KM, Huang D, Ma L. Reduced field-of-view DTI segmentation of cervical spine tissue. Magn Reson Imaging. 2013;31(9):1507–1514.

35. Dawood AA, Moosa A. Hand and ECG tremor in spinal muscular atrophy. Arch Dis Child. 1983;58(5):376–378.

36. El Mendili MM, Cohen-Adad J, Pelegrini-Issac M, Rossignol S, Morizot-Koutlidis R, Marchand-Pauvert V, et al. Multi-parametric spinal cord MRI as potential progression marker in amyotrophic lateral sclerosis. PLoS One. 2014;9(4).

37. Vos SB, Jones DK, Viergever MA, Leemans A. Partial volume effect as a hidden covariate in DTI analyses. Neuroimage. 2011;55(4):1566–1576.

38. Chou SM, Nonaka I. Werdnig-Hoffmann disease: Proposal of a pathogenetic mechanism. Acta Neuropathol. 1978;41(1):45–54.

39. Haakma W, Froeling M, Pedersen M, Uhrenholt L, Douven P, Leemans A, et al. Post-mortem diffusion MRI of the cervical spine and its nerve roots. J Forensic Radiol Imaging. 2018;12(1):50-56

40. Carter GT, Abresch RT, Fowler WM, Johnson ER, Kilmer DD, McDonald CM. Profiles of neuromuscular diseases. Spinal muscular atrophy. Vol. 74, American journal of physical medicine & rehabilitation / Association of Academic Physiatrists. 1995. S150-159.

41. DeBoy CA, Zhang J, Dike S, Shats I, Jones M, Reich DS, et al. High resolution diffusion tensor imaging of axonal damage in focal inflammatory and demyelinating lesions in rat spinal cord. Brain. 2007;130(8):2199–2210.

42. Kuru S, Sakai M, Konagaya M, Yoshida M, Hashizume Y, Saito K. An autopsy case of spinal muscular atrophy type III (Kugelberg-Welander disease). Neuropathology. 2009;29(1):63–67.

43. Kimura T, Budka H. Glial bundles in spinal nerve roots - An immunocytochemical study stressing their nonspecificity in various spinal cord and peripheral nerve diseases. Acta Neuropathol. 1984;65(1):46–52.

44. Budde MD, Janes L, Gold E, Turtzo LC, Frank JA. The contribution of gliosis to diffusion tensor anisotropy and tractography following traumatic brain injury: Validation in the rat using Fourier analysis of stained tissue sections. Brain. 2011;134(8):2248–2260.

45. Tagliafico A, Calabrese M, Puntoni M, Pace D, Baio G, Neumaier CE, et al. Brachial plexus MR imaging: accuracy and reproducibility of DTI-derived measurements and fibre tractography at 3.0-T. Eur Radiol. 2011;21(8):1764–1771.

46. Vargas MI, Viallon M, Nguyen D, Delavelle J, Becker M. Diffusion tensor imaging (DTI) and tractography of the brachial plexus: feasibility and initial experience in neoplastic conditions. Neuroradiology. 2010;52(3):237–245.

47. Froeling M, Nederveen AJ, Nicolay K, Strijkers GJ. DTI of human skeletal muscle: the effects of diffusion encoding parameters, signal-to-noise ratio and T2 on tensor indices and fiber tracts. NMR Biomed. 2013 Nov;26(11):1339–1352.

48. Bastin ME, Armitage PA, Marshall I. A theoretical study of the effect of experimental noise on the measurement of anisotropy in diffusion imaging. Magn Reson Imaging. 1998;16(7):773–785.

49. Schlaffke L, Rehmann R, Froeling M, Kley R, Tegenthoff M, Vorgerd M, et al. Diffusion tensor imaging of the human calf: Variation of inter- and intramuscle-specific diffusion parameters. Journal of Magnetic Resonance Imaging. 2017;46(4):1137-1148.

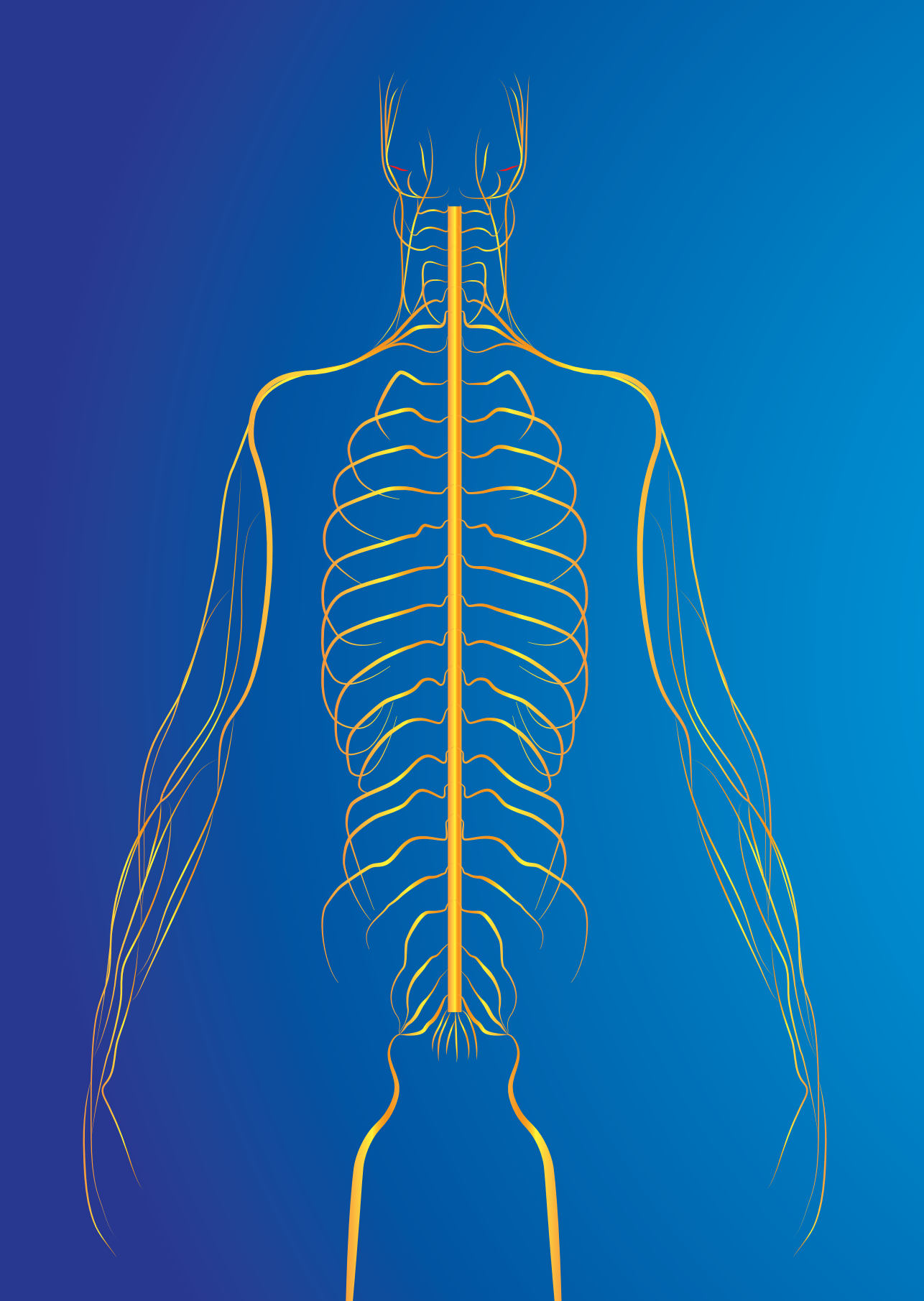

Chapter 7

Diffusion tensor imaging of the auditory nerve in patients with long-term single-sided deafness

Sjoerd B. Vos
Wieke Haakma
Huib Versnel
Martijn Froeling
Lucienne Speleman
Pieter Dik
Max A. Viergever
Alexander Leemans
Wilko Grolman

Hearing Research 2016; 323; 1-8, DOI: 10.1016/j.heares.2015.01.010

Abstract

A cochlear implant (CI) can restore hearing in patients with profound sensorineural hearing loss by direct electrical stimulation of the auditory nerve. Therefore, the viability of the auditory nerve is vitally important in successful hearing recovery. However, the nerve typically degenerates following cochlear hair cell loss, and the amount of degeneration may considerably differ between the two ears, also in patients with bilateral deafness. A measure that reflects the nerve's condition would help to assess the best of both nerves and decide accordingly which ear should be implanted for optimal benefit from a CI. Diffusion tensor MRI (DTI) may provide such a measure, by allowing noninvasive investigations of the nerve's microstructure. In this pilot study, we show the first use of DTI to image the auditory nerve in five normal-hearing subjects and five patients with long-term profound single-sided sensorineural hearing loss. A specialized acquisition protocol was designed for a 3T MRI scanner to image the small nerve bundle. The nerve was reconstructed using fiber tractography and DTI metrics - which reflect the nerve's microstructural properties - were computed per tract. Comparing DTI metrics from the deaf-sided with the healthy-sided nerves in patients showed no significant differences. There was a small but significant reduction in fractional anisotropy in both auditory nerves in patients compared with normal-hearing controls. These results are the first evidence of possible changes in the microstructure of the bilateral auditory nerves as a result of single-sided deafness. Our results also indicate that it is too early to assess the degenerative status of the auditory nerve of a subject-specific basis.

Introduction

In patients with severe or profound hearing loss, hearing can be restored by a cochlear implant (CI). One of the crucial aspects in the successful hearing restoration following CI is thought to be the state of the auditory nerve (1,2), which connects the cochlea to the central nuclei of the auditory system. Typically, the nerve progressively degenerates following cochlear deafness as demonstrated in humans (2–5) and in animal models of deafness (3,6,7). Because the extent of hearing loss may differ between the two sides, the condition of the nerves may differ as well (2). Since unilateral CI is the common treatment, particularly in adults, the CI should be placed in the ear that would provide the highest yield in terms of hearing recovery, which is expected to be the ear with the nerve in the best condition. A direct measure of the nerve's viability is its ability to conduct electrical impulses and although there are methods to measure this (e.g., electrically evoked compound action potentials), these methods are only available after implantation (8) and are therefore of no use in choosing which side to implant.

Magnetic resonance imaging (MRI) is a suitable candidate to non-invasively investigate the auditory nerve. Diffusion MRI in particular would be ideal because of its ability to probe the neuronal tissue on a microstructural level. Diffusion MRI is a non-invasive MRI technique that can provide information about tissue microstructure and the directional organization of neural tissue in vivo by measuring the self-diffusion of water molecules (9,10). In healthy neural fiber bundles, diffusion of water is less hindered along than perpendicular to axons, making the local diffusion dependent on microstructure (11,12). Diffusion tensor MRI (DTI) is a way to describe and quantify the magnitude and orientation of the estimated diffusion (13). Microstructural damage, e.g., axonal or myelin loss, typically reduces the hindrance and restriction that diffusing water molecules experience, which affects DTI parameters such as the fractional anisotropy (FA) and mean diffusivity (MD). Following the assumption that diffusion is largest parallel to axons, the main orientation of diffusion as obtained from the diffusion tensor can be used to virtually reconstruct neural fiber pathways, a process called fiber tractography (FT, (14)). DTI parameters have been shown to reveal pathological changes in the brain and predict the development of lesions before they are visible on more conventional MR images (15).

In the auditory system DTI has for instance been used to investigate aging in Heschl's gyrus (16), tracts between the inferior colliculus and auditory cortex and connections to non-auditory areas in tinnitus patients (17), and subcortical

connections in patients with auditory nerve deficiencies (18). DTI has also been used to examine the brain's microstructure in patients scheduled for CI. Chang et al have shown that in children, FA of central elements of the auditory system – specifically the medial geniculate, genu of the corpus callosum, and Broca's area – correlates with auditory performance after implantation (19). This is important information, highlighting which areas should function properly to have optimal use of a CI. These areas, however, are all upstream of the brainstem from where the laterality of the auditory information is obscured. Thus, investigations of those regions do not reveal which ear would be the ideal candidate for implantation in bilaterally deaf patients. Our intention is to investigate the one neural fiber structure that contains the unilateral information, aiming to find a predictor of which side to implant in bilaterally deaf patients.

In this pilot study, we will show the first explorations of using DTI and fiber tractography to reconstruct the auditory nerve and to investigate its microstructural properties in vivo. Using a group of patients with long-term single-sided deafness and a group of healthy controls, we will examine whether DTI can be used to detect laterality differences in the auditory nerves between a patient's deaf and healthy ear, and whether these are distinguishable from the auditory nerve in healthy subjects. The nerve of the deafened ear is expected to be considerably degenerated (2,20). Since degeneration includes loss of neurons, and demyelination and shrinkage of surviving neurons (3,21,22), which all affect diffusion, we hypothesize that DTI measures of the auditory nerve differ between the deafened and control ears.

Materials and methods

DTI background

DTI is a method to quantify and analyze a collection of diffusion-weighted MR images. Diffusion-weighted MRI (DWI) creates an imaging contrast based on the diffusion of water molecules in tissue. In a medium such as water, water molecules are able to diffuse freely, and diffusion is equal in all directions, isotropic. In tissue, diffusing molecules are limited in their motion by the cellular microstructure, including the cell membrane and cell nucleus. In neural tissue, diffusion of water molecules is rather unrestricted along the elongated structure of axons but restricted perpendicular to the axes of axons, resulting in very anisotropic diffusion. This enables us to reconstruct the three-dimensional architecture of neuronal tissue. Diffusion-weighting in MRI is typically achieved by applying a magnetic gradient, next to all the normal gradients and pulses required to make an MR image (9). Such a diffusion-weighting gradient is applied along a certain axis and

will only be affected by diffusion along that axis. Given that diffusion in neural tissue is anisotropic, applying diffusion-weighting gradients along different axes allows us to measure this anisotropic diffusion in neural tissue in vivo (11,12).

DTI is a method that takes one conventional T2-weighted image and multiple diffusion-weighted images from at least six different gradient orientations and models the measured diffusion signal at each imaged voxel as a tensor (13). Conceptually, a tensor can be visualized as an ellipsoid where its surface represents the surface of equal probability of finding a molecule that has diffused for a given time from the ellipsoid's center (**Figure 1A**). The diffusion tensor can be redefined as having three perpendicular vectors, called eigenvectors (ε_1, ε_2, and ε_3), each with a given magnitude of diffusion along these eigenvectors, called eigenvalues (λ_1, λ_2, and λ_3). Here, the first eigenvalue denotes the highest diffusion coefficient, and consequently the first eigenvector denotes the orientation along which the diffusion is highest (**Figure 1C**). Assuming that this dominant diffusion orientation is parallel to the fiber pathways, ε_1 reflects the main axis of these fiber trajectories (14,23).

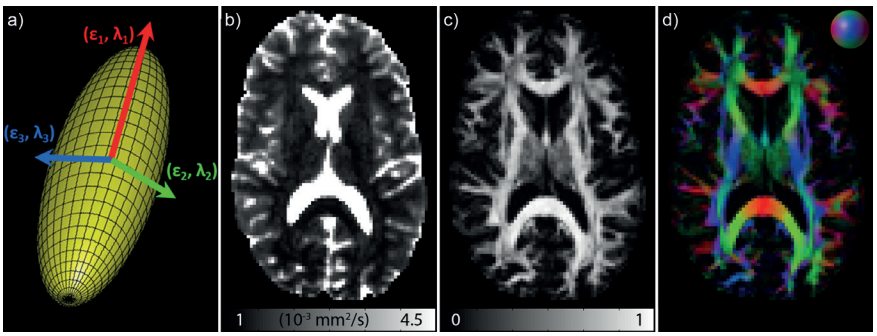

Figure 1: The diffusion tensor can be visualized as an ellipsoid (a). The eigenvectors (ε_1 – ε_3) and eigenvalues (λ_1 – λ_3) describe the principal diffusion directions and their magnitudes, respectively. The mean diffusivity (b) and fractional anisotropy (c) values can be computed from the tensor's eigenvalues and are often used to quantify diffusion magnitude and anisotropy, respectively. The directionally-encoded-color map is a fractional anisotropy map color-encoded by the direction of largest diffusion (d). As indicated by the color index sphere in the top right corner, green indicates anterior-posterior, red means left-right, and blue is inferior-superior.

The two main quantitative values that can be derived from the tensor are the mean diffusivity (MD) and the fractional anisotropy (FA, (24,25)). The MD quantifies the amount of diffusion, calculated by the average of the eigenvalues. The FA value is a measure of the degree of anisotropy with which diffusion occurs, and essentially represents the standard deviation of the eigenvalues, scaled between 0, isotropic, and 1, totally anisotropic (24). Example images of these two DTI metrics are shown in **Figure 1B and C**. The local fiber orientation can be visualized in a directionally-encoded color (DEC) map, where the FA image is color-encoded based on the orientation of largest diffusion, ε_1 (**Figure 1D**). Since the magnitude and anisotropy of diffusion (quantified by the MD and FA, respectively) are influenced by the neural microstructure, changes in FA and MD as a result of various pathologies have been detected, for instance in Alzheimer's disease (26), multiple sclerosis (27), and spina bifida (28). For a more detailed introduction into DTI, please see (29) and (30).

Subject population

Five patients with single-sided deafness and five healthy normal-hearing subjects were included. All control subjects had normal middle ear function, with no acute middle ear infection or tympanic membrane perforations and an air-bone gap <10 dB. Here, normal-hearing subjects were defined as having a hearing threshold ≤20 dB hearing level (HL) for individual frequencies of 0.5, 1, 2, and 4 kHz, with an average over these four frequencies ≤15 dB HL. Patients were included only if one ear had hearing thresholds ≥70 dB HL and the other ear had thresholds ≤30 dB HL for each of these four frequencies. Subject demographics and hearing thresholds are shown in **Table 1**. All subjects gave written informed consent to participate in this study under a protocol approved by the University Medical Center Utrecht ethics committee.

Data acquisition

DTI data were acquired from all subjects on a 3.0 T Philips Achieva MRI system (Philips Healthcare, Best, the Netherlands) using a single-shot spin echo echo-planar imaging (EPI) sequence with an 8-channel head coil. To maximize the spatial resolution the acquisition had a limited field-of-view (FOV) of 79 mm in the anterior-posterior direction using fold-over suppression. The FOV of 79 × 230 mm^2 (AP × LR) was imaged with a 44 × 128 matrix, and 20 axial slices with thickness 1.8 mm were acquired without gap, resulting in an isotropic resolution of 1.8 mm^3. SENSE-acceleration by a factor of 2.1 was applied in the AP-direction, resulting in a TE of 58 ms and a TR of 3215 ms, and a band-width of 48.3 Hz/pixel. A single non-diffusion-weighted image was acquired (6 number of signal averages,

Table 1: Subject characteristics

Subject	Age (y)	Gender	Hearing threshold [0/5, 1, 2, 4 kHz] (dB)		Age at first symptoms (y)
			Left	Right	
Patient 1	36	male	[95 90 95 100]	[10 10 5 10]	21
Patient 2	34	female	[– 120 – 115]*	[0 0 0 0]	5
Patient 3	67	female	[80 120 120 115]	[20 15 30 30]	13
Patient 4	52	male	[5 10 10 20]	[– 120 – 110]*	6
Patient 5	64	male	[10 0 5 20]	[115 120 120 115]	Early childhood
Control 1	36	male	[10 5 0 20]	[10 5 5 10]	-
Control 2	29	male	[5 5 5 10]	[5 5 5 10]	-
Control 3	51	male	[10 5 0 10]	[10 5 5 15]	-
Control 4	30	female	[5 0 5 5]	[0 5 10 5]	-
Control 5	57	female	[0 10 15 15]	[5 5 10 15]	-

* The hearing loss values at 1 and 4 kHz lie on the edge of the measurable range. The loss at 0.5 and 2 kHz is therefore not measured.

NSA) along with 22 gradient directions (3 NSA) with a b-value of 1000 s/mm^2 (δ/Δ: 12.4/28.3 ms) (31). This set of 23 images was acquired twice to improve the signal-to-noise ratio, for a total acquisition time of 7:49 minutes. Additionally, an axial 3D T2-weighted TSE image with DRIVE (DRIVen Equilibrium) was acquired with a FOV of 130 × 130 × 25 mm^3 (AP × LR × IS) with an acquisition matrix of 276 × 276 × 25 and a reconstructed voxel size of 0.25 × 0.25 × 0.50 mm^3. TE and TR were 200 and 2000 ms, respectively, for an acquisition time of 4:32 minutes.

Image processing

Prior to data analysis, the acquired diffusion MRI data were corrected for signal drift (32) and corrected for eddy current induced geometric distortions and subject motion by realigning all diffusion-weighted images (DWIs) to the b=0-images (non-diffusion weighted images) with elastix (33) using an affine coregistration technique (12 degrees of freedom). In this procedure, the diffusion gradients were adjusted with the proper b-matrix-rotation as described by (34). The diffusion tensor was fitted using the iterative weighted linear least squares approach (35). All processing was performed in ExploreDTI (www.exploreDTI.com) (36).

Tractography

Compared to the large white matter fiber bundles in the brain typically reconstructed with tractography, the auditory nerve is a very small structure, and thus heavily influenced by partial voluming with the surrounding cerebrospinal

fluid. It therefore has relatively low FA values. To select the accurate starting point for fiber tractography, the cochlea was manually outlined on the 3D T2-weighted image (**Figure 2A**). On the same image, the mid-sagittal plane was determined using a global symmetry-based method (37). The 3D T2 image was then rigidly registered to the DTI data and the cochlea segmentations and mid-sagittal plane were transformed accordingly. The registered cochlea segmentations (approximately 150 mm^3) were used to seed the fiber tractography. The registered mid-sagittal plane was translated 10 voxels (18 mm) to the left and right and used as termination points for the tractography to select the left and right auditory nerves, respectively (**Figure 2B and C**). Because of the small cross-section of the auditory nerve, it is quickly lost in the complex architecture of the brainstem (38). For this reason, a tract segment was extracted that terminated 18 mm lateral of the mid-sagittal plane – roughly upon entering the brainstem. Tractography step size was 0.5 mm, and tracking was stopped if the angle between two subsequent points was larger than 20˚.

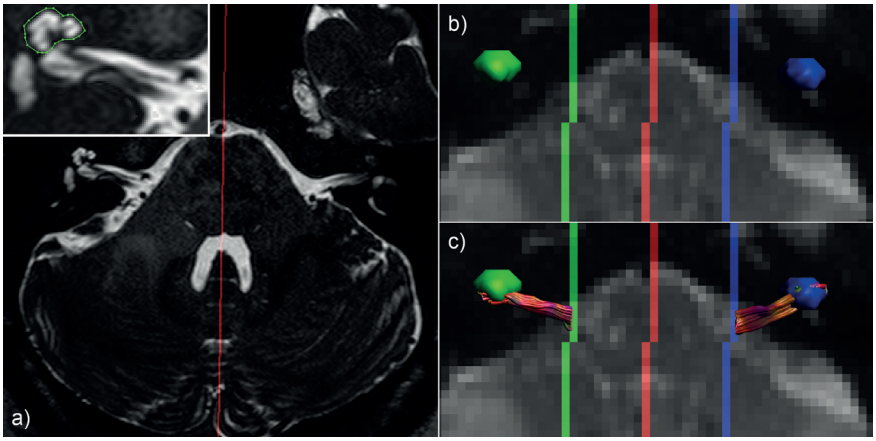

Figure 2: Example of the anatomical 3D T2-weighted (a) and non-diffusion-weighted (b, c) images. The T2 image (a) is used to delineate the cochlea on both sides (shown for the right cochlea in the inset). The mid-sagittal plane that best divides the two hemispheres is also determined on this image (red line). The mid-sagittal plane is transformed onto the non-diffusion-weighted image (red row of voxels in b and c). This is transposed 10 voxels to either side to generate the tract bundle selecting regions of interest (green and blue lines for the right and left regions, respectively). The segmented cochlear volumes are also transformed onto the DWI data (green and blue volumes for the right and left volumes, respectively). Tracts are seeded from this volume and will terminate upon reaching the bundle selecting regions (c).

The whole processing procedure was performed twice, to evaluate the reproducibility of the analysis. For both repeats of the obtained bundles, mean FA and MD values per bundle segment were calculated. This allows for evaluation of reproducibility both in terms of the obtained tractography results as well as diffusion metrics.

Statistical evaluation

Overall group analysis consists of two steps. First, average FA and MD per bundle segment will be compared using paired t-tests to investigate laterality differences in FA and MD. In healthy controls this is done between the tracts from the left and right hemisphere, in the patient group between tracts from the healthy and deaf hemispheres. Secondly, the values from the healthy subjects' tracts are compared separately against the values from the patients' deaf ears and healthy ears to determine whether either of these deviates from the normal range of values. All statistical tests were performed on only the first of the two repeats of the tractography analyses, not both.

To look at the diffusion properties on a more local scale, we will also investigate the FA and MD along the tract as in (39).

Results

Bundle-average analysis

Reconstructed fiber tract bundles of the auditory nerve are shown for two healthy controls and two patients for both repeats of the tractography analysis in **Figure 3**. The reconstructed tracts between the two repeats are very similar, with only one clear change in the number of tracts (Fig. 3E) and minor differences in tract endpoints (**Figure 3B**). For all tractography results, DTI values were quantified for each subject and shown in **Table 2**.

Statistical analyses were performed on the first set of FA and MD values from **Table 2**. In healthy subjects, no laterality differences were observed, neither in FA ($p=0.73$) nor in MD ($p=0.77$). Similarly for patients, no differences were detected between diffusion values from the tracts in the deaf and healthy sides (FA: $p=0.95$; MD: $p=0.82$).

Comparison of the diffusion values in the tracts of patients to the healthy controls showed a significantly lower FA in the patients' tracts, both in the healthy-sided ($p=0.013$) and the deaf-sided tracts ($p=0.030$). No differences in MD were detected, neither when comparing the controls to the patients' healthy-sided ($p=0.09$)

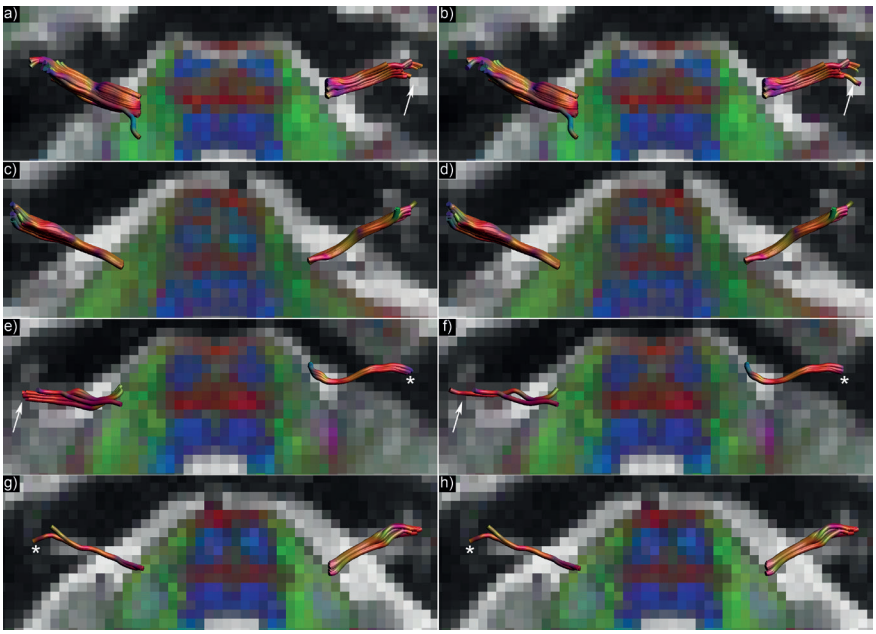

Figure 3: Tractography results for four subjects for the two repeats of the analysis (a and b, c and d, e and f, and g and h). The fiber tract segments are shown as streamtubes with a 1 mm thickness over an axial slice of the b = 0-image and the directionally-encoded color map. Panels a&b and c&d show two healthy controls (1 and 2, respectively); e&f and g&h show results of two patients (1 and 5, respectively). A clear difference in the number of tracts can be seen between panels e) and f), as indicated by the arrows. This is the largest and only clear difference in tractography results from all ten subjects. A few minor change appear in the tract endpoints, as indicated by the arrows in panels a) and b). The asterisks in e-h indicate the deafened sides.

nor deaf-sided (p=0.27) tracts. The apparent higher significance in the patients' healthy tracts compared to the patients' deaf-sided tracts appears to be caused by a larger standard deviation of FA and MD values in the deaf side rather than a larger difference in mean (**Table 2**). Because no differences between the left and right tracts of healthy controls were observed, these tests were performed using values averaged over the left and right segments for each control subject.

Along-tract analysis

Results from the along-tract analysis are shown for all subjects in **Figures 4 and 5**. All tracts from each bundle segment (corresponding to the left column of **Figure 3**) were averaged into one average tract to facilitate visualization of the FA and MD values along the tract. Mean FA and MD values are shown as a function of distance from

Table 2: Diffusion tensor measures for all subjects (mean ± standard deviation over all points of all tracts in fiber bundle) as well as per group (mean ± standard deviation over subjects within the group) for both repeats of the tractography analysis.

Subject		Fractional anisotropy		Mean diffusivity (10^{-3} mm^2/s)	
		Deaf	Healthy	Deaf	Healthy
Patient 1	repeat 1	0.09 ± 0.04	0.12 ± 0.03	1.27 ± 0.52	1.48 ± 0.31
	repeat 2	0.09 ± 0.04	0.10 ± 0.03	1.32 ± 0.51	1.37 ± 0.38
Patient 2	repeat 1	0.14 ± 0.06	0.10 ± 0.04	1.41 ± 0.42	1.67 ± 0.40
	repeat 2	0.14 ± 0.06	0.11 ± 0.04	1.40 ± 0.42	1.63 ± 0.43
Patient 3	repeat 1	0.09 ± 0.03	0.08 ± 0.03	1.63 ± 0.40	1.41 ± 0.43
	repeat 2	0.10 ± 0.03	0.08 ± 0.03	1.62 ± 0.40	1.41 ± 0.43
Patient 4	repeat 1	0.11 ± 0.03	0.07 ± 0.02	1.48 ± 0.36	1.65 ± 0.40
	repeat 2	0.11 ± 0.03	0.07 ± 0.02	1.48 ± 0.36	1.65 ± 0.40
Patient 5	repeat 1	0.06 ± 0.02	0.11 ± 0.03	1.71 ± 0.42	1.42 ± 0.46
	repeat 2	0.06 ± 0.02	0.11 ± 0.03	1.71 ± 0.42	1.42 ± 0.46
Mean	repeat 1	0.10 ± 0.03	0.10 ± 0.02	1.50 ± 0.17	1.53 ± 0.12
	repeat 2	0.10 ± 0.03	0.09 ± 0.02	1.51 ± 0.16	1.50 ± 0.13
		Left	Right	Left	Right
Control 1	repeat 1	0.14 ± 0.05	0.14 ± 0.06	1.23 ± 0.26	1.27 ± 0.31
	repeat 2	0.14 ± 0.05	0.14 ± 0.06	1.23 ± 0.26	1.27 ± 0.31
Control 2	repeat 1	0.12 ± 0.03	0.13 ± 0.05	1.40 ± 0.28	1.30 ± 0.30
	repeat 2	0.12 ± 0.03	0.13 ± 0.05	1.40 ± 0.28	1.30 ± 0.30
Control 3	repeat 1	0.15 ± 0.07	0.13 ± 0.07	1.26 ± 0.30	1.54 ± 0.41
	repeat 2	0.15 ± 0.07	0.13 ± 0.07	1.26 ± 0.29	1.52 ± 0.40
Control 4	repeat 1	0.12 ± 0.04	0.14 ± 0.05	1.52 ± 0.24	1.45 ± 0.33
	repeat 2	0.12 ± 0.04	0.14 ± 0.05	1.55 ± 0.24	1.45 ± 0.33
Control 5	repeat 1	0.13 ± 0.04	0.11 ± 0.05	1.63 ± 0.41	1.32 ± 0.39
	repeat 2	0.13 ± 0.04	0.11 ± 0.05	1.63 ± 0.41	1.31 ± 0.38
Mean	repeat 1	0.13 ± 0.01	0.13 ± 0.01	1.41 ± 0.17	1.38 ± 0.11
	repeat 2	0.13 ± 0.02	0.13 ± 0.01	1.42 ± 0.17	1.37 ± 0.11

the brainstem. Along-tract variability in DTI values along the tract is pronounced, with the FA and MD showing strong dependence on the distance from the brainstem (starting 18 mm from the mid-sagittal plane).

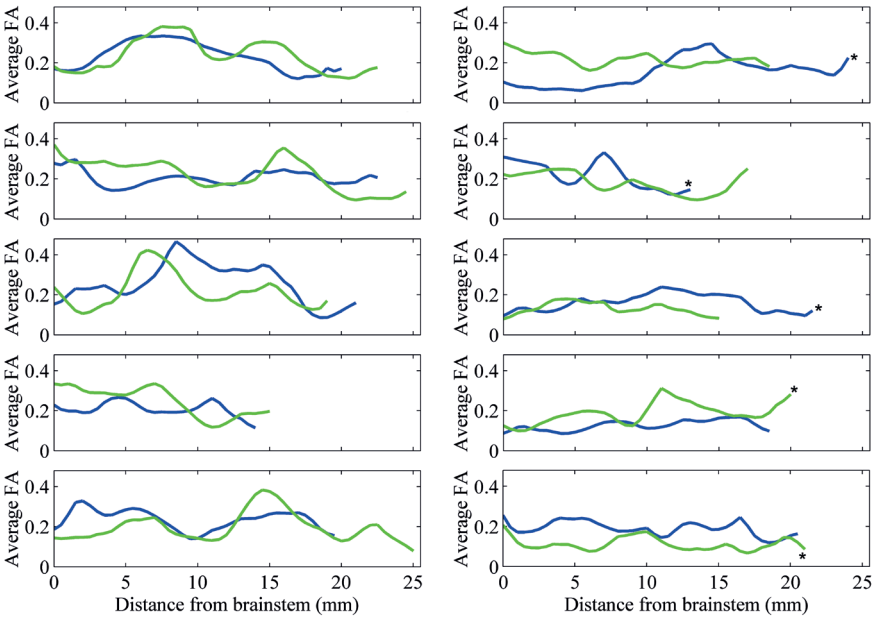

Figure 4: Fractional anisotropy (FA) values shown as a function of distance from the tract-selecting region of interest in the brainstem, where the blue and green lines indicate values from the left and right tracts, respectively. The left column of panels shows values from the five healthy controls, the right from the patients. For the patients, the profiles from the deaf-sided tract are indicated by the asterisk.

Discussion

In this work we have used diffusion tensor-based fiber tractography to reconstruct the auditory nerve and investigate its microstructural properties. We found a significantly lower FA in the auditory nerves in patients with long-term single-sided deafness compared to healthy controls. This reduction in FA was present in both the patients' healthy-sided fiber bundles and the deaf-sided bundles (**Table 2**). No differences were observed between the tracts from the deaf ears and from the healthy ears.

From **Figure 3** one can see that the vast majority of the reconstructed bundle segments is identical when the analysis is repeated. This high reproducibility is a result of a clearly visible cochlea on the 3D T2-weighted image – making it easy to delineate – and because the automatic mid-sagittal plane estimation is very robust (37).

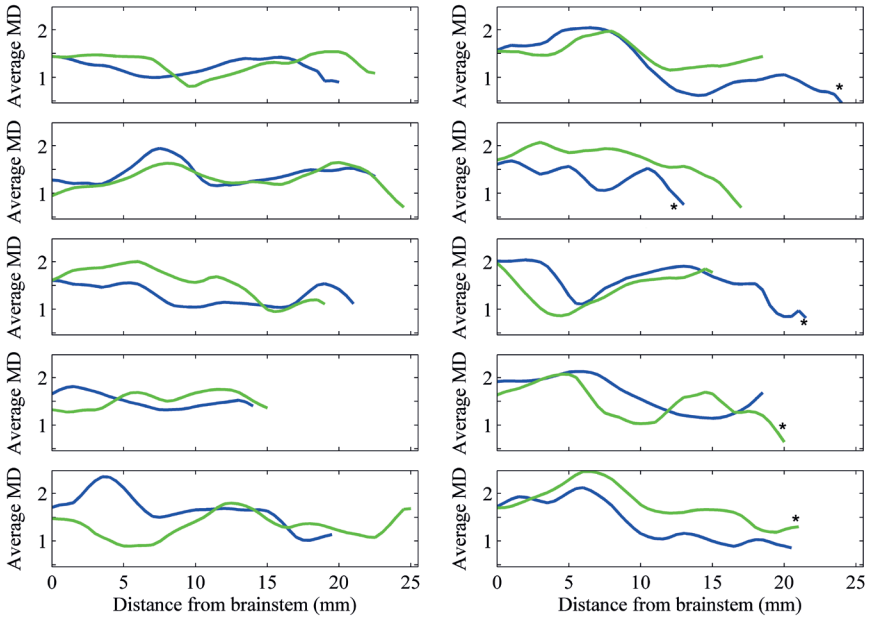

Figure 5: Mean diffusivity (MD, 10^{-3} mm^2/s) values shown as a function of distance from the tract-selecting region of interest in the brainstem, where the blue and green lines indicate values from the left and right tracts, respectively. The left column of panels shows values from the five healthy controls, the right from the patients. For the patients, the profiles from the deaf-sided tract are indicated by the asterisk.

All patients had lost hearing in one ear 15 or more years ago, and normal (4 patients) and near-normal (1 patient) hearing in their healthy ear. After such a long period of deafness the human auditory nerve has typically substantially degenerated with 10-50% survival as indicated by studies in bilaterally deaf subjects (2,4,5) and in unilateral deafness (20). Our results, albeit in a small subject group, do not show any FA reduction between tracts from the healthy ear and the deaf ear. Rather, FA decreases were observed in both auditory nerves from the patients compared to controls, indicating bilateral differences in microstructure of the auditory nerve in unilaterally deaf subjects. These results are the first to show a change in microstructure of the auditory nerve in patients with single-sided deafness.

In the entire auditory system, from the initial innervation of the auditory nerve to the brain areas that process sound, only the auditory nerve contains unilateral auditory information. Upon reaching the brainstem, the nerve impulses enter a

system of binaural processing, including the olivary nuclei and the inferior and superior colliculi, after which the information from one ear is transferred to the bilateral auditory cortices (40–42). If any fiber structure within the auditory system should be indicative of unilateral deafness, the auditory nerve would logically be that structure. Our results, indicating a bilateral decrease in FA in single-sided deafness patients, appear to contrast with that theory. Although remote, one possibility of the contralateral nerve to be affected by the deaf ear resides in the small population of efferent fibers in the auditory nerve, which run from the olivary complex in the brainstem (43). Effects of deafness on the efferent system are not well known, but cannot be excluded. For instance, since the olivary complex is affected by unilateral deafness (44), this may in turn have an effect on the efferent axons in the bundle on both sides.

Along-tract analysis

More specific along-tract investigations of DTI metrics in the auditory nerve did not reveal more subtle differences that whole-tract investigations would miss. In some patients similarities could be observed while in others such similarities are not present (Figures 4 and 5). The patterns of FA and MD as a function of distance from the brainstem varied too much between subjects to provide any valuable local information. Given the short length of the auditory nerve segment, roughly 2 cm, less gain is expected by using this along-tract analysis compared to the major white matter fiber bundles of over 10 cm in length (39).

Limitations

Note that the auditory nerve after leaving the cochlea joins with the vestibular nerve to form the vestibulocochlear nerve (or eighth cranial nerve), which then runs along near the facial nerve (45). DTI will not distinguish the different parts of the vestibulocochlear nerve and facial nerve, making our results less specific but nonetheless very informative. The facial and vestibular nerves are small compared to the auditory nerve, making the expected effect on the information captured using DTI rather small. Furthermore, it is more likely that the observed FA differences between deaf and normal-hearing subjects originate from changes in the auditory nerve than from the facial or vestibular nerves.

Imaging the auditory nerve

The cochlea and auditory nerves are located in between the inferior temporal poles and the brainstem, and this region is very prone to susceptibility-induced artefacts caused by air-bone-tissue interfaces. Standard clinical DTI, being an EPI-based technique, is especially sensitive to this, and the magnetic susceptibility

differences between air, bone, and soft tissue can cause pronounced geometric distortions (i.e., that the image is distorted and no longer represents the anatomy, (46)). The DTI acquisition was therefore optimized to minimize the distortions by limiting the FOV in the phase-encoding (AP) direction to 79 mm. This reduced the distortions to a level significantly lower than for standard neuroscientific (factor 2.5 compared to e.g. (47) and standard clinical protocols (factor 1.5 compared to e.g. (48)), even for the higher spatial resolution of our data.

The cross-sectional size of the auditory nerve, on the order of half a millimeter, is as yet beyond the resolution of DTI on clinical MRI scanners (typically 2 mm) to resolve. To more specifically image the auditory nerve, e.g., to distinguish it from the facial nerve, higher resolution DTI data is required. Increasing the resolution of the DTI scan, however, decreases the signal-to-noise ratio, and more importantly increases the geometric distortions of the standard EPI-based sequences (in-plane resolution only). This suggests that DTI acquisition methods should be considered with inherently lower geometric distortions, such as PROPELLER or readout-segmented EPI – both of which require longer acquisitions (49,50).

Analysis of diffusion

The diffusion tensor model was used in this study to investigate the auditory nerve. The FA and MD, derived from the tensor, are known to be affected by partial-voluming with cerebrospinal fluid (e.g. (51,52)). More advanced diffusion MRI methods, such as diffusion kurtosis imaging (DKI) and apparent fiber density (AFD), are theoretically less affected by this (53,54). Both DKI and AFD give a more direct indication of intra-cellular diffusion which may inform more specifically on the axons than the MD does (53). These methods, however, require acquisitions that are more demanding than the protocol used in this work (including a higher maximum b-value).

Study population

The sample size in this study, consisting of five patients and five controls, is relatively small. Nevertheless, a small but significant difference was observed in FA values in the auditory nerves between patients and controls. If any differences in microstructure are present in the tracts from each patient's healthy and deaf ear, our population size was not sufficient to detect this. Histological studies show strong evidence that such a difference can be expected (2–5), and future studies will investigate the auditory nerve's microstructure in a larger population to determine if these expected effects can be found.

Conclusions

In this work we have used DTI and tractography to show reduced FA values in both auditory nerves in patients with single-sided deafness compared to normal-hearing controls. Although the patients had normal and near-normal hearing in their healthy ear, the reduction in FA was bilateral. No differences in FA were found in the auditory nerves of the healthy and deaf side in patients. This means that, currently, DTI of an individual patient cannot be used to assess the condition of the nerve.

Acknowledgements

The authors would like to thank Feike de Graaff, Luuk Voskuilen, Paula Bos, and Lidy Kuster for their contributions in scan optimization and subject inclusion, and Niels Blanken en Guus Wisse for acquiring the MRI data.

References

1. Pfingst BE, Zhou N, Colesa DJ, Watts MM, Strahl SB, Garadat SN, et al. Importance of cochlear health for implant function. Vol. 322, Hearing Research. 2015. 77–88.
2. Seyyedi M, Viana LM, Nadol JB. Within-Subject Comparison of Word Recognition and Spiral Ganglion Cell Count in Bilateral Cochlear Implant Recipients. Otol Neurotol. 2014;1–5.
3. Spoendlin H, Schrott A. Analysis of the human auditory nerve. Hear Res. 1989;43(1):25–38.
4. Khan AM, Handzel O, Burgess BJ, Damian D, Eddington DK, Nadol JB. Is word recognition correlated with the number of surviving spiral ganglion. Cells and electrode insertion depth in human subjects with cochlear implants? Vol. 115, Laryngoscope. 2005. 672–677.
5. Fayad JN, Linthicum FH. Multichannel cochlear implants: Relation of histopathology to performance. Laryngoscope. 2006;116(8):1310–1320.
6. Webster M, Webster DB. Spiral ganglion neuron loss following organ of Corti loss: a quantitative study. Brain Res. 1981;212(1):17–30.
7. Versnel H, Agterberg MJH, de Groot JCMJ, Smoorenburg GF, Klis SFL. Time course of cochlear electrophysiology and morphology after combined administration of kanamycin and furosemide. Hear Res. 2007;231(1–2):1–12.
8. Smoorenburg GF, Willeboer C, Van Dijk JE. Speech perception in nucleus CI24M cochlear implant users with processor settings based on electrically evoked compound action potential thresholds. Audiol Neuro-Otology. 2002;7(6):335–347.
9. Stejskal EO, Tanner JE. Spin Diffusion Measurements: Spin Echoes in the Presence of a Time-Dependent Field Gradient. J Chem Phys. 1965;42(1):288–292.
10. Cleveland GG, Chang DC, Hazlewood CF, Rorschach HE. Nuclear magnetic resonance measurement of skeletal muscle: anisotrophy of the diffusion coefficient of the intracellular water. Biophys J. 1976;16(9):1043–1053.
11. Moseley ME, Cohen Y, Kucharczyk J, Mintorovitch J, Asgari HS, Wendland MF, et al. Diffusion-weighted MR imaging of anisotropic water diffusion in cat central nervous system. Radiology. 1990;176(2):439–445.
12. Beaulieu C. The basis of anisotropic water diffusion in the nervous system - a technical review. NMR Biomed. 2002;15(7–8):435–455.
13. Basser PJ, Mattiello J, LeBihan D. MR diffusion tensor spectroscopy and imaging. Biophys J. 1994;66(1):259–267.
14. Basser PJ, Pajevic S, Pierpaoli C, Duda J, Aldroubi A. In vivo fiber tractography using DT-MRI data. Magn Reson Med. 2000 Oct;44(4):625–632.
15. De Groot M, Verhaaren BFJ, De Boer R, Klein S, Hofman A, Van Der Lugt A, et al. Changes in normal-appearing white matter precede development of white matter lesions. Stroke. 2013;44(4):1037–1042.
16. Lutz J, Hemminger F, Stahl R, Dietrich O, Hempel M, Reiser M, et al. Evidence of Subcortical and Cortical Aging of the Acoustic Pathway: A Diffusion Tensor Imaging (DTI) Study. Acad Radiol. 2007;14(6):692–700.

17. Crippa A, Lanting CP, van Dijk P, Roerdink JBTM. A diffusion tensor imaging study on the auditory system and tinnitus. Open Neuroimag J. 2010;4:16–25.

18. Wu C-M, Ng S-H, Wang J-J, Liu T-C. Diffusion tensor imaging of the subcortical auditory tract in subjects with congenital cochlear nerve deficiency. AJNR Am J Neuroradiol. 2009;30(9):1773–1777.

19. Chang Y, Lee H-R, Paik J-S, Lee K-Y, Lee S-H. Voxel-Wise Analysis of Diffusion Tensor Imaging for Clinical Outcome of Cochlear Implantation: Retrospective Study. Clin Exp Otorhinolaryngol. 2012;5:S37.

20. Nadol JB. Degeneration of cochlear neurons as seen in the spiral ganglion of man. Hear Res. 1990;49(1–3):141–154.

21. Agterberg MJH, Versnel H, de Groot JCMJ, Smoorenburg GF, Albers FWJ, Klis SFL. Morphological changes in spiral ganglion cells after intracochlear application of brain-derived neurotrophic factor in deafened guinea pigs. Hear Res. 2008;244(1–2):25–34.

22. Spoendlin H. Retrograde degeneration of the cochlear nerve. Acta Otolaryngol. 1975;79(3–4):266–275.

23. Mori S, Crain BJ, Chacko VP, van Zijl PC. Three-dimensional tracking of axonal projections in the brain by magnetic resonance imaging. Ann Neurol. 1999;45(2):265–269.

24. Basser PJ. Inferring microstructural features and the physiological state of tissues from diffusion-weighted images. NMR Biomed. 1995;8(7):333–344.

25. Pierpaoli C, Jezzard P, Basser PJ, Barnett A, Di Chiro G. Diffusion tensor MR imaging of the human brain. Radiology. 1996;201(3):637–648.

26. Bozzali M, Falini A, Franceschi M, Cercignani M, Zuffi M, Scotti G, et al. White matter damage in Alzheimer's disease assessed in vivo using diffusion tensor magnetic resonance imaging. J Neurol Neurosurg Psychiatry. 2002;72(6):742–746.

27. Roosendaal SD, Geurts JJG, Vrenken H, Hulst HE, Cover KS, Castelijns JA, et al. Regional DTI differences in multiple sclerosis patients. Neuroimage. 2009;44(4):1397–1403.

28. Haakma W, Dik P, Ten Haken B, Froeling M, Nievelstein R a J, Cuppen I, et al. Diffusion tensor MRI and fiber tractography of the sacral plexus in children with spina bifida. J Urol. 2014;192(3):927–933.

29. Tournier J-D, Mori S, Leemans A. Diffusion tensor imaging and beyond. Magn Reson Med. 2011;65(6):1532–1556.

30. Jones DK. Diffusion MRI Theory, Methods, and Applications. Oxford University Press. 2010.

31. Jones DK, Horsfield MA, Simmons A. Optimal strategies for measuring diffusion in anisotropic systems by magnetic resonance imaging. Magn Reson Med. 1999;42(3):515–525.

32. Vos SB, Tax C, Visser F, Luijten P, Leemans A, Froeling M. The importance of correcting for B0-drift-induced global signal decrease in diffusion MRI. Proc 22th Annu Meet Int Soc Magn Reson Med Milan, Italy. 2014;4460.

33. Klein S, Staring M, Murphy K, Viergever MA, Pluim JPW. Elastix: A toolbox for intensity-based medical image registration. IEEE Trans Med Imaging. 2010;29(1):196–205.

34. Leemans A, Jones DK. The B-matrix must be rotated when correcting for subject motion in DTI data. Magn Reson Med. 2009;61(6):1336–1349.

35. Veraart J, Sijbers J, Sunaert S, Leemans A, Jeurissen B. Weighted linear least squares estimation of diffusion MRI parameters: Strengths, limitations, and pitfalls. Neuroimage. 2013;81(0):335–346.

36. Leemans A, Jeurissen B, Sijbers J, Jones D. ExploreDTI: a graphical toolbox for processing, analyzing, and visualizing diffusion MR data. Proc 17th Sci Meet Int Soc Magn Reson Med. 2009;17(2):3537.

37. Kuijf H, Leemans A, Viergever M, Vincken K. Assessment of methods to extract the mid-sagittal plane from brain MR images. SPIE Med Imaging. 2013;8673:86731K1-e86731K7.

38. Aggarwal M, Zhang J, Pletnikova O, Crain B, Troncoso J, Mori S. Feasibility of creating a high-resolution 3D diffusion tensor imaging based atlas of the human brainstem: a case study at 11.7 T. Neuroimage. 2013;74:117–127.

39. Colby JB, Soderberg L, Lebel C, Dinov ID, Thompson PM, Sowell ER. Along-tract statistics allow for enhanced tractography analysis. Neuroimage. 2012;59(4):3227–3242.

40. Rubel EW, Fritzsch B. Auditory system development: primary auditory neurons and their targets. Annu Rev Neurosci. 2002;25:51–101.

41. Fitzgerald MJT, Gruener G, Mtui E. Clinical Neuroanatomy and Neuroscience. 2007. 428

42. Solntseva GN. Morphology of the auditory and vestibular organs in mammals, with emphasis on marine species. Morphology of the Auditory and Vestibular Organs in Mammals, with Emphasis on Marine Species. 2007. 1-244

43. Warr W. Organization of the human superior olivary complex. In: In: Webster, D.B., Popper, A.N., Fay RR (Eds., editor. Organization of Olivocochlear efferent systems in mammals. 1992.

44. Russell F, Moore D. Effects of unilateral cochlear removal on dendrites in the gerbil medial superior olivary nucleus. Eur J Neurosci. 1999;11(4):1379–1390.

45. Zhang Y, Chen Y, Zou Y, Zhang W, Zhang R, Liu X, et al. Facial nerve preservation with preoperative identification and intraoperative monitoring in large vestibular schwannoma surgery. Acta Neurochir (Wien). 2013;155(10):1857–1862.

46. Skare S, Newbould RD, Clayton DB, Bammer R. Propeller EPI in the other direction. Magn Reson Med. 2006;55(6):1298–1307.

47. Vos SB, Viergever MA, Leemans A. Multi-fiber tractography visualizations for diffusion MRI data. PLoS One. 2013;8(11):e81453.

48. Reijmer YD, Leemans A, Heringa SM, Wielaard I, Jeurissen B, Koek HL, et al. Improved Sensitivity to Cerebral White Matter Abnormalities in Alzheimer's Disease with Spherical Deconvolution Based Tractography. PLoS One. 2012;7(8):e44074.

49. Pipe JG, Farthing VG, Forbes KP. Multishot diffusion-weighted FSE using PROPELLER MRI. Magn Reson Med. 2002;47(1):42–52.

50. Holdsworth SJ, Skare S, Newbould RD, Guzmann R, Blevins NH, Bammer R. Readout-segmented EPI for rapid high resolution diffusion imaging at 3T. Eur J Radiol. 2008;65(1):36–46.

51. Pasternak O, Sochen N, Gur Y, Intrator N, Assaf Y. Free water elimination and mapping from diffusion MRI. Magn Reson Med. 2009;62(3):717–730.

52. Vos SB, Jones DK, Viergever MA, Leemans A. Partial volume effect as a hidden covariate in DTI analyses. Neuroimage. 2011;55(4):1566–1576.

53. Jensen JH, Helpern J a, Ramani A, Lu H, Kaczynski K. Diffusional kurtosis imaging: the quantification of non-gaussian water diffusion by means of magnetic resonance imaging. Magn Reson Med. 2005;53(6):1432–1440.

54. Raffelt D, Tournier JD, Rose S, Ridgway GR, Henderson R, Crozier S, et al. Apparent Fibre Density: A novel measure for the analysis of diffusion-weighted magnetic resonance images. Neuroimage. 2012;59(4):3976–3994.

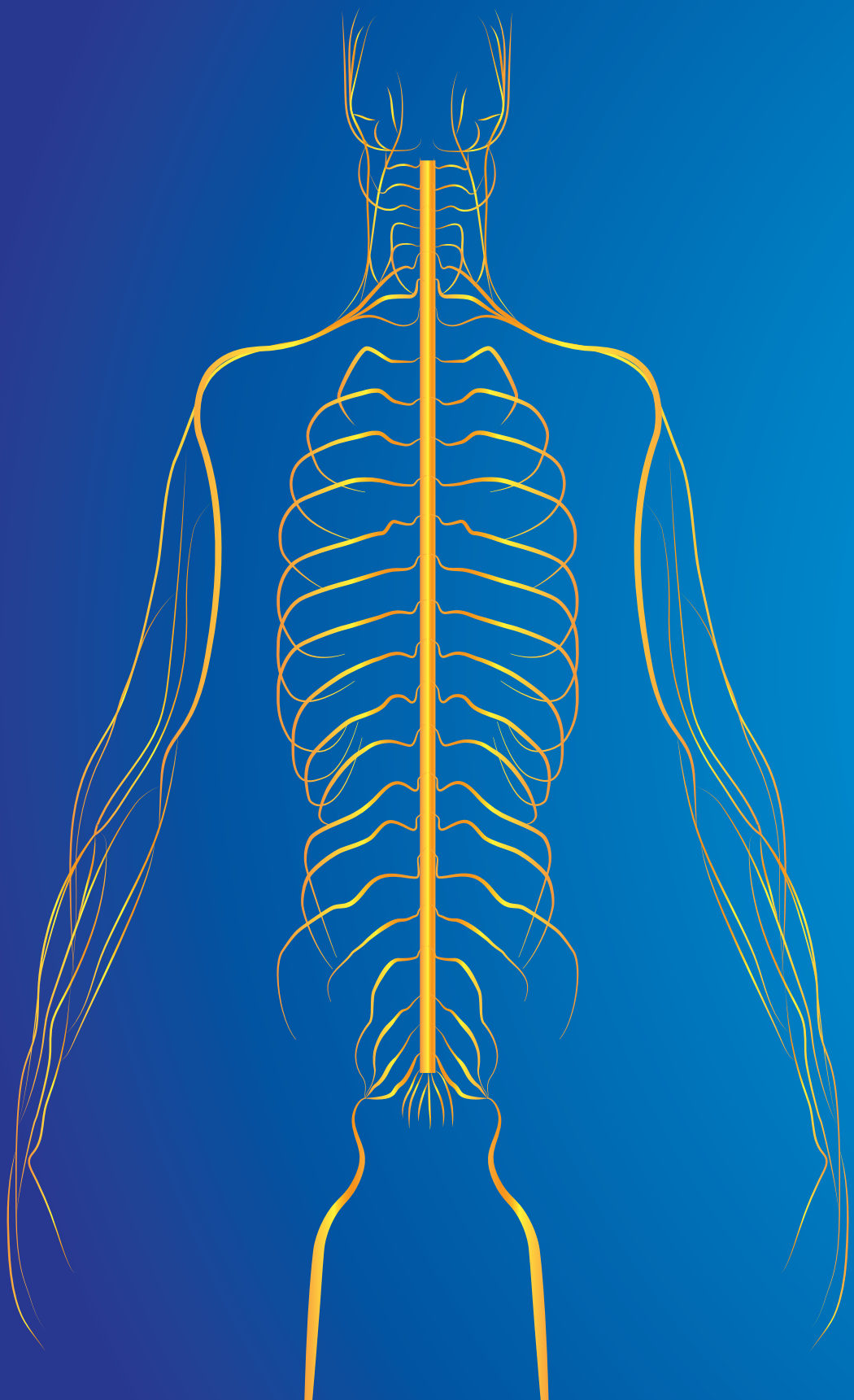

Chapter 8

Summary and general discussion

Summary

The peripheral nervous system is a network of nerves which transmits signals from the central nervous system to the body and vice versa. It regulates and controls body functions and activity. In the nerves, sensory neurons transmit the signal from the sensory receptors in the peripheral nervous system back to the central nervous system. Motor neurons transmit signal from the central nervous system back to the effectors. Damage to (part of) the nerves may cause distortion in transmission of the signal from the central nervous system to the innervated area and vice versa, which in turn may lead to muscle weakness or muscle wasting.

The underlying pathophysiological processes leading to nerve degeneration are not always evident. New insights regarding these processes are needed to better understand disease mechanisms. Furthermore, there is a need for non-invasive imaging modalities that can diagnose and monitor disease progression, or therapeutic effects in neurological disorders.

A non-invasive imaging technique that allows for the visualization of nerve tissue is magnetic resonance imaging (MRI). MRI has many different ways of generating contrast. Diffusion tensor imaging (DTI) is an MRI technique which is sensitive to the random motion of water molecules and can be used to measure the diffusion of water molecules in tissue. In nerve tissue this diffusion is more oriented along the nerve than perpendicular to it (anisotropic diffusion). This makes it a potential valuable method to investigate peripheral nerve tissue in neurological disorders. In this thesis MRI and DTI are applied in different neurological disorders to explore its potential value in a clinical setting.

In **chapter 2**, the reproducibility of DTI in the lumbosacral nerves was investigated. DTI was found to be reproducible and can therefore be reliably used in cross-sectional studies in a clinical setting. Small differences in inter-week comparison highlight that one needs to be careful when interpreting diffusion measures in longitudinal studies, since small differences can also be caused by factors other than disease progression or therapy response.

In **chapter 3**, the application of DTI in the lumbosacral plexus in spina bifida patients is demonstrated. The asymmetry and disorganization of the nerves, especially at the level of the myelomeningocele, indicate that the sacral plexus in these patients is different from healthy controls. Differences in diffusion values demonstrated nerve abnormalities in these patients, and could be indicative for reduced intrinsic

diffusion in the intra-axonal space due to cytoskeletal breakdown. Although spina bifida is a complex pathology, we expect that abnormal diffusion parameters can be indicative for affected or dysfunctional nerves.

To determine the clinical value of fiber tractography and diffusion parameters, we assessed the applicability in compressed nerves of lumbar disc herniated patients in **chapter 4**. We found differences in the fractional anisotropy (FA) and radial diffusivity (RD) between the affected nerves in patients and healthy controls. However, we did not observe differences when comparing the compressed side with the contralateral side in the same patient. Additionally, we showed that the location of sampling is important since diffusion values are different along the nerve roots, with lower FA and higher mean diffusivity (MD), axial diffusivity (AD) and RD values proximal than distal. This is an important aspect which needs to be considered in the study design of DTI experiments.

In **chapter 5** we determined the added value of MRI and DTI to distinguish multifocal motor neuropathy (MMN) patients from amyotrophic lateral sclerosis (ALS) patients and healthy controls. In the nerves of the forearm, we found differences in AD and enlarged cross-sectional areas in MMN patients compared to ALS patients and healthy controls. Although future studies should focus on improving patient comfort, we expect that the application of MRI and DTI may become relevant in distinguishing between these diseases and can help to provide insight into pathological mechanisms.

In **chapter 6** we investigated the application of MRI and DTI in spinal muscular atrophy (SMA) patients in the cervical spinal cord and the nerve roots at the spinal cord level of C3-C8. Cross-sectional area measurements of the cervical spinal cord segments were consistently smaller in SMA patients compared to healthy controls. Additionally, diffusion in the cervical nerve roots in patients was lower compared to healthy controls. Based on these findings we expect that MRI and DTI are promising techniques to monitor SMA progression and treatment effects.

In **chapter 7** we demonstrate the application of DTI in the auditory nerve. We showed a reduction in FA in both auditory nerves in patients with single-sided deafness compared to healthy controls. No differences in FA were found between the auditory nerves of the healthy and deaf side in patients. This means that, currently, DTI cannot be used to assess the condition of the nerve in an individual patient.

In conclusion, the various studies in this thesis show that MRI and DTI are promising techniques in the evaluation of peripheral nerve tissue in neurological disorders. The evaluated methods may contribute to the improvement of diagnosis and prognosis of different neurological disorders. However, in some patient groups the hypothesized intra-subject differences were not found. Furthermore, in the longitudinal follow-up of patients, one should be careful with the interpretation, since differences in diffusion values may also be caused by other factors than disease progression or therapeutic effects.

General discussion

This thesis focusses on the application and validation of DTI in clinical practice to determine the added value of DTI as a tool to evaluate neurological disorders. One of the aims of this thesis was to develop reliable acquisition and post-processing methods that enable DTI to be used in a clinical setting. Furthermore, we investigated the feasibility and robustness of DTI in peripheral nerve tissue in various neurological disorders and anatomical locations. Based on our findings we expect that MRI and DTI will be of added value in the diagnosis, monitoring, or investigation of pathophysiological processes in peripheral nerve tissue affected by neurological disorders.

The application of DTI to investigate peripheral nerve tissue is not straightforward. Currently, there are no standardized protocols for the acquisition and post-processing which makes the application in clinical practice challenging. In this section different technical and practical considerations for the application of DTI in clinical practice are reviewed. Additionally, we discuss the future of DTI as a clinical application in neurological disorders.

Setting up a DTI experiment for clinical applications

When setting up DTI sequences for diagnostic purposes, the sequences should be robust, reliable, and the data obtained from these sequences should contain all the relevant and essential anatomical detail. More specifically, it is desirable to have DTI data with a high resolution and high signal-to-noise ratio (SNR) within a short scan time to reduce patient discomfort. Unfortunately each of these factors will come at the cost of the other (1). This means that there is a tradeoff between resolution, SNR, and scan time. Scan time in clinical practice is limited and is often also restricted to what a patient can handle. Especially for patients with neurological disorders it can be very challenging to lie still for a longer period of time, since body parts can be very stiff and patients can be affected by pain associated with the disease. In the study where we scanned participants in prone position with their arm above the head, we experienced much discomfort among patients, and to a lesser extent also among healthy controls. But also in the study where were investigated spinal muscular atrophy patients, which were positioned in supine position, we experienced that some of the patients had difficulties with lying still. This was also related to the tremor these patients typically have (2). In general, the entire scan MRI protocol should be limited to 35 minutes, to reduce patient discomfort and motion artifacts affecting the images. It is crucial to have a sufficient SNR, as DTI is very sensitive to the effects of noise, which may affect the eigenvalues estimation

(3) and reliability of tractography (1). Peripheral nerves are typically between 2-10 mm in diameter (4). Depending on the anatomy and size of the specific nerves of interest, a minimally required resolution should be determined. To visualize the lumbosacral plexus we used a voxel size of $3 \times 3 \times 3$ mm^3, where the diameter of the lumbar nerve roots is around 2.8 mm (5). For the forearm we used a voxel size of $1.5 \times 1.5 \times 4$ mm^3, where the diameter of the median nerve is around 3 mm and the ulnar nerve is around 2.6 mm (6). In the case of nerves with a high level of curvature, such as in the lumbosacral and cervical region, one should aim at developing a protocol with isotropic resolution. In the case where the trajectory of the nerves is quite straight such as in the forearm, the isotropic protocols are not essential and the slice thickness along the nerve can be increased, which leads to shorter scan time and/or higher in plane resolution.

Practical considerations

In clinical practice, one should be aware of unforeseen difficulties while scanning patients. In the case of scanning the extremities, it is imperative to position the extremity as close to the isocenter of the magnet as possible as B0 inhomogeneities can increase with increasing distance from the magnet isocenter (4,7). Patients of which the forearm is scanned are therefore typically scanned in prone position. However, this is very uncomfortable for the patient, and it can be very challenging to lie still for the entire duration of the protocol. During the scan, pain associated with the disease can make this even more challenging. Since protocol development is usually based on healthy controls, one should be aware of patient induced factors interfering with the acquisition of high quality data. In some diseases tremor may be present, which will induce patient movement and therefore decrease scan quality. Furthermore, logistical problems may occur in cases where patients are very stiff, such as in SMA patients, and are unable to reposition themselves in such a way that they fit in the scanner. In those cases the bore size of the scanner is an important aspect to consider. An MRI scanner with a field strength of 3 Tesla is strongly preferred over 1.5 Tesla because of increased SNR. Furthermore, coils dedicated to the body part under examination should be used (4). Guggenberger et al investigated the inter-scanner variability in FA and MD values of the median nerve on three different 3 Tesla scanners. They showed small but significant differences between the scanners. Although the vendor measurement bias was still small enough to detect a difference between normal and pathological conditions, they recommend to use the same scanner to examine the patients (8). In our studies we therefore used the same scanner for all participants per study. For each area of interest and each patient group the development and the setup

of the protocol should be specifically designed to obtain the best quality of DTI data. In the projects concerning this thesis, a close collaboration between the neurology department and the radiology department was established. In this way expertise regarding patient group and clinical concerns and expertise regarding protocol development and technical considerations for MRI were combined and are essential in order to obtain such protocols.

Processing

There are various methods for processing diffusion data. The steps required in order to correct for potential artifacts are typically optimized for brain and need to be adjusted before use in peripheral nerves. Before continuing with any of the processing steps it is important to check the quality of the data. High quality data is important and identifying artifacts and issues at an early stage is essential for obtaining reliable results. In general DTI parameters are very sensitive and can thus easily be affected by artifacts and data quality. More detail regarding artifacts in the data is given below. The data quality check can be done by simply 'eyeballing' the raw data (9). By viewing the data in for example a movie loop, and going through the different diffusion-weighted volumes, one can already get an understanding of what the quality of the data is and outliers can easily be detected (9). Residual maps of the fitting procedure can also be used to identify artefacts caused by for example motion or pulsatility in the data (9). When correcting for subject motion, the rotations obtained from registering the images, must also be applied to the diffusion encoding vectors (10).

When performing fiber tractography, there are different parameters which can be used as a threshold in order to obtain only those tracts belonging to the peripheral nerves. Such parameters are, for instance, the FA, the turning angle, and the fiber length (4). Caution should be taken when selecting these parameters, since the choice of setting these parameters depends on the geometry of the nerve being studied. When the input of these parameters are set too strict, the tracking algorithm may stop too early which may result in unfinished fiber tracts, or when parameters are set too tolerant, this can result in the inclusion of false tracts in the fiber tractography which do not belong to the nerve tract.

DTI has the disadvantage that it has a relatively low spatial resolution. In the studies of this thesis investigating the lumbosacral nerves the spatial resolution was 2.5 to 3 mm isotropic, whereas the diameter of the nerves in the lumbosacral plexus are around the same size or smaller (5). Therefore, partial volume effects are likely to occur and can affect the fiber tractography and the diffusion parameters, especially

in the smaller nerve roots (5,11). A higher resolution will reduce these effects, but will increase scan time and reduce SNR of the data (1). Several more advanced sequence designs have been proposed to reduce scan time including parallel imaging, and multi-band imaging (12).

Artifacts

Diffusion weighted images are usually based on spin echo sequences with an echo planar imaging read-out (SE-EPI). Although these sequences are fast (13), they are more prone to artifacts such as eddy-current and magnetic field inhomogeneities (14,15). Artifacts in the data may result in distortion of the images. If the artifacts are too extensive the data is unusable for further analysis. When the artifacts present in the data are insufficient corrected this may lead to incorrect quantitative diffusion values. To prevent such artifacts from occurring, artifacts should be resolved preferably during the acquisition. This can be done by shimming which improves homogeneity of the magnetic field. However, establishing a homogeneous field can be difficult in areas with complex anatomy and air-tissue boundaries. Other methods have been proposed to reduce susceptibility artefacts such as the DW-SLICE approach in which the EPI acquisition module is replaced by a single-shot turbo spin echo (TSE) module (16). Furthermore, post-processing methods should include steps to correct for such artifacts (15). Nevertheless, when abnormalities in the fiber tractography and diffusion parameter results are found, one should still consider that these can also be caused by deformations or other artifacts present in the data (17).

Interpretation of fiber tractography and DTI parameters

While fiber tractography can map the 3D architecture of nerve tissue and can provide striking images, the technology has not been used extensively to visualize peripheral nerve tissue and the interpretation is not straightforward. One of the major questions remains how representative these images are for wat we think they present. It is therefore important to consider that abnormalities in fiber tractography and diffusion parameters can be associated with the clinical characteristics and pathophysiological processes patients present themselves with (18), but they can also be due to deformities in the data introduced by the imaging technique itself, or limitations of the fiber tractography methods (11,17).

In human tissue, diffusion processes are mainly influenced by cellular microstructures. In nerves, this is based on the composition of the neurological tissue, which consists of different barriers and compartments such as the intracellular and extracellular space, neurons, axons, and for example myelin (19). Changes in

diffusion parameters can be associated with biological processes in the tissue or (patho)physiological processes. The diffusion weighted MRI measurement reflects the amount of water diffusion that occurs along the axis of the applied diffusion gradient, averaged over the voxel (9). As such, conventional DTI acquisition and processing methods cannot provide direct information on cellular-level axonal connectivity. Axonal structures can be very complex and can merge or branch out of one voxel. It is therefore difficult to process and interpret data from voxels containing more than one population of axonal tracts with different orientations. Another limitation is that the afferent and efferent pathways of axonal tracts cannot be distinguished from the direction of water diffusion, as DTI can only identify the orientation of the diffusion and not its direction (20). DTI can therefore not directly be used to distinguish between sensor and motor involvement.

In general, the FA and MD are mostly used to represent microstructural properties in the tissue. A drop in FA is usually associated with neurological damage. However, when interpreting this decrease, there are different explanations: 1) the AD is decreased (i.e. largest eigenvalue, λ_1), 2) RD is increased (i.e. perpendicular diffusivity, $(\lambda_2 + \lambda_3)/2)$), or 3) both happen simultaneously. This may be associated with a larger axon diameter, a lower packing density, both of these processes (which means fewer barriers to diffusion in a given space), or due to increased membrane permeability (9). In animal studies a drop in FA was associated with mechanical disruption, tearing of myelin sheaths and fibers, and also Wallerian degeneration (21). A change in MD should be evaluated similarly. A decrease of MD can arise from a decrease in AD, in RD, or both. It is therefore important to calculate the AD and RD in order to determine what the underlying cause of change is (22). In earlier research a decrease in AD has been associated with axonal loss, whereas an increase in RD has been correlated with demyelination (23–26). However, this does not always hold, since axonal loss may lead to a decrease in AD, but a decrease in AD does not necessarily mean that there is axonal loss (22). In areas with low FA, crossing fibers, or partial volume effected voxels, AD and RD may not always reflect the same underlying microstructural characteristics (27), although crossing fibers are considered of lesser relevance in peripheral nerves since they are typically longitudinally oriented (28).

Implementation in clinical practice

DTI has demonstrated to be a valuable method to visualize the lumbosacral plexus and brachial plexus. Conventional ultrasound techniques and electrophysiological studies have their limitations, due to the deep location and complex anatomy

of these nerves (29). Before DTI can be implemented in clinical practice, the reproducibility should be assessed. Earlier studies investigating the use of DTI in the brachial plexus and the upper leg showed good reproducibility between test-retest on the same day (30,31). However, the small but significant differences in diffusion values found in the inter-week comparison in chapter 2, suggests that in the evaluation of longitudinal studies, one should be careful with the interpretation of potential differences in diffusion values and fiber tractography results.

To determine the exact clinical value of DTI, diffusion parameters should be correlated to clinical parameters such as (quantitative) clinical outcome measurements, EMG, nerve conduction studies, or ideally to histology (32,33) However, the latter is difficult to retrieve in vivo studies. We aimed at correlating the diffusion parameters to the clinical tests and EMG measurements in chapter 5 and 6. However, correlation between these two functional markers and DTI are not always present, and interpretation is therefore not straightforward. Several studies have investigated the correlation of DTI with clinical assessment in polyneuropathies and other peripheral nerve diseases (34,35). Some studies have found a correlation between DTI measures and nerve conduction properties or clinical tests (36–40), others were not able to find this correlation (40–42). As these studies all used small sample sizes, larger sample sizes are needed to investigate the exact origin of the variation of this correlation further.

The diffusion tensor describes the magnitude, the degree of anisotropy, and the orientation of diffusion anisotropy (43). Although it is a promising technique to quantify microstructural properties of tissue, it is important to know its potential value and its pitfalls. Changes in diffusion of water within the tissue, may be associated with changes in the tissue microstructures (43). However, to determine whether DTI is the best technique to be used for a specific research question, knowledge about disease characteristics is needed. When the aim is to investigate the anatomical features of the nerves, DTI may not always be the preferable method to use.

Future directions

Nowadays, segmentation methods to track the fiber tracts still rely for a large part on manual segmentation which is prone to bias and is time-consuming. The application and evaluation of DTI as a tool to assess peripheral nerves requires careful oversight by both trained scientists and radiologists or clinicians interpreting the

data. Future research should focus on the development of dedicated sequences and coil design to improve SNR, the spatial resolution and to reduce scan time. Automated post-processing techniques, such as atlas based analysis techniques, which are already applicable for the brain (44,45), are needed specifically designed for peripheral nerve tissue to improve the robustness of this technique and to make it clinically applicable on a larger scale (4). These techniques should enable automated selection of nerve tissue, which will reduce observer dependent bias on the one hand and save a substantial amount of post-processing time for the user on the other hand.

Clinical applications

Diffusion MRI has already been proven to play an important role in the detection of stroke (46). After this, clinical applications of DTI expanded and DTI together with functional MRI have been shown helpful for preoperative planning of brain tumors (47,48).

Other purposes for which DTI can be used include post-mortem applications (49). An earlier study by Scheurer et al has suggested to use DTI to estimate the time span between death and examination. DTI may provide a more objective estimate of this interval especially after 30 hours of death (50). In cases where trauma is expected but no external sign of violence is present such as in cases of babies who have been violently shaken, DTI may also be helpful (51).

DTI has been used to investigate peripheral neuropathies. When this is applied in a post-mortem setting, it can be used to better understand pathological mechanisms as it can be compared to histology (33). Investigating neurological disorders in a post-mortem setting may be helpful to contribute to a better understanding of pathogenesis and disease progression.

In light of new therapeutic developments, DTI may also play an important role. Recently, the first survival motor neuron therapy for spinal muscular atrophy patients has been approved (52,53). In this context the evaluation of this new therapy becomes important, since this new therapy is extremely expensive. Effectiveness per patient should be evaluated based on sensitive quantitative outcome measures to identify whether or not an individual patient will benefit from the new treatment and also to reduce costs (54). DTI may be a potential candidate for the assessment of these therapeutic effects since it is very sensitive to changes in tissue.

Apart from that, we expect that DTI may also be helpful in the preoperative planning of neurofibromatosis patients. In these patients benign tumors grow out of the (peripheral) nervous system. It is often difficult to determine what part of the peripheral nerves is still functional. Future research should focus on investigating what the added value of DTI is as a preoperative tool in which fiber tractography and diffusion measures may help to detect what part of the nervous system belongs to the functional peripheral nerves and what part is tumor tissue. This information can then be used by the surgeon to determine which tissue needs to be dissected.

With some technical improvements for both acquisition and post-processing we expect that DTI will become valuable to monitor disease progression or treatment effects in peripheral nerve tissue affected by neurological disorders.

References

1. Froeling M, Nederveen AJ, Nicolay K, Strijkers GJ. DTI of human skeletal muscle: the effects of diffusion encoding parameters, signal-to-noise ratio and T2 on tensor indices and fiber tracts. NMR Biomed. 2013;26(11):1339–1352.
2. Dawood AA, Moosa A. Hand and ECG tremor in spinal muscular atrophy. Arch Dis Child. 1983;58(5):376–378.
3. Bastin ME, Armitage PA, Marshall I. A theoretical study of the effect of experimental noise on the measurement of anisotropy in diffusion imaging. Magn Reson Imaging. 1998;16(7):773–785.
4. Jeon T, Fung MM, Koch KM, Tan ET, Sneag DB. Peripheral nerve diffusion tensor imaging: Overview, pitfalls, and future directions. J Magn Reson Imaging. 2017;1–19.
5. Hogan Q. Size of human lower thoracic and lumbosacral nerve roots. Anesthesiology. 1996;85(1):37–42.
6. Haakma W, Jongbloed BA, Froeling M, Goedee HS, Bos C, Leemans A, et al. MRI shows thickening and altered diffusion in the median and ulnar nerves in multifocal motor neuropathy. Eur Radiol. 2017;27(5); 2216-2224.
7. Johnson D, Stevens KJ, Riley G, Shapiro L, Yoshioka H, Gold GE. Approach to MR Imaging of the Elbow and Wrist: Technical Aspects and Innovation. Vol. 23, Magnetic Resonance Imaging Clinics of North America. 2015. 355–366.
8. Guggenberger R, Nanz D, Bussmann L, Chhabra A, Fischer MA, Hodler J, et al. Diffusion tensor imaging of the median nerve at 3.0 T using different MR scanners: agreement of FA and ADC measurements. Eur J Radiol. 2013;82(10):e590-596.
9. Jones DK, Knösche TR, Turner R. White matter integrity, fiber count, and other fallacies: The do's and don'ts of diffusion MRI. Neuroimage. 2013;73(0):239–254.
10. Leemans A, Jones DK. The B-matrix must be rotated when correcting for subject motion in DTI data. Magn Reson Med. 2009;61(6):1336–1349.
11. Vos SB, Jones DK, Viergever MA, Leemans A. Partial volume effect as a hidden covariate in DTI analyses. Neuroimage. 2011;55(4):1566–1576.
12. Mitsuda M, Suzuki Y, Kunimatsu A, Kasahara A, Watanabe Y, Ino K, et al. Feasibility of Diffusion Tensor Imaging at 1.5T Using Multi-Band Echo Planar Acquisition. Magn Reson Med Sci. 2017;16(2):169–175.
13. Oudeman J, Nederveen AJ, Strijkers GJ, Maas M, Luijten PR, Froeling M. Techniques and applications of skeletal muscle diffusion tensor imaging: A review. Vol. 43, Journal of Magnetic Resonance Imaging. 2016. 773–788.
14. Irfanoglu MO, Walker L, Sammet S, Pierpaoli C, Machiraju R. Susceptibility distortion correction for echo planar images with non-uniform B-spline grid sampling: A diffusion tensor image study. In: Lecture Notes in Computer Science (including subseries Lecture Notes in Artificial Intelligence and Lecture Notes in Bioinformatics). 2011. 174–181.
15. Jones DK, Cercignani M. Twenty-five pitfalls in the analysis of diffusion MRI data. NMR Biomed. 2010;23(7):803–820.

16. Schakel T, Hoogduin JM, Terhaard CHJ, Philippens MEP. Technical Note: Diffusion-weighted MRI with minimal distortion in head-and-neck radiotherapy using a turbo spin echo acquisition method. Med Phys. 2017;44(8):4188–4193.

17. Tournier JD, Calamante F, King MD, Gadian DG, Connelly A. Limitations and requirements of diffusion tensor fiber tracking: An assessment using simulations. Magn Reson Med. 2002;47(4):701–708.

18. Haakma W, Dik P, Ten Haken B, Froeling M, Nievelstein R a J, Cuppen I, et al. Diffusion tensor MRI and fiber tractography of the sacral plexus in children with spina bifida. J Urol. 2014;192(3):927–933.

19. Beaulieu C. The basis of anisotropic water diffusion in the nervous system - a technical review. NMR Biomed. 2002;15(7–8):435–455.

20. Mori S, van Zijl PCM. Fiber tracking: principles and strategies - a technical review. NMR Biomed. 2002;15(7–8):468–480.

21. Nevo U, Hauben E, Yoles E, Agranov E, Akselrod S, Schwartz M, et al. Diffusion anisotropy MRI for quantitative assessment of recovery in injured rat spinal cord. Magn Reson Med. 2001;45(1):1–9.

22. Tournier J-D, Mori S, Leemans A. Diffusion tensor imaging and beyond. Magn Reson Med. 2011;65(6):1532–1556.

23. Beaulieu C, Does MD, Snyder RE, Allen PS. Changes in water diffusion due to Wallerian degeneration in peripheral nerve. Magn Reson Med. 1996;36(4):627–631.

24. Song S-K, Sun S-W, Ramsbottom MJ, Chang C, Russell J, Cross AH. Dysmyelination Revealed through MRI as Increased Radial (but Unchanged Axial) Diffusion of Water. Neuroimage. 2002;17(3):1429–1436.

25. Song SK, Yoshino J, Le TQ, Lin SJ, Sun SW, Cross AH, et al. Demyelination increases radial diffusivity in corpus callosum of mouse brain. Neuroimage. 2005;26:132–140.

26. Aung W, Mar S, Benzinger T. Diffusion tensor MRI as a biomarker in axonal and myelin damage. Imaging Med. 2013;5(5):427–440.

27. Wheeler-Kingshott CAM, Cercignani M. About "axial" and "radial" diffusivities. Magn Reson Med. 2009;61(5):1255–1260.

28. Simon NG, Kliot M. Diffusion weighted MRI and tractography for evaluating peripheral nerve degeneration and regeneration. Neural Regen Res. 2014;9(24):2122–2124.

29. Noguerol TM, Barousse R, Socolovsky M, Luna A. Quantitative magnetic resonance (MR) neurography for evaluation of peripheral nerves and plexus injuries. Quant Imaging Med Surg. 2017;7(4):398–421.

30. Ho MJ, Manoliu A, Kuhn FP, Stieltjes B, Klarhöfer M, Feiweier T, et al. Evaluation of Reproducibility of Diffusion Tensor Imaging in the Brachial Plexus at 3.0 T. Invest Radiol. 2017;52(8):482–427.

31. Simon NG, Lagopoulos J, Gallagher T, Kliot M, Kiernan MC. Peripheral nerve diffusion tensor imaging is reliable and reproducible. J Magn Reson Imaging. 2015;43(4):962–969.

32. Haakma W, Froeling M, Pedersen M, Uhrenholt L, Douven P, Leemans A, et al. Post-mortem diffusion MRI of the cervical spine and its nerve roots. J Forensic Radiol Imaging. 2018;12(1);50-56.

33. Schmierer K, Wheeler-Kingshott CAM, Boulby PA, Scaravilli F, Altmann DR, Barker GJ, et al. Diffusion tensor imaging of post mortem multiple sclerosis brain. Neuroimage. 2007;35(2):467–477.

34. Cardenas-Blanco A, MacHts J, Acosta-Cabronero J, Kaufmann J, Abdulla S, Kollewe K, et al. Structural and diffusion imaging versus clinical assessment to monitor amyotrophic lateral sclerosis. NeuroImage Clin. 2016;11:408–414.

35. Breckwoldt MO, Stock C, Xia A, Heckel A, Bendszus M, Pham M, et al. Diffusion Tensor Imaging Adds Diagnostic Accuracy in Magnetic Resonance Neurography. Invest Radiol. 2015;50(8):498–504.

36. Lindberg PG, Feydy A, Le Viet D, Maier MA, Drape JL. Diffusion tensor imaging of the median nerve in recurrent carpal tunnel syndrome - initial experience. Eur Radiol. 2013;23(11):3115–3123.

37. Wang C-K, Jou I-M, Huang H-W, Chen P-Y, Tsai H-M, Liu Y-S, et al. Carpal tunnel syndrome assessed with diffusion tensor imaging: Comparison with electrophysiological studies of patients and healthy volunteers. Eur J Radiol. 2012;81(11):3378–3383.

38. Heckel a., Weiler M, Xia A, Ruetters M, Pham M, Bendszus M, et al. Peripheral Nerve Diffusion Tensor Imaging: Assessment of Axon and Myelin Sheath Integrity. PLoS One. 2015;10(6):1–13.

39. Baümer P, Pham M, Ruetters M, Heiland S, Heckel A, Radbruch A, et al. Peripheral Neuropathy : Detection with Diffusion-Tensor Imaging. Radiology. 2014;273(1):185–193.

40. Mathys C, Aissa J, Zu Hörste GM, Reichelt DC, Antoch G, Turowski B, et al. Peripheral Neuropathy: Assessment of Proximal Nerve Integrity By Diffusion Tensor Imaging. Muscle Nerve. 2013;48(6):889–896.

41. Hiltunen J, Kirveskari E, Numminen J, Lindfors N, Goransson H, Hari R. Pre- and post-operative diffusion tensor imaging of the median nerve in carpal tunnel syndrome. Eur Radiol. 2012;22(6):1310–1319.

42. Kakuda T, Fukuda H, Tanitame K, Takasu M, Date S, Ochi K, et al. Diffusion tensor imaging of peripheral nerve in patients with chronic inflammatory demyelinating polyradiculoneuropathy: A feasibility study. Neuroradiology. 2011;53:955–960.

43. Alexander AL, Lee JE, Lazar M, Field AS. Diffusion tensor imaging of the brain. Neurotherapeutics. 2007;4(3):316–329.

44. Kersbergen KJ, Leemans A, Groenendaal F, van der Aa NE, Viergever MA, de Vries LS, et al. Microstructural brain development between 30 and 40 weeks corrected age in a longitudinal cohort of extremely preterm infants. Neuroimage. 2014;103:214–224.

45. Lebel C, Walker L, Leemans A, Phillips L, Beaulieu C. Microstructural maturation of the human brain from childhood to adulthood. Neuroimage. 2008;40(3):1044–1055.

46. Warach S, Gaa J, Siewert B, Wielopolski P, Edelman RR. Acute human stroke studied by whole brain echo planar diffusion- weighted magnetic resonance imaging. Ann Neurol. 1995;37(2):231–241.

47. Ulmer JL, Salvan C V, Mueller WM, Krouwer HG, Stroe GO, Aralasmak A, et al. The role of diffusion tensor imaging in establishing the proximity of tumor borders to functional brain systems: implications for preoperative risk assessments and postoperative outcomes. Technol Cancer Res Treat. 2004;3(6):567–576.

48. Talos I, O'Donnell L, Westin C. Diffusion tensor and functional MRI fusion with anatomical MRI for image-guided neurosurgery. Medial Image Comput Comput Invervention. 2003;6(1):407–415.

49. Haakma W, Pedersen M, Froeling M, Uhrenholt L, Leemans A, Boel LWT. Diffusion tensor imaging of peripheral nerves in non-fixed post-mortem subjects. Forensic Sci Int. 2016;263:139–146.

50. Scheurer E, Lovblad KO, Kreis R, Maier SE, Boesch C, Dirnhofer R, et al. Forensic application of postmortem diffusion-weighted and diffusion tensor MR imaging of the human brain in situ. Am J Neuroradiol. 2011;32(8):1518–1524.

51. Biousse V, Suh D, Newman N, Davis P, Mapstone T. Diffusion-weighted magnetic resonance imaging in shaken baby syndrome. Am J Ophthalmol. 2002; 133(2):249-255

52. Chiriboga CA. Nusinersen for the treatment of spinal muscular atrophy. Expert Rev Neurother. 2017;17(10):955–962.

53. Finkel RS, Mercuri E, Darras BT, Connolly AM, Kuntz NL, Kirschner J, et al. Nusinersen versus Sham Control in Infantile-Onset Spinal Muscular Atrophy. N Engl J Med. 2017;377(18):1723–1732.

54. Bertini E, Burghes A, Bushby K, Estournet-Mathiaud B, Finkel RS, Hughes RAC, et al. 134th ENMC international workshop: Outcome measures and treatment of spinal muscular atrophy 11-13 February 2005 Naarden, the Netherlands. Neuromuscul Disord. 2005;15(11):802–816.

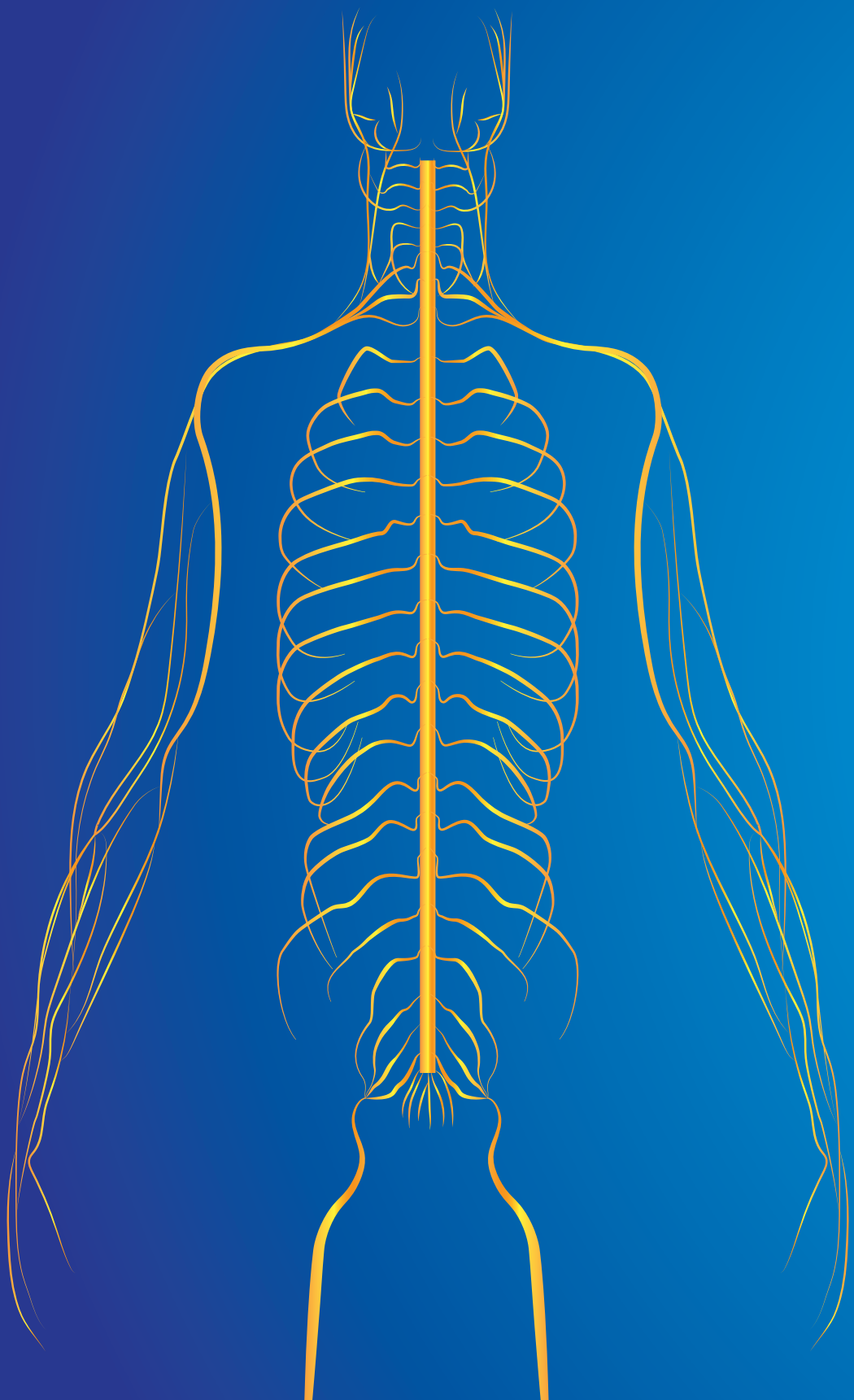

Addendum

Dutch summary
(Nederlandse samenvatting)

Het perifeer zenuwstelsel bevat alle zenuwen die buiten het centraal zenuwstelsel (hersenen en ruggenmerg) liggen. Het geeft signalen door van het centrale zenuwstelsel naar de rest van het lichaam en vice versa. Ook reguleert en controleert het lichaamsfuncties en activiteit. Als er schade ontstaat aan (delen van) de zenuwen kan dit leiden tot verstoring in het doorgeven van signalen van het centrale zenuwstelsel naar het door de zenuw aangestuurde gebied en weer terug. Als gevolg van dit gebrek aan aansturing kan spierzwakte en uiteindelijk zelfs spieruitval ontstaan.

De onderliggende pathofysiologische processen die leiden tot zenuwdegeneratie zijn niet altijd eenvoudig te verklaren. Het verkrijgen van meer informatie omtrent deze processen is wenselijk om meer inzicht te krijgen in deze ziektemechanismen en daarmee de mogelijke behandelingen. Daardoor is er niet alleen een sterke behoefte aan non-invasieve methoden om deze ziektebeelden beter te kunnen diagnosticeren, maar ook om iets te kunnen zeggen over de progressie van de ziekte en om het effect van de gekozen therapie te meten.

Het zenuwstelsel kan non-invasief in beeld worden gebracht met magnetic resonance imaging (MRI). Een geschikte kandidaat om afwijkingen aan het zenuwstelsel te onderzoeken is diffusion tensor imaging (DTI). DTI is een MRI techniek die sensitief is voor de willekeurige beweging van watermoleculen, diffusie, en kan gebruikt worden om deze diffusie van watermoleculen te kwantificeren. In het zenuwweefsel is diffusie meer georiënteerd in de richting van de zenuw dan loodrecht op de zenuw. Deze georiënteerde diffusie wordt anisotrope diffusie genoemd. Verstoringen in de (anisotrope) diffusie van de zenuw kunnen met DTI worden gemeten en zo mogelijk een beeld geven over de staat van de zenuw. In dit proefschrift worden MRI en DTI toegepast in verschillende perifere zenuwaandoeningen om zo de waarde van deze technieken in een klinische setting te onderzoeken.

In **hoofdstuk 2** hebben we de reproduceerbaarheid van DTI in de lumbosacrale (onderrug) zenuwen onderzocht. We vonden een hoge reproduceerbaarheid van DTI wat betekent dat deze techniek betrouwbaar kan worden toegepast in cross-sectioneel onderzoek in een klinische setting. Tussen herhaalde metingen gedaan met een week interval vonden we kleine verschillen. Dit toont aan dat het belangrijk is om voorzichtig te zijn met de interpretatie van diffusiewaarden gemeten in longitudinale studies, omdat kleine verschillen ook kunnen worden veroorzaakt door andere factoren dan ziekteprogressie en respons op de therapie.

In **hoofdstuk 3** demonstreerden we de toepassing van DTI in de lumbosacrale plexus bij kinderen met spina bifida. We vonden asymmetrie en disorganisatie van de zenuwen in spina bifida patiënten, waarbij met name op het niveau van de myelomeningocèle een duidelijk verschil te zien was t.o.v. gezonde controles. De zenuwen van patiënten hadden lagere diffusiewaarden dan gezonde controles. Het mechanisme achter spina bifida is erg complex, waardoor de interpretatie van onze bevindingen moeilijk is. Desalniettemin verwachten we dat de abnormale diffusiewaarden een indicatie zijn voor aangedane of disfunctionele zenuwen.

Om de klinische waarde van fiber tractografie en diffusie parameters te bepalen, hebben we de toepasbaarheid van DTI in gecomprimeerde zenuwen van patiënten met een lumbale discus hernia onderzocht in **hoofdstuk 4**. We vonden verschillen in fractionele anisotropie en radiale diffusie tussen aangedane zenuwen van patiënten en zenuwen van gezonde controles. We konden echter geen verschil vinden in diffusiewaarden tussen de gecomprimeerde zenuwen en de contralaterale zijde in dezelfde patiënt. Wel hebben we laten zien dat de locatie waarop gemeten wordt een effect heeft op de diffusiewaarden, waarbij een lagere fractionele anisotropie en hogere gemiddelde diffusie, axiale diffusie en radiale diffusiewaarden werden gevonden in het proximale gedeelte ten opzichte van de rest van de zenuw. In toekomstig onderzoek zal dus nauwkeurig moeten worden bepaald op welke locatie in de zenuw gemeten zal worden.

In **hoofdstuk 5** hebben we onderzocht wat de mogelijke diagnostische waarde van MRI en DTI is, waarbij we de zenuwen van multifocale motor neuropathie (MMN) patiënten hebben vergeleken met die van amyotrofe laterale sclerosis (ALS) patiënten en gezonde controles. We vonden verschillen in axiale diffusie en in oppervlakte metingen van de zenuwen in de onderarm tussen patiënten met MMN en ALS patiënten en gezonde controles. Tijdens ons onderzoek werd duidelijk dat er in toekomstig onderzoek aandacht besteed moet worden aan het verbeteren van het comfort van de patiënt tijdens het onderzoek in de scanner. Met aanpassingen op dit gebied verwachten we dat de toepasbaarheid van MRI en DTI om onderscheid te maken tussen deze verschillende ziektebeelden zeer relevant zal worden en dat het bovendien zal helpen om meer inzicht te geven in de pathologische mechanismen van deze ziektebeelden.

In **hoofdstuk 6** hebben we onderzocht hoe MRI en DTI gebruikt kunnen worden bij het in kaart brengen van het cervicale ruggenmerg en de zenuwwortels op het niveau van C3-C8 bij patiënten met spinale musculaire atrofie (SMA). Oppervlakte metingen in het cervicale ruggenmerg lieten in SMA patiënten een consistent

kleiner oppervlakte zien dan in gezonde controles. Diffusiewaarden in de cervicale zenuwwortels waren kleiner dan in gezonde controles. We verwachten dat MRI en DTI een belangrijke en veelbelovende techniek zal zijn om ziekteprogressie en mogelijke therapeutische effecten in SMA patiënten beter te kunnen monitoren.

In **hoofdstuk 7** laten we de toepassing van DTI in de gehoorzenuw zien. We zagen een verlaging van fractionele anisotropie in beide gehoorzenuwen van patiënten die aan één kant doof waren ten opzichte van gezonde controles. We vonden echter geen verschillen in fractionele anisotropie tussen de beide gehoorzenuwen (gezond versus aangedaan) binnen een individuele patiënt. Dit betekent dat DTI op dit moment nog niet gebruikt kan worden om de conditie van de gehoorzenuw in de individuele patiënt aan te tonen.

Concluderend kan gesteld worden dat MRI en DTI veelbelovende technieken zijn in het onderzoeken van perifere zenuwaandoeningen. MRI en DTI kunnen mogelijk het diagnosticeren en het in kaart brengen van de prognose van verschillende zenuwaandoeningen verbeteren. De cross-sectionele studies die zijn uitgevoerd in dit proefschrift laten verschillen zien in diffusie parameters en fiber tractografie tussen patiënten en gezonde controles, wat impliceert dat deze technieken waardevol kunnen zijn in het beoordelen van perifere zenuwaandoeningen. In sommige patiëntengroepen zagen we deze verschillen in de individuele patiënt echter niet terug. In longitudinale studies is het belangrijk dat men voorzichtig is met de interpretatie van veranderingen in diffusiewaarden, omdat mogelijke verschillen ook kunnen ontstaan door andere factoren dan ziekteprogressie en de respons op therapie.

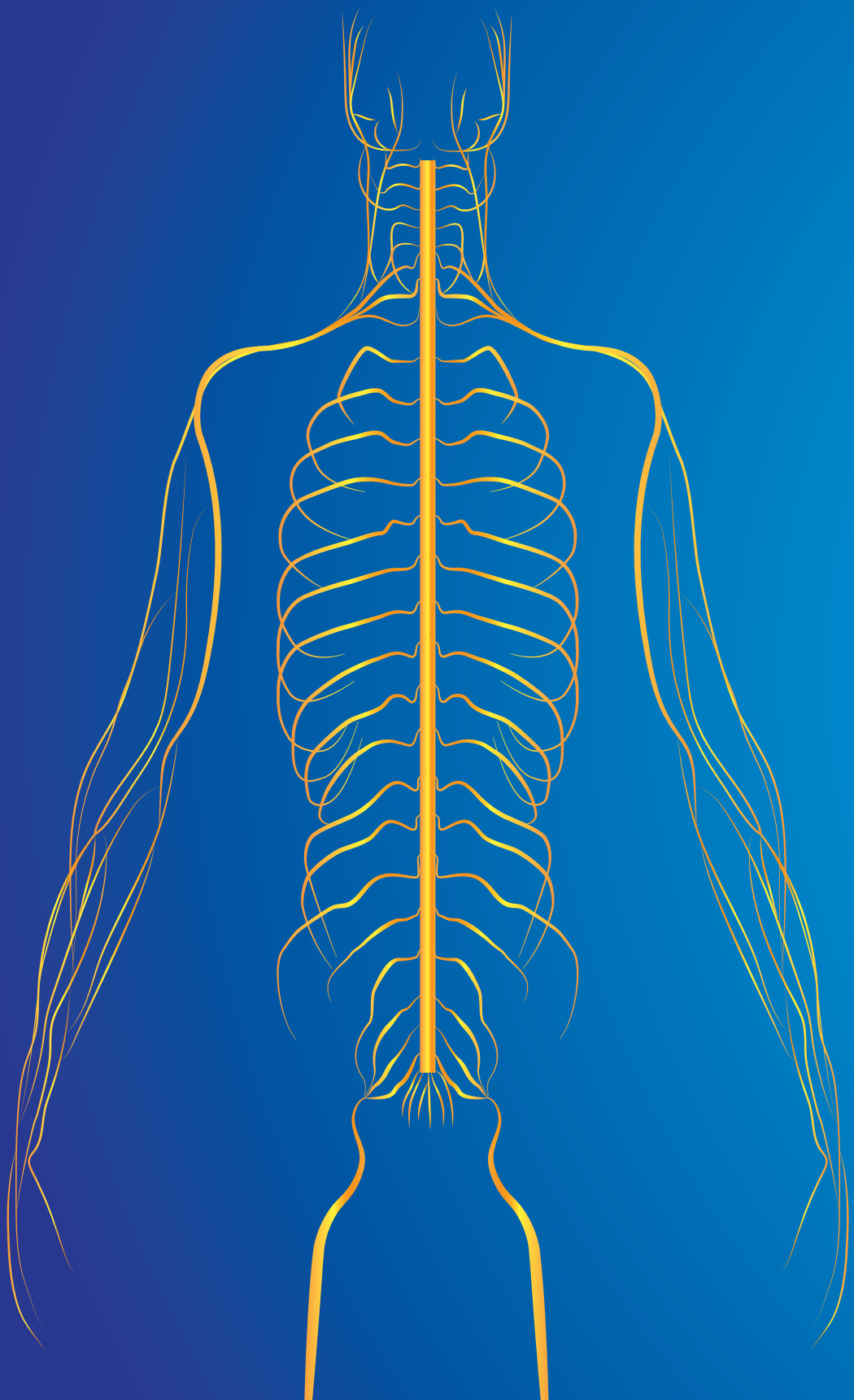

Addendum

List of publications

This thesis

Haakma W, Dik P, Ten Haken B, Froeling M, Nievelstein RAJ, Cuppen I, De Jong TPVM, Leemans A.
Diffusion tensor MRI and fiber tractography of the sacral plexus in children with spina bifida Journal of Urology, 2014;192(3):927-933

Vos SB, **Haakma W**, Versnel WH, Froeling M, Speleman L, Dik P, Viergever MA, Leemans A, Grolman W.
Diffusion tensor imaging of the auditory nerve in patients with acquired single-sided deafness
Hearing Research, 2016;323:1-8

Haakma W, Jongbloed BA, Froeling M, Goedee HS, Bos C, Leemans A, Van den Berg LH, Hendrikse J, Van der Pol WL.
MRI shows thickening and altered diffusion in the median and ulnar nerves in multifocal motor neuropathy
European Radiology, 2016;27(5):2216-2224

Haakma W, Hendrikse J, Uhrenholt L, Leemans A, Warner Thorup Boel L, Pedersen M, Froeling M.
Multicenter reproducibility study of diffusion MRI and fiber tractography of the lumbosacral nerves
Journal of Magnetic Resonance Imaging, 2018; [Epub ahead of print]

Haakma W, Froeling M, Dik P, Leemans A, Linn FHH, Nieuwkamp D, Dorhout Mees S, Biessels GJ, Hendrikse J.
Diffusion tensor imaging of the compressed nerve roots in lumbar disc herniation
Submitted

Haakma W*, Stam M*, Kuster L, Froeling M, Philippens MEP, Bos C, Leemans A, Otto LAM, Van den Berg LH, Hendrikse J^, Van der Pol WL^.
Magnetic resonance imaging of the spinal cord in spinal muscular atrophy
Submitted
* and ^: These authors contributed equally to this work

Other

Haakma W, Pedersen M, Froeling M, Uhrenholt L, Leemans A, Warner Thorup Boel L.
Diffusion tensor imaging of peripheral nerves in non-fixed post-mortem subjects
Forensic Science International, 2016;263:139–146

Haakma W, Rohde M, Kuster L, Uhrenholt L, Pedersen M, Warner Thorup Boel L.
Post-mortem computed tomography angiography utilizing barium sulfate to identify microvascular structures: a preliminary phantom model and case study
Journal of Forensic Radiology and Imaging, 2016;7:38-42

Jongbloed BA, **Haakma W**, Goedee HS, Bos JW, Bos C, Hendrikse J, Van den Berg LH, Van der Pol WL.
Comparative study of peripheral nerve MRI and ultrasound in multifocal neuropathy and amyotrophic lateral sclerosis
Muscle and Nerve, 2016;54(6):1133-1135

Haakma W, Rohde M, Uhrenholt L, Pedersen M, Warner Thorup Boel L.
Identification of discrete vascular lesions in the extremities using post-mortem computed tomography angiography – Case reports
Journal of Forensic Radiology and Imaging, 2017;9:47-50

Haakma W, Froeling M, Pedersen M, Uhrenholt L, Douven P, Leemans A, Warner Thorup Boel L.
Post-mortem diffusion MRI of the cervical spine and its nerve roots
Journal of Forensic Radiology and Imaging, 2018;12:50-56

Vaeggemose M, **Haakma W**, Pham M, Ringgaard S, Tankisi H, Ejskjaer N, Heiland S, Poulsen PL, Andersen H.
Diffusion Tensor Imaging MR Neurography Detects Polyneuropathy in Type 2 Diabetes
Submitted

Conferences presentations (first author only)

Haakma W, Dik P, Ten Haken B, Froeling M, Nievelstein RAJ, Cuppen I, De Jong TPVM, Leemans A.
Diffusion tensor MRI and fiber tractography of the sacral plexus in children with spina bifida
Oral ESPU 2014, Innsbruck, Austria
Oral ISMRM 2014, Milan, Italy

Haakma W, Pedersen M, Froeling M, Uhrenholt L, Leemans A, Warner Thorup Boel L.
Diffusion tensor imaging of peripheral nerves in non-fixed post-mortem subjects
Oral ISMRM Benelux 2015, Gent, Belgium
Poster ISMRM 2015, Toronto, Canada
Oral ISFRI 2015, Leicester, UK

Haakma W, Jongbloed BA, Froeling M, Goedee HS, Bos C, Leemans A, Van den Berg LH, Hendrikse J, Van der Pol WL.
Diffusion tensor imaging of forearm nerves for early diagnosis of multifocal motor neuropathy
Poster ISMRM 2015, Toronto, Canada

Haakma W, Froeling M, Pedersen M, Uhrenholt L, Douven P, Leemans A, Warner Thorup Boel L.
Post-mortem diffusion MRI of the cervical spine and its nerve roots
Oral ISMRM Benelux 2016, Eindhoven, the Netherlands
Oral ISMRM 2016, Singapore, Singapore
Oral ISFRI 2016, Amsterdam, the Netherlands

Haakma W, Hendrikse J, Heemskerk AM, Luijten P, Pedersen M, Leemans A, Froeling M.
7T diffusion MRI of the forearm nerves
Poster ISMRM 2016, Singapore, Singapore

Haakma W, Stam M, Kuster L, Froeling M, Philippens MEP, Bos C, Leemans A, Otto LAM, Van den Berg LH, Hendrikse J, Van der Pol WL.
Magnetic resonance imaging of the spinal cord in spinal muscular atrophy
Poster ISMRM Benelux 2017, Tilburg, the Netherlands
Poster ISMRM 2017, Honolulu, Hawaii

Awards

Diffusion tensor MRI and fiber tractography of the sacral plexus in children with spina bifida
Summa Cum Laude award ISMRM 2014

Post-mortem diffusion MRI of the cervical spine and its nerve roots
Magna Cum Laude award ISMRM 2016

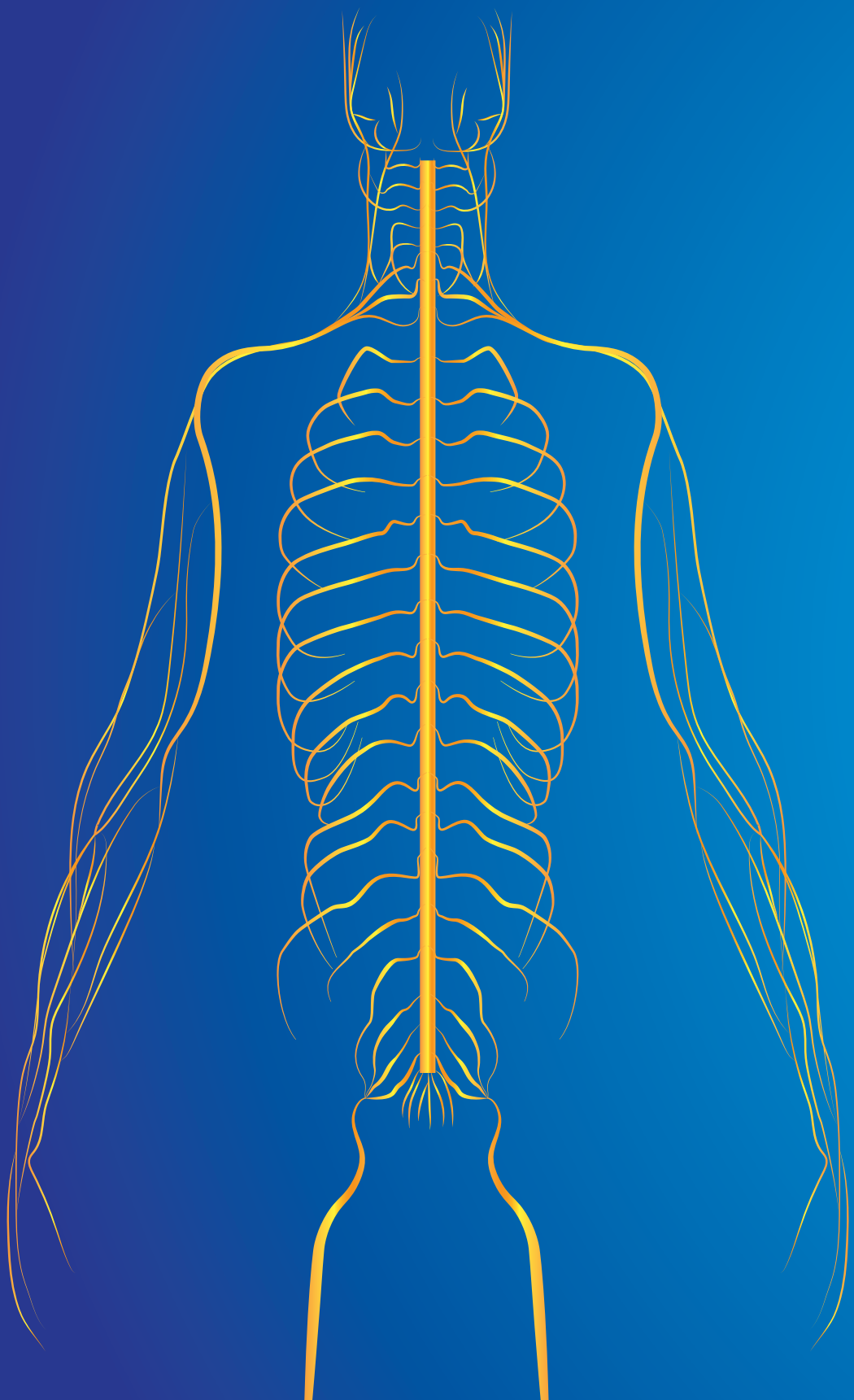

Addendum

Acknowledgements
(Dankwoord)

Graag wil ik iedereen bedanken die op welke manier dan ook heeft bijgedragen aan dit proefschrift. Zonder jullie steun en bijdrage was het tot stand komen van dit proefschrift niet gelukt. In het bijzonder wil ik de deelnemers aan mijn studies bedanken. Zonder hen was het doen van onderzoek niet mogelijk geweest.

Prof. Dr. Hendrikse, beste Jeroen, het was me een waar genoegen om onder jouw supervisie dit promotietraject te doorlopen. Ik heb altijd bewondering gehad voor jouw betrokkenheid en dat je bij elk onderzoek ook nog van de hoed en de rand weet. De frequente bezoekjes aan onze kamer waarbij je binnen kwam waaien om te vragen hoe het er voor stond en de 'laten we even koffie halen, loop je mee' gesprekken ben ik gaan waarderen. Ik ben dankbaar voor de ruimte die je me hebt gegeven om mijn eigen pad te bewandelen en me te ontwikkelen als onderzoeker en als persoon.

Prof. Dr. Luijten, beste Peter, ik ben blij dat ik onderdeel mocht uitmaken van de 7T groep. De diversiteit en de betrokkenheid van deze groep heeft mij enorm geholpen in het uitvoeren van mijn onderzoeken. Ook de openheid en de laagdrempeligheid van alle collega's in de groep heeft geleid tot een ontzettend leuke werksfeer waarin ik veel van anderen heb kunnen leren.

Dr. Leemans, beste Alexander, ik weet nog goed dat, toen ik als master student je kantoor binnen kwam, ik erg onder de indruk was van alle kennis die je in huis hebt. Ik ben dan ook blij dat je me tijdens dit promotietraject hebt begeleid en ik heb veel van je opgestoken. Je bent altijd betrokken geweest bij mij en bij mijn onderzoeken en ik heb me er menig maal over verbaasd hoe je altijd binnen 2 minuten op je mail kunt reageren. Ik wil je bedanken dat je te allen tijde voor me klaarstond.

Dr. Froeling, beste Martijn, vanaf de start van mijn promotie ben je altijd betrokken geweest bij mijn onderzoek. Ik heb een hoop van je geleerd mede dankzij de vele uren van sleutelen aan protocollen achter de MRI scanner. Je intensieve begeleiding op afroep sloot goed aan op mijn manier van werken. Ik kon altijd bij je binnenlopen als ik ergens niet uitkwam of gefrustreerd over was. Dank daarvoor!

Dear Lene, Michael and Lars, thanks for the supervision in Denmark. I really enjoyed working in such an inspiring scientific environment where 'impossible' is not an option.

Prof. dr. Pasterkamp, Prof. dr. Dijkhuizen, Prof. dr. Moonen, Prof. dr. Biessels, and Prof. dr. Pedersen, thank you for all the time and effort spend in assessing this thesis.

Dr. Dik, beste Pieter, bij jou begon dit avontuur. Toen ik bij jou startte met mijn laatste master stage met het onderzoek bij spina bifida patiënten had ik niet verwacht dat het zou eindigen in twee promotietrajecten. Je gevoel voor humor en je frisse blik op de wereld leveren vaak weer tal van nieuwe ideeën op voor onderzoek. Ik ben je dankbaar dat je in deze jaren betrokken bent gebleven en dat ik altijd even bij je binnen kon lopen om bij te praten over koetjes en kabouters.

Ik wil alle co-auteurs bedanken voor de fijne samenwerking in alle onderzoeksprojecten. Clemens en Mariëlle, dank voor jullie hulp bij het opzetten van de MRI protocollen. Clemens, ik heb altijd bewondering voor je gehad om de manier waarop jij complexe MRI materie zo simpel kunt uitleggen. Je was er als ik weer eens je hulp nodig had, heel erg bedankt!
Mariëlle, ik vond het bijzonder leuk om met jou samen te mogen werken. Jij zorgde voor de finetuning van onze protocollen en ook je outfit ziet er altijd gefinetuned en fleurig uit. Onze gezellige gesprekken fleurden mijn dag altijd weer op.
Bas, we hebben zitten zwoegen om de patiënten voor de MMN studie te includeren. Gelukkig resulteerde het harde werken en de vele uren achter de scanner (zelfs op kerstavond) in twee mooie publicaties!
Marloes, het was soms even bikkelen en zwoegen, maar dat lag niet aan onze samenwerking. We vulden elkaar mooi aan en ik denk dat we een goed team waren! Er ligt nu toch maar mooi een manuscript en tevens is er financiering voor vervolgonderzoek op basis van onze resultaten.

Alle collega's van de 7T groep, bedankt voor de open en relaxte werkomgeving. De vele uitjes en de congressen waren altijd enorm plezierig om met jullie te ondernemen

Colleagues of the diffusion group, dear Szabolcs, Hamed, Alberto, Samuel, Alexander, Martijn, Sjoerd, Chantal, Anneriet, Fenghua, Victor and Hanna. Thanks for all the informative, inspiring, and fun diffusion meetings. The yearly dinners were always something to look forward to. Thanks that you were always willing to help me out with diffusion matters.

Beste Sylvia, Marja en Annet, hartelijk dank voor jullie hulp bij het regelen van allerlei praktische zaken rondom het doen van onderzoek! Ook vond ik het fijn dat ik af en toe gewoon even langs kon lopen om een praatje te maken.

Beste Shanta, Saskia en Anneke, ik vond het ontzettend fijn dat jullie er waren voor de ondersteuning van klinische onderzoeksprojecten. Heel erg bedankt voor jullie hulp bij het opzetten en uitvoeren van mijn klinische projecten.

Beste Roy, Karin en Chris, hartelijk dank voor jullie hulp bij het maken van posters en figuren voor mijn promotieonderzoek. Roy, heel erg bedankt voor het maken van de lay-out en binnenwerk van dit proefschrift en je flexibele werkwijze!

Collega's van de zaak, beste Esther, Remko en Wouter. Dank voor het kunnen delen van euforische momenten zoals het submitten van een paper, revisies, resubmissies, submissies naar een ander journal en uiteindelijk accepted papers (immers elke mijlpaal binnen je PhD moet gevierd worden!). Door jullie was naar 'kantoor' gaan altijd een feestje.

Oud-kamergenoten en huidige kamergenoten, beste Jill, Bertine, Lara, Bernard, Richard, Csilla, Lieke, Ria en Peter, dank voor het kunnen sparren en spuien van alles wat met wetenschap en daarbuiten te maken had.

Collega's van Q1 en de vissenkom, beste Margot, Caren, Josanne, Frans, Annemarie, Dhabia, Ludwike, Bianca, Robbert, Wouter, Jonas, Mimount, Suzanne, Marilot, Ahmed, Sander en Martina. Teruggekomen van zwangerschapsverlof hebben jullie mij met open armen ontvangen. Dank voor al die koffie/chocoladekokosmelk momentjes waarin ik altijd mijn euforie en frustratie met jullie heb kunnen delen.

ImagO commissieleden, beste Hanke, Tristan, Tijl, Erwin, Ellis, Annemarie en Bas, ik heb met veel plezier samen met jullie de ImagO (mid)dagen georganiseerd. De samenwerking liep altijd gestroomlijnd en ook onze werkbesprekingen in de vorm van een drankje op het terras bevielen mij altijd goed.

Thanks to all my Danish colleagues in particular Trine, Mia, Henrik and Kasper. Thanks for the moments eating 'stroopwafels' and 'rugbrød med marinerede sild'.

Lieve dispuutsgenoten, lieve meiden van Nefertiti, ook in Utrecht zijn we nog steeds een hechte groep. Ik ben jullie dankbaar dat jullie er vanaf mijn studententijd voor mij zijn geweest en dat we er nu en altijd voor elkaar zullen zijn.

Lieve 'broertjes en zusjes', lieve Remy, Martijn, Anique en Evelien. Door het lot verenigd en nog steeds een hechte (doe)groep. De uitjes, Sinterklaasavonden en avonturen die we samen hebben beleefd, maakten mijn promotietijd mooier.

Lieve paranimfen, lieve Esther en Annemarie, wat had ik zonder jullie gemoeten… Jullie stonden altijd voor mij klaar zowel in het werkende leven als daarbuiten. Esther, dank voor alle steun die je me door de jaren heen altijd hebt gegeven. Ik kon voor alles bij je terecht, PhD problematiek, persoonlijke dingen, vaccinaties, het was je allemaal niet te gek. Annemarie, ik begrijp soms niet hoe je het allemaal

doet. Altijd behulpzaam, nuchter, vindingrijk en ook goede verhalen. Hoe druk je zelf ook bent, je bent nooit te beroerd om mij weer eens uit de brand te helpen met al mijn vragen. Ik ben je daar enorm dankbaar voor. 👍

Lieve schoonfamilie, lieve Jaap, Olga, Saskia en Jurjen, dank voor de oneindige steun die jullie me de afgelopen jaren hebben gegeven. Dank voor het kunnen delen van lief en leed.

Lieve broers en zussen, lieve Sido, Lieke, Ineke en Nick, er is veel gebeurd, van promoties tot gezinsuitbreiding het kon allemaal niet gekker. Dank dat ik altijd op jullie kon rekenen in goede en in slechte tijden.

Lieve pap en mam, dank voor jullie onvoorwaardelijke steun en liefde. Ik kan bij jullie altijd voor alles terecht, dag en nacht. Het is met woorden niet eens uit te drukken hoeveel ik mij gezegend voel met jullie als ouders. Ik ben gewoon heel blij dat jullie er voor mij zijn.

Lieve Remy, wat een avontuur de afgelopen jaren. Ik ben je dankbaar dat je me altijd de ruimte hebt gegeven om te kunnen schipperen tussen Nederland en het Vikingland. Bij elke reis die ik ondernam was het beste hiervan om weer bij jou thuis te komen. Dank voor je liefde, je onvoorwaardelijke steun en je rotsvaste vertrouwen. Ik prijs mijzelf bijzonder gelukkig met jou en nu ook onze twee prachtige dochters Jasmijn en Nynke in mijn leven. Met jou is het leven mooier!

Remy,
Jasmijn, Nynke,
Nellie, Bauke, Ineke,
Nick, Sido, Lieke, Tessa,
Daan, Nyssa, Vamke,
Olga, Jaap, Saskia,
Jurjen, Wobbe, Peter,
Jeroen, Alexander,
Martijn, Lene ,
Michael, Lars,
Marianne,
Remko, Esther,
Wouter,
Bertine, Jill, Lara,
Bernard, Csilla, Richard,
Nikki, Jolanda, Carlo, Alberto, Chantal, Sjoerd, Hamed,
Szabolcs, Fenghua, Bruno, Victor, Hanna, Jelmer, Bob, Anneriet,
Thessa, Dennis, Hans, Fredy, Jaco, Natalia, Jeroen, Alex, Sylvia, Renée,
Tijl, Jannie, Alexander, Anja, Joep, Ronald, Arjan, Irene, Anna, Hanke,
Marlijne, Arthur, Niels, Rashid, Stefano, Matthew, Lisa, Arjen, Maarten,
Tine, Jeanine, Tim, Frank, Janot, Oscar, Mike, Sam, Bart, Anneloes, Sander,
Annemarie, Dhabia, Margot, Caren, Bianca, Josanna, Frans, Marilot, Robbert,
Wouter, Ludwike, Suzanne, Mimount, Gerke, Jonas, Ahmed,
Sander, Martina, Roy, Björn, Alexandra, Anouk, Erika, Marjolein,
Gisela, Ellis, Lennart, Deji, Quincy, Marja, Annet, Marloes, Bas, Ludo,
Shanta, Anneke, Clemens, Marielle, Peter, Erwin, Pieter, Tristan,
Trine, Mia, Christian, Louise, Perla, Lidy, Szuszanne, Michael,
Sofie, Maria, Lone, Henrik, Kasper, Jesper, Esben, Tymen, Viviane,
Femke, Hans, Lotte, Klaas, Anna, Elko, Sandra, Tanja,
Rasmus, Liana, Hetty, Martin, Henk, Jikke, Sanne, Niels, Eise,
Bettie, Ron, Pake, Christine, Esther, Marjan, Bjorn, Ingmar, Zoë, Anne,
Tineke, Joop, Marion, Evelien, Anique, Martijn, Mathilde, Lex, Lisanne,
Nicole, Niels, Sharon, Nanda, Wietske, Yoël, Willem, Sara, Anneke,
Bauke, Hanneke, Nefertiti, Ilse, Bas, Roos, Frank, Simone, Erwin, Jori,
Sophie, Wendie, Inge, Kristin, Maaike, Mo, Mirte, Sanne, Willemijn,
Maarten, Céline, Bernd, Suzanne, Stef, Stefan, Ferry, Kim, Fien, Joren,
Marina, Menno, Elisabeth, Janita, Maryse, Lizette, Marco Miek

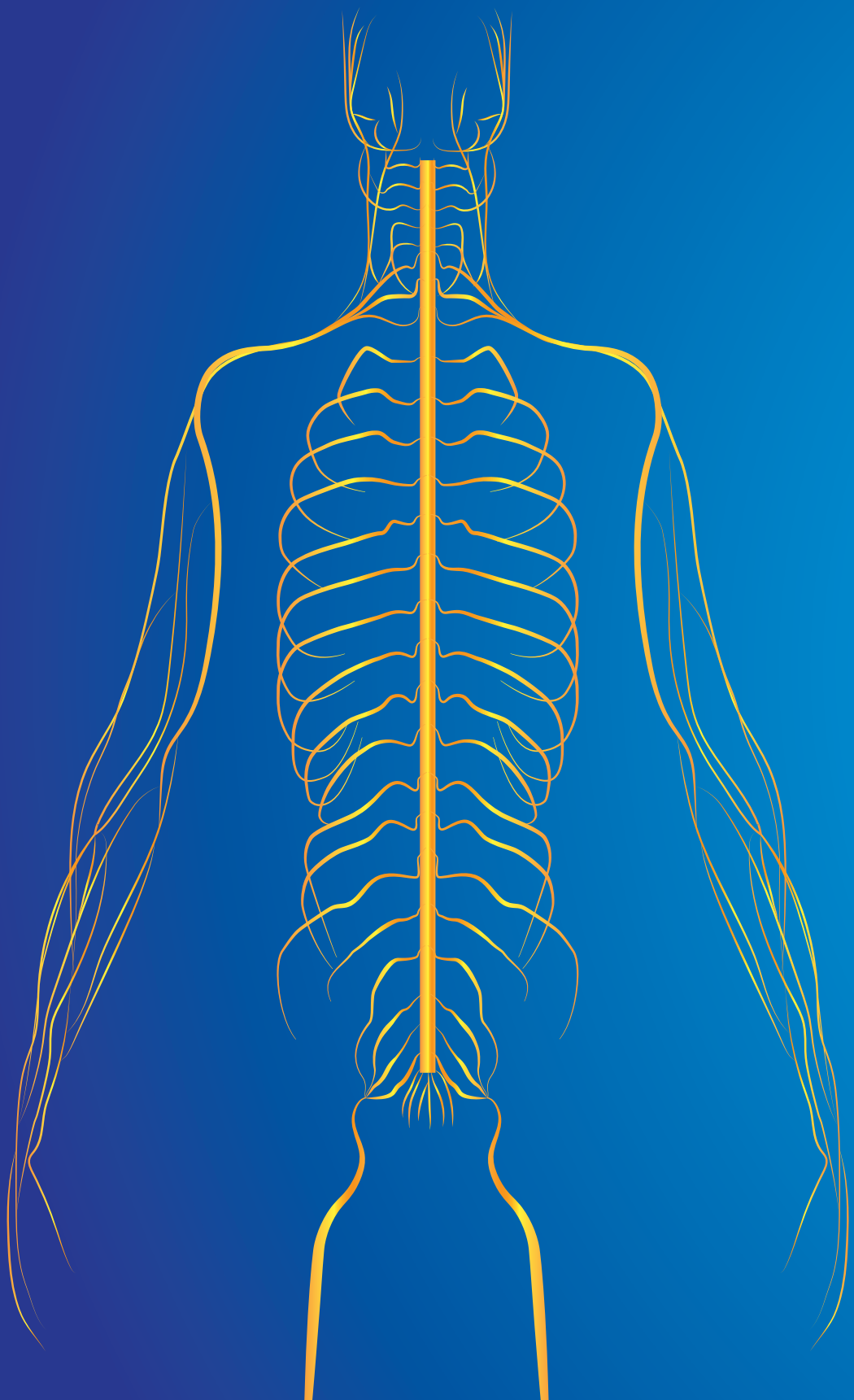

Addendum

Autobiography

Wieke Haakma was born on January 28th, 1988 in Beetsterzwaag. Eager to learn about technology and health care she attended the University of Twente to study Technical Medicine and Health Sciences in 2006. In 2011, she received her master degree *cum laude* in Health Sciences. Her final master internship of Technical Medicine brought her to the Wilhelmina Kinderziekenhuis where she started working on imaging peripheral nerves with diffusion tensor imaging under the supervision of Dr. P. Dik. During this internship she visited the University of Aarhus to apply this technique in a clinical setting. She received her master degree in Technical Medicine in 2013.

Enthusiastic about this imaging technique and its potential applications accompanied by her curiosity to work in another institute abroad, she started working on a double PhD degree. This was a collaboration between the department of radiology at the University Medical Center Utrecht under the supervision of Prof. Dr. J. Hendrikse, Prof Dr. P.R. Luijten, Dr. A. Leemans, and Dr. M. Froeling and at the forensic department and comparative medicine lab of the University of Aarhus in Denmark under the supervision of Prof. Dr. L. Warner Thorup Boel, Prof. Dr. M. Pedersen, and Dr. L. Uhrenholt. At Aarhus University she worked on her PhD thesis entitled: 'Advances in forensic imaging – CT angiography and diffusion MRI of the nervous system', which she completed in 2017. At the University Medical Center in Utrecht she studied peripheral nerve structures in different neurological disorders *in vivo* of which this thesis is the final result.

She lives with her husband Remy and their two children Jasmijn and Nynke in Utrecht.